Diplomarbeit

Prozessvergleich zwischen Monoethanolamin Prozess und Chilled Ammonia Prozess zur CO_2 Wäsche - basierend auf Modellierung und Simulation

ausgeführt zum Zwecke der Erlangung des akademischen Grades eines Diplom-Ingenieurs unter der Leitung von

Univ. Prof. Dipl. Ing. Dr. techn. Markus Haider
Proj. Ass. Dipl. Ing. Sebastian Posch
Institut für Energietechnik und Thermodynamik (E302)
Forschungsbereich Thermodynamik und Wärmetechnik

eingereicht and der Technischen Universität Wien
Fakultät für Maschinenwesen und Betriebswissenschaften

von

Thomas Steinparzer
Matr. Nr.: 0526090
E734
Dießenleitenweg 4
4040-Linz
E-mail: e0526090@student.tuwien.ac.at

Wien, im Juni 2010

_____

Master Thesis

MEA Process and CAP - A comparison based on simulation

in fulfillment of the thesis requirement for the degree of Diplom-Ingenieur

Supervisors:
Univ. Prof. Dipl. Ing. Dr. techn. Markus Haider
Project. Ass. Dipl. Ing. S. Posch
Institute of Energy Systems and Thermodynamics (E302)

presented to the Vienna University of Technology
Faculty of Mechanical Engineering

by

Thomas Steinparzer
Matr. No.: 0526090
E734
Dießenleitenweg 4
4040-Linz
E-mail: e0526090@student.tuwien.ac.at

Vienna, June 2010

_____

Acknowledgements

I would like to express my thanks to all those who have assisted and supported me doing this thesis.

- First of all, I would like to thank DI *Sebastian Posch* for all the scientific support and the interesting discussion about energy issues during doing this thesis.
- Further, I would like to express my thanks to Univ.-Prof. DI Dr. *Markus Haider* for giving me the possibility of doing this thesis and the quick support.
- Moreover, I would like to thank my parents *Elfriede* and *Karl Steinparzer* for supporting me emotionally and financially during my whole education and for being such good parents.
- I also like to thank *Stefanie Pohn* for supporting me at all times.

Abstract

Objective of this work was the process comparison of the two post-combustion capture processes based on an aqueous MEA solution or an aqueous ammonia solution. The CO_2 absorption based on the aqueous NH_3 solution was done at chilled conditions.

Due to the change in climate, carbon dioxide got into the focus of research for reduction of GHG (Greenhouse Gas) emissions.
For power plants three main technologies exist for reducing the CO_2 emissions. These are: pre-combustion, oxyfuel-combustion and post-combustion. Post-combustion technologies are interesting, because of the retrofit possiblity of existing power plants.

Therefore two of the most developed post-combustion processes (MEA Process and CAP) were compared to each other. This process comparison was based on simulation results calculated with the simulation tool ASPEN Plus^{TM}.
Therefore, simulation models for each process with property data sets were adopted from various sources.

The simulation results showed that both processes have a partikular minimum for the specific reboiler duty at a certain washing solvent to flue gas ratio. By the variation of the main operation parameters the optimum process parameters for both capture processes were determined.
For each process the main operation data (specific reboiler duty, specific cooling duty, specific power duty, specific solvent flow, specific water and solvent consumption) were calculated and considered in the evaluation.

The process comparison showed that the CAP has an advantage with respect to the specific reboiler duty and the necessary specific solvent flow compared to the MEA Process. On the other hand, the higher power demand and cooling water consumption for the refrigeration system of the CAP leads to a larger loss in net power than for the MEA Process.
Further, an approximate evaluation of the investment costs for both processes was done. This comparison resulted in the fact that the CAP is slightly more expensive than the to the MEA Process due to the taller columns and costs for auxiliary components.
The qualitative ecologic comparison of the systems came to the result that ammonia is more toxic to the environment than monoethanolamine.

Kurzfassung

Ziel dieser Arbeit war der Prozessvergleich zwischen zwei post-combustion capture Prozessen basierend einerseits auf einer wässrigen Monoethanolamin Lösung und andererseits auf einer wässrigen Ammoniak Lösung. Die CO_2 Absorption mit Hilfe der wässrigen Ammoniak Lösung wurde unter gekühlten Bedingungen durchgeführt.

Auf Grund der möglichen Änderung des Klimas ist CO_2 in den Fokus der Forschung zur Reduktion der Treibhausgase gekommen.
Für Kraftwerke gibt es grundsätzlich drei mögliche Technologien, die zur CO_2 Abscheidung genutzt werden können. Diese sind im Wesentlichen: pre-combustion, Oxyfuel Verbrennung und post-combustion. Besonders die post-combustion Prozesse haben ein großes Potential, da bei ihnen die Möglichkeit der Nachrüstung besteht.

In dieser Arbeit wurden zwei post-combustion capture Prozesse (Monoethanolamin Prozess und Chilled Ammonia Prozess) miteinander verglichen, die aktuell im Fokus der Forschung liegen. Der Prozessvergleich baut auf Ergebnisse, die mit Hilfe der Prozesssimulationssoftware ASPEN Plus^{TM} erzielt wurden.
In Anlehnung an verschiedene Quellen wurden Modelle zur Prozesssimulation für beide CO_2 Abscheideverfahren entworfen.

Die Simulationsergebnisse zeigten, dass für beide Prozesse ein Minimum des Reboilerbedarfs bei einem bestimmten Verhältnis von Waschflüssigkeit zu Rauchgas existiert. Durch Veränderung der wichtigsten Anlagenparameter wurde für beide Prozesse ein Optimum der Betriebsparameter fixiert.
Für jeden Prozess wurden die Anlagenparameter (spezifischer Reboilerbedarf, spezifische Kühlleistung, spezifische elektrische Leistung, spezifischer Waschmittelmassenstrom und spezifischer Wasser- und Waschmittelverbrauch) berechnet und miteinander verglichen.

Der Prozessvergleich kam zu dem Ergebnis, dass der Chilled Ammonia Prozess in Bezug auf spezifischen Reboilerbedarf und Waschmittelmassenstrom gegenüber dem Monoethanolamin Prozess begünstigt ist. Hingegen führt der größere Bedarf an elektrischer Energie sowie der höhere Kühlwasserbedarf zu einem größeren Leistungsverlust für das Kraftwerk.
Eine grobe und qualitative Abschätzung der Investitionskosten wurde ebenfalls für beide Systeme durchgeführt. Diese kam zu dem Schluss, dass die Investitionskosten für den Chilled Ammonia Prozess etwas höher liegen als für den Monoethanolamin Prozess. Grund dafür sind die höheren Kolonnen und die zusätzlichen Hilfsaggregate.
Durch einen ökologischen Vergleich der Systeme wurde rein qualitativ festgestellt, dass Ammoniak eine höhere Toxizität für die Umwelt besitzt als Monoethanolamin.

Contents

1 Introduction

Nowadays, many researchers agree that anthropogenic GHG provoke a change in climate, although it is not certain. Nevertheless, a significant contribution to stop global warming must be yet done. The reason is, that when this theory is going to be verified, it may be too late to stop the global warming.
Since 1750 the global atmospheric concentrations of carbon dioxide, methane and nitrous oxide increased vehemently due to human activities. The global increase in CO_2 has mainly been caused by fossil fuel use and land use. Whereas, methane and nitrous oxide are created by agriculture (cf. [1]).

In a short term, fossil fuels will remain abundant for worldwide energy supply. As a matter of fact, fossil energy use causes about 85% of the anthropogenic CO_2 emissions produced annually (see [1], chapter 4, p. 265). Besides methane, carbon dioxide is seen as the most important antropoghenic GHG, since it belongs to the long-lived GHG and has the strongest radiative forcing according to [1]. Besides, the major reason of the importance of carbon dioxide in the fight against global warming is the large emission. If the emissions of greenhouse gases like carbon dioxide shall be reduced significantly in the next few years, "'*either current uses of fossil energy will have to shift toward low- and zero-carbon sources, and/or technologies will have to be adopted that capture and store the CO_2 emissions*"' (see [2]). Carbon capture and storage (CCS) technologies will be needed for reducing emissions of atmospheric CO_2 (cf. [1]). Although prices increase, fossil fuels enjoy economic advantages at the moment, because of their availability and proven technology.

The Kyoto Protocol (see [3], 1997) entered into force in February 2005. The objective of the Kyoto Protocol is the stabilization of GHG concentrations in the atmosphere at a level that would prevent dangerous interference with the climate system. A reduction of emmissions should be done by -5.2% compared to the CO_2 level in the atmosphere of 1990. Overall, 183 states are parties to the protocoll (e.g.: European Union, Russia, China,...). For achieving the targets the so called Kyoto flexible mechanisms (Emissions Trading, Clean Development Mechanism, Joint Implementation) can be used to achieve emissions cutback cost-effectively in other countries.
This extension to the Rio Declaration [4] made the reduction of GHG obligatory for the participating industrialized countries.
Besides, the flexible mechanism of emission trading (credits) gets especially new technologies into the focus of this contract to achieve the reduction targets. In other words, if buying of additional credits from other countries is getting too expensive, the Kyoto Protocol could be seen as the legal basis for the needed development of CCS technologies.

The potential of carbon capture and storage is expected as very high, according to IPCC Special Report on CCS in 2005 [1]. The two main advantages of CCS are the increase of flexibility in achieving GHG emission limits and the reduction of overall costs for mitigation.
There are three basic technologies to capture the carbon dioxide:

1. pre-combustion
2. oxyfuel-combustion
3. post-combustion.

Post combustion capture (PCC) processes are mainly based on chemical absorption. In this process the CO_2 of the flue gas is absorbed by chemical solvents. Afterwards, the solvent is

regenerated. The main energy entry in this process is the reboiler heat duty for the regeneration of the solvent (cf. [5]).
A special advantage of the post-combustion capture by chemical solvents is the commercial availability of similar processes already today. Further, this technology can be adopted to almost all different kinds of combustion systems emitting carbon dioxide (e.g.: power plants, steel production, cement production, ammonia production) (cf. [1]).
"At this point in time, absorption processes based on chemical solvents offer high capture efficiency, selectivity and the lowest energy use", according to [1].
A certain fact, that makes CCS technologies very attractive is the option of building capture ready plants. Those capture ready plants can be upgraded afterwards with the best developed capture process for the particular circumstances. This alternative makes it possible to build power plants, which can fit a capture process in the future. Another possibility is to retrofit existing power plants, primary pulverized coal (PC) plants. This option makes PCC an important strategic point for the retrofit of existing power plants, which will be in service for many years (see [6]).
In most literature the use of Monoethanolamine (MEA) as a chemical solvent is seen as reference process. This process is commercially and industrial widley spread, for example in natural gas conditioning. Nevertheless, the conditions for the carbon capture process deviate strongly from the operating conditions of these systems. The main differences are lower gas pressure, lower CO_2 concentration in the flue gas and higher flow rates (cf. [5]).

As a result, the use of more efficient solvents is a main request for the success of post combustion capture systems based on chemical absorption.
Thus, the absorption of CO_2 in aqueous ammonia at chilled conditions is an interesting approach for carbon capture. This process is patented by EIG Inc [7]. Alstom has made intensive efforts in the development of the Chilled Ammonia Process (CAP). Furthermore, Alstom already handled some industrial projects for PCC with CAP.

1.1 Objective of this work

The objective of this work is to build up two process models for a capture process based on monoethanolamine and on chilled ammonia. Additionally, a literature research on the topics Carbon Capture and Storage, and Post-Combustion Capture based on monoethanolamine and aqueous ammonia was conducted.
Those two processes were compared to each other in an energetic, ecologic (qualitative) and economic (qualitative) way. The energetic comparison was based on simulation. The monoethanolamine scrubbing is used as a reference process.

1.2 Modeling and simulation of chemical processes

Simulation programs are widley used in chemical engineering. Moreover, most results of this work are based on process simulation. Therefore, the main terms are defined in the following:

- **Model**: Reproduction of a real process with its main correlations.
- **Simulation**: Prediction of the behaviour of a real process based on the mathematic model of the process by using a computer.

Pre-condition for doing a process simulation is that physical and chemical correlations of the process are fully known and that the process can be formally described.

Part I
Theoretical Basics

2 Carbon Capture and Storage - Technologies

In this chapter an overview of the most important CCS technologies is given.

2.1 Carbon capture technologies - general

In principle, there are three basic methods for carbon capture technologies. Carbon dioxide capture is done either in a pre-combustion, post-combustion or oxyfuel-combustion process. In the following, a short description of those three main types is given according to [8] and [9].

2.1.1 Oxyfuel

The technical term "*Oxyfuel*" describes the combustion of a fuel with pure oxygen. The combustion of carbon containing fuels with pure oxygen leads to a flue gas containing primarily CO_2 and H_2O. The water can be removed by condensation. Finally, the flue gas remains almost pure gaseous carbon dioxide. The process scheme is visualized in figure 2.1
Nevertheless, inert gas has to be added to the combustion process to control the combustion

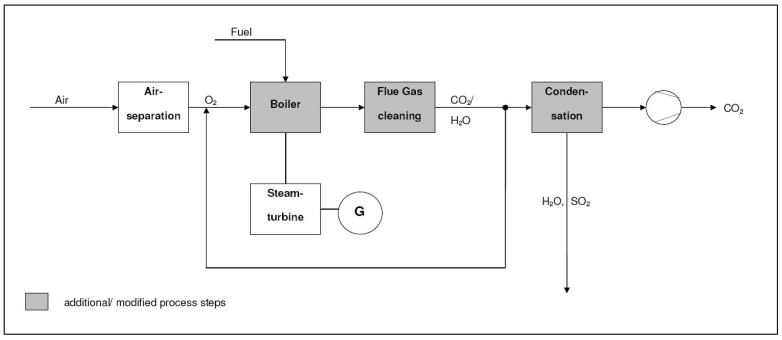

Fig. 2.1: Scheme of an Oxyfuel combustion, [10]

temperature. Gas recirculation of carbon dioxide is used for the realization. There are two principle ways for the combustion:

- Direct combustion in a conventional steam power plant and
- Combustion in a gas turbine.

The main counterpart of the simple carbon capture step is the necessary upstream air separation system. This process step has a high energy effort (cf. [11]).
Summarized, the advantages of this technology are:

- Industrial avialability of the components
- Simple CO_2 separation
- Lower energy effort and costs for the CO_2 capture step.

The disadvantages are:

- High energy effort for the air separation unit
- Investment costs
- Higher safty standards because of the pure oxygen.

2.1.2 Pre-Combustion

Pre-combustion systems generate a carbonless fuel-gas for the combustion. The production of the carbonless gas is possible through an Integrated-Gasification-Combined-Cycle (IGCC).
Coal gasfication processes use pure oxygen or steam as fumigators. As a result, the synthetic gas contains mostly CO and H_2. In the so-called *CO-shift* (equation 2.1), the CO is converted into CO_2 and H_2 by an exothermic reaction.

$$CO + H_2O \rightarrow CO_2 + H_2 \tag{2.1}$$

After the shift reaction the synthetic gas contains mainly CO_2 and H_2. The carbon dioxide is then captured by an absorption or adsorption process before the combustion of the synthetic gas. The processes scheme is shown in figure 2.2.
The advantage is that due to the high partial pressure of CO_2 in the synthetic gas the absorption is easy. Especially the adsorption process for the carbon capture is very attractive for this technology.
The additional process steps like the CO-shift and the carbon capture are widley developed in

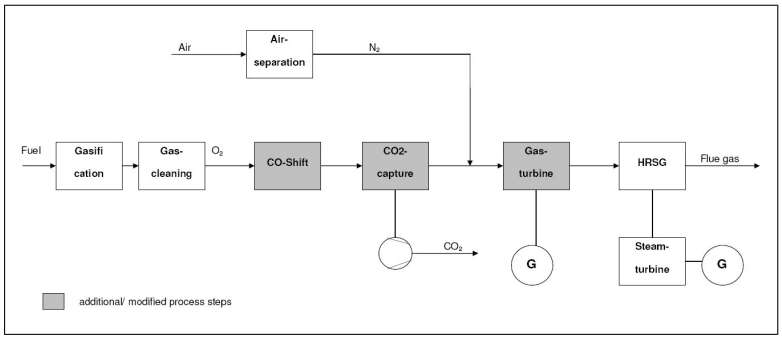

Fig. 2.2: Scheme of a pre-combustion process [10]

the petrochemical industry.
Nevertheless, there are no industrial realizations of this method at the moment.
Another problem is the necessary development of a hydrogen turbine, which is not available yet.
The advantages of this technology are:

- Industrial avialability of almost all components
- Lowest energy effort and costs for new power plants.

The main disadvantage is:

- the complexity of the IGCC-Process and high generation costs in the basic process without CCS.

Although, this process is seen to be the best option for new built power plants (lowest efficiency loss), there is no technical realization of this process yet.

2.1.3 Post-Combustion Capture

At Post Combustin Capture systems the CO_2 is separated at low concentrations/ partial pressure from the fluegas. The effort of capturing depends on the concentration of CO_2. Therefore, the power plant is just modified by a downstream process (cf. [11]). The basic configuration is given by figure 2.3. This method will be described in detail in section 2.4.1.

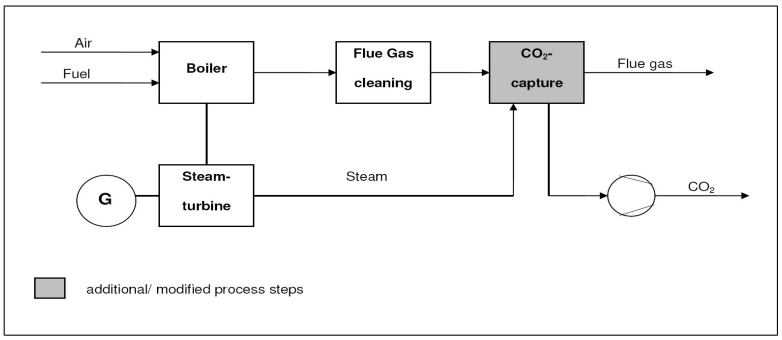

Fig. 2.3: Scheme of a post-combustion processes [10]

2.2 Transport

After the capture of the carbon dioxide, it has to be transported to a deposit. It can be transported in gaseous, liquid or solid state. The prefered aggregate state for transport is the subcooled liquid state at ambient temperature (see [12]).
The main options for the transport are:

- Pipelines,
- Ships,
- Trains,
- Lorries or
- Combination of all four options.

According to [11] the most reasonable ways are the transport by pipelines or by ships.
In Austria only the transport by pipelines seems reasonable.
Other countries like the United States of America for example have already realized a widely developed pipeline system and operate it sucessfully, since the oil industry uses CO_2 for generating higher pressure in the natural gas deposits.

The main disadvantage of pipeline transport is the pressure drop. Therfore, cost-intensive pressure increase stations will be necessary. The high pressure in the system is necessary to avoid two-phase flow because of the isothermal ambient conditions. This would cause material loss because of cavitation.

The phase diagramm of CO_2 is shown in figure 2.4. The minimal pressure for the liquid transport at 15°C is 50 bar (cf. [11]).

2.3 Storage

In this section the storage possibilities for liquid CO_2 are shortly mentioned.

2.3.1 Storage options

Various systems are considered as suitable for the carbon storage.
They are:

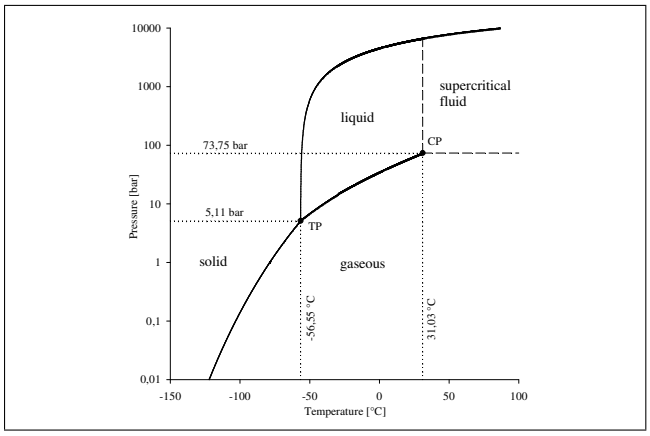

Fig. 2.4: CO_2 phase diagram

- **Depleted Oil and Gas fields:** onshore or offshore depleted oil and gas fields represent a possibility for the carbon dioxide storage with high capacities, for example in the EU (see [13]).

- **Deep saline aquifers:** These sedimentary rock formations are seen to have the greatest potential for the carbon dioxide storage (see [13]). Their porous and permeable structure allows the storage of great volumes of CO_2 and the flow of fluids.

- **Unmineable coal seems:** In Enhanced Coal Bed Methane projects the carbon dioxide is adsorbed by the coal and enhances the methane production. This option with its limited potential is in development, but gives another cheap opportunity for the carbon dioxide storage (cf. [13]).

- **Enhanced Oil or Gas Recovery (EOR):** are seen as an intermediate step. CO_2 is injected into mature oil or gas fields for improving the oil or gas recovery. It increases the production by 4-20%. This method is already operated in several large projects (cf. [13]). Besides, it must be mentioned that this method conduce to recovery and not primary to storage.

2.3.2 Situation in Austria

Primarily, exhaust oil and natural gas deposition could be used for carbon storage (cf. [11]). According to [14] the capacity of carbon storage in Austria is about 400 mio. tons. In the study by Heinemann [14] two locations for carbon storage in Austria were proposed:

- **Lower Austria:** Baumgarten-Schönkirchen, operated by OMV AG, with an estimated capacity of 60 mio. tons.

- **Upper Austria:** Atzbach-Schwanenstadt-Voitsdorf, operated by RAG, with an estimated capacity of 30 mio. tons.

2.4 PCC - Post Combustion Capture in general

In this section the PCC technology will be described more precisely.

2.4.1 Processes

Post-Combustion Capture systems have a large potential for existing energy systems.
The main advantages of this technology for carbon capture are:

- Simple adaption of the process for existing power plants
- Retrofit.

On the other hand, there are some disadvantages:

- Additional steam consumption of the regeneration step
- Loss of power and lower efficiency of the power plant
- High investment costs.

2.4.2 Outline

There are various processes which can be used for PCC systems. Figure 2.5 gives an overview of the different process, which could be used for the capture step. These are shortly explained in

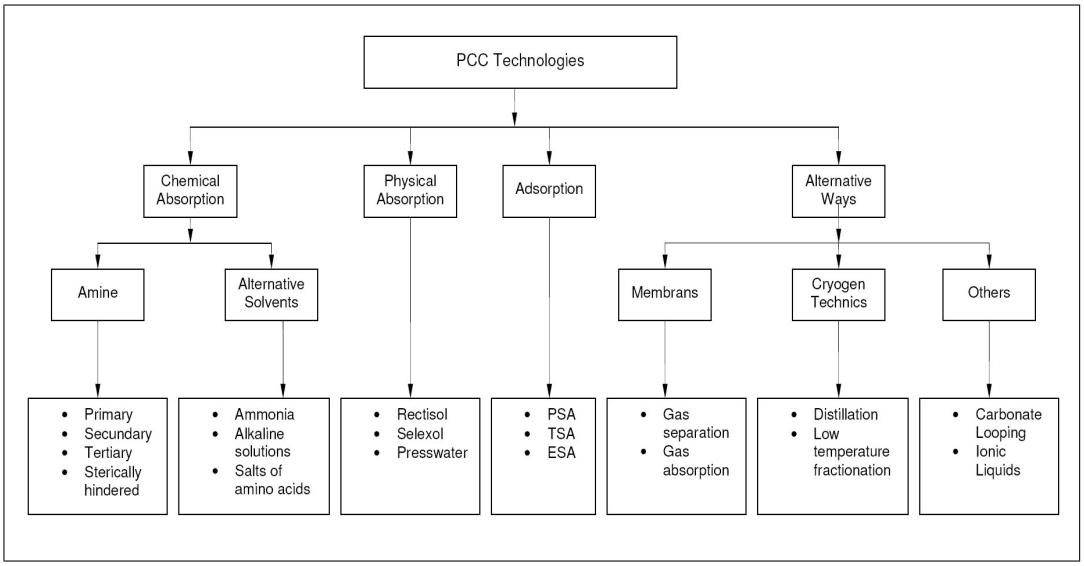

Fig. 2.5: Overview of post combustion capture processes (cf. [5])

the following.

2.4.3 Chemical absorption

In the chemical absorption the carbon dixiode is linked by a chemical reaction to the solvent. During the regeneration of the solvent the carbon dioxide is released. The regeneration is done by the use of energy (mostly steam).
This capture method must be used at low partial pressure of the separated component (solute).

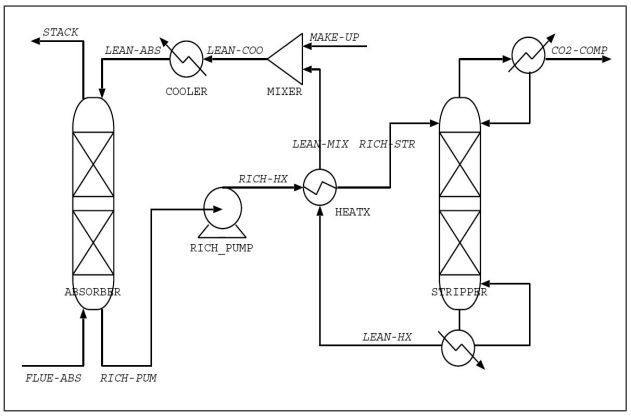

Fig. 2.6: Flow sheet of a chemical absorption process [15]

Technical description: In the process gaseous CO_2 is absorbed by a liquid washing solvent in countercurrent flow (CO_2 *Absorber* in figure 2.6). The absorption step runs at lower temperatures (exothermic reaction). Therefore, cooling systems for the flue gas are necessary.
After the absorption step the loaded solvent is regenerated at higher temperatures and pressures in the desorber/ stripper (endothermic reaction). The necessary heat exchanger, pumps and the CO_2 *Stripper* are shown in figure 2.6. In this step the carbon dioxide is separated from the washing solvent (cf. [11]).

2.4.4 Physical absorption

Here carbon dioxide is physically solved at higher pressure in a washing solvent. The physical absorption is used for gases at high pressure, for example natural or synthetic gas. The process is mostly run at pressures in the range of 20 to 160 bar and temperatures lower than 60°C.
The desorption of the CO_2 is executed by expanding the loaded solvent to atmospheric pressure. This method can only be used for highly concentrated gases (cf. [11]).

2.4.5 Adsorption

The adsorption process uses the ability of gases to accumulate at solid surfaces.

PSA - Pressure Swing Adsorption uses different adsorbents, like activated coal, to adsorb the CO_2 at high pressure out of the flue gas. Because of the compression there is a very high energy effort on this method. Thus, it can't be used for carbon capture.

TSA - Temperature Swing Adsorption is run at low temperatures (under 60°C). Here the regeneration of the adsorbent is done at a high temperature (about 200°C). This process could be a possiblity for CCS technologies. The main disadvantage of adsorption processes is the applicability only for low flow rates (cf. [11]).

2.4.6 Alternative ways

Membranes These separate the components because of their selective permeability in a thin coat and because of the pressure gradient. This method is used for the separation of low-molecular components out of a gas mixture. Because polymer membrans are used, gas temperatures lower than 100°C are necessary.

At the moment, the application of membranes in CCS technologies is limited to the separation of H_2 from the synthetic gas in IGCC systems than for carbon capture.

Cryogen techniques These express the separation of CO_2 by low temparture fractionation or direct freezing. Although, a carbon dioxide reduction of 100% would be possible, cryogen techniques have many disadvantages. Upstream drying for example would be necessary to avoid freezing of the cooling surface. Furthermore, wet CO_2 is corrosive and a high energy effort is necessary for the cooling system.

Others: *Chemical Looping Combustion (CLC) / Carbonate Looping* are expected to be capture methods with a very low efficiency loss. These processes use two fluidized beds and metal oxide (CLC) or lime (Carbonate Looping), which is circulated between them. Because the overall process is run at a high temperature (about 600°C) the whole energy effort is used for the generation of electricity.
Ionic liquids are salts with a melting temperature below the boiling point of water. Most ionic liquids have an organic cation and an inorganic anion. Besides, it should be mentioned that these substances have nearly no vapor pressure. These materials would fit perfectly for the absorption of acid gases like CO_2. The focus in the development of these liquids for chemical absorption is to achieve lower viscosities. Other disadvantages are the currently high costs and the low experience.

3 Chemical Absorption by MEA and CAP

In this section the chemical absorption by the chemical solvents monoethanolamine and aqueous ammonia and their theoretical background are going to be explained more detailed.

3.1 Thermodynamic equilibrium

The basic equations of the thermodynamic equilibrium of a reactive system are valid for the monoethanolamine solution and the aqueous ammonia.
Primary, two systems must be in thermal, mechanical and diffusive equilibrium to be said in thermodynamic equilibrium. These relations are declared by the equilibrium conditions.

3.1.1 Equilibrium conditions for a multi-component two phase system

The equilibrium conditions (equation (3.1)) have to be fulfilled in every phase of the system.

$$T^{'} = T^{''} = const \qquad p^{'} = p^{''} = const \qquad \mu_i^{'} = \mu_i^{''} = const \tag{3.1}$$

In other words, temperature, pressure and chemical potential of every individual component have to be equal in the phase. Figure 3.1 illustrates this correlation (cf. [16]).

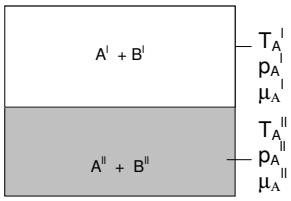

Fig. 3.1: Equilibrium conditions

3.1.2 Chemical equilibrium

The chemical equilibrium of a reactive system is described by the law of mass action (equation (3.3)). It depends on the concentrations of the components, whereas the equilibrium constant is a function of temperature and pressure.

$$\nu_A \cdot A + \nu_B \cdot B \overset{K}{\longleftrightarrow} \nu_C \cdot C + \nu_D \cdot D \tag{3.2}$$

$$K = \frac{[C]^{\nu_C} \cdot [D]^{\nu_D}}{[A]^{\nu_A} \cdot [B]^{\nu_B}} \tag{3.3}$$

Generally equation 3.3 can be written as

$$K = \frac{\Pi(z_{Products})^{\nu_{Product}}}{\Pi(z_{Educts})^{\nu_{educt}}} \tag{3.4}$$

where z represents either the concentration (like in equation 3.3), the activity a, the partial pressure p or the substance amount fraction x.

3.1.3 Dissociation Equilibrium

The mechanisms during chemical absorption are described by equilibrium constants.
Mainly there are two types of equilibria - chemical reaction dissociation equilibria (equation (3.6)), which are a special form of the chemical equilibrium, and vapour-liquid phase equilibria (3.36) - for molecular species used (cf. [17]).

Dissociation Equilibrium The dissociation equilibria for molecular electrolytes can be written as

$$K = \prod_i a_i^{\nu_i} \tag{3.5}$$

$$K = \Pi_i (x_i \gamma_i)^{\nu_i} \tag{3.6}$$

In terms of the reference state Gibbs free energy of the system, which is defined in section 3.2.1, the chemical equilibrium constant can be defined as (cf. [18])

$$lnK = -\frac{\Delta G^0}{RT} \tag{3.7}$$

The reference state for ionic species in various mixed solvent electrolyte systems is the ideal, infinitely dilute aqueous solution used. By choosing this standard/ reference state it is allowed to use equilibrium constants for reactions, which are reported in literature. Therefore, the solution is treated as a mixed solvent (cf. [17]).

3.2 Thermodynamic basics for mixtures

In the following the basic thermodynamic correlations for mixtures of gases and liquids are given.

3.2.1 Gibbs fundamental equation

The Gibbs Fundamental equation (equation (3.8)) expresses the free energy of a component as a function of its enthalpy, entropy and temperature.

$$G = U + PV - TS = H - TS \tag{3.8}$$

This equation is valid for homogenous closed systems. By partial derivation of the Gibbs function many important parameters of a system can be calculated (see table 3.1).

Tab. 3.1: Partial derivation of the Gibbs function

$(\frac{\partial G}{\partial p})_{T,n_i}$	$= V$
$(\frac{\partial G}{\partial T})_{p,n_i}$	$= -S$
$(\frac{\partial G}{\partial n_i})_{T,p,n_i \neq n_j}$	$= \mu(T,p,x_i)$
$-T^2 \cdot (\frac{\partial G/T}{\partial T})_{p,n_i}$	$= H$

For open homogenous systems the relation for the inner energy has to be extended by the chemical potential μ_i.

$$dG = \Sigma \mu_i \cdot dn_i + V dp - S dT \tag{3.9}$$

The chemical potential expresses the inner energy per mole of a component and is defined as follows.

$$\mu_i = [\frac{\partial U}{\partial n_i}]_{S,V,n_j \neq n_i} \tag{3.10}$$

3.2.2 Mixing Variables

A non-ideal mixture deviates from its ideal characteristics depending on the mole fraction of the components.
Therefore, mixing variables are defined as deviations of state variables (equation (3.11)). In the following equations the parameter d stands for any state variable.

$$\Delta d_{mix} = d - \Sigma(d_i x_i) \qquad \Delta D_{mix} = n\Delta d_{mix} \tag{3.11}$$

Those can also be defined by the use of partial molar variables (equations (3.12) - (3.13)).

$$\Delta d_{mix} = \Sigma[x_i(\overline{d_i} - d_i)] \tag{3.12}$$

$$\overline{d}_i = (\frac{\partial(nd)}{\partial n_i})_{T,p,n_j \neq n_i} \tag{3.13}$$

Ideal mixtures are defined as mixtures which have the same mixing behaviour as ideal gas mixtures.
The deviations from ideality are called excess variables for mixtures (equation (3.14)) and residual variables for gases. Because of the higher importance of the excess variables in solution processes like PCC only those are mentioned in the following (cf. [19]).

$$\Delta d_{mix} = d^E \tag{3.14}$$

Finally, the state variable of a non-ideal mixture can be written as the sum of the ideal and the excess variable (cf. [20]):

$$d = d^{IM} + d^E \tag{3.15}$$

3.3 Fundamental equations for interface equilibrium

The following equations describe the correlations at interface equilibrium, which are the basics for physical absorption. These equations are valid for vapour-liquid equilibria.

When a gas gets into contact with liquids, a certain amount of gas molecules will always be absorbed physically into the liquid. The amount depends on the physical solubility of the solvent. In a first approximation the physical solubility is proportional to the partial pressure of the gas (Henry's Law) and it is decreasing with rising temperature (cf. [21]).

3.3.1 Ideal behaviour

For ideal gases and liquids the following equations can be used to describe their physical characteristics.

Ideal Gas Law This equation of state (equation (3.16)) expresses the behaviour of an ideal gas (dilute and low pressure).

$$p \cdot V = n \cdot R \cdot T \tag{3.16}$$

Dalton's Law (equation (3.17)) describes the ideal partial pressure of component i in a gas mixture.

$$P = \sum_i^n p_i \qquad p_i = y_i \cdot P \tag{3.17}$$

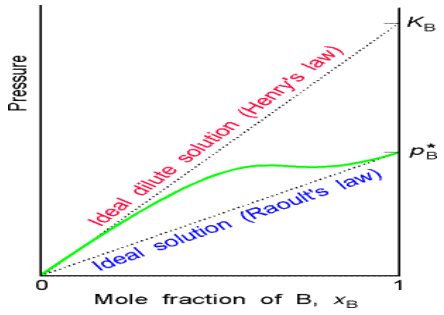

Fig. 3.2: Non-ideal systems - Henry's and Raoult's law

Raoult's Law (equation 3.18) expresses the vapour/ partial pressure of component i above a liquid mixture including i.

$$p_i = c_i \cdot p_i^0 \qquad\qquad p_i = x_i \cdot p_i^0 \tag{3.18}$$

Raoult's Law is valid for highly concentrated liquids (cf. [22]). It expresses the solubility of subcritical gases in a liquid at high mole fraction (≈ 1).

3.3.2 Non-ideal Behaviour

Henry's Law (equation (3.19)) describes the solubility of a gas into a liquid. This equation is valid for a low concentration in the gas and aqueous phase. In other words, Henry's law has to be used for dilute solutions and supercritical gases.

$$p_i = H_i \cdot x_i \qquad\qquad p_i = H_i \cdot a_i \tag{3.19}$$

The so called Henry's constant $H_i(T)$ is a function of temperature.
By the combination of Henry's and Dalton's law (equation (3.20)) a equilibrium constant m_i (equation (3.21)) is defined.

$$y_i \cdot P = H_i \cdot x_i \tag{3.20}$$

$$m_i = \frac{y_i}{x_i} = \frac{H_i}{P} \tag{3.21}$$

By the equilibrium constant m_i the minimal solvent flux for the physical absorption is fixed (cf. [23]).

$$\dot{L}_{min} = m_i \cdot \dot{G} \tag{3.22}$$

Raoult's Law For non-ideal mixtures Raoult's law is expressed by the following equation.

$$f_i = a_i \cdot f_i^0 \tag{3.23}$$

In this equation the liquid concentration and the partial pressure are replaced by activity and fugacity, which are introduced in the next paragraph.
Henry's law (equation (3.19)) and Raoult's law (equation (3.23)) have to be seen as border laws. The real behavior of a system is described by both laws. In fact, the real characteristics of the system are described by the activity coefficient. Henry's constant and the saturation vapour pressure can be seen as the limiting constants for the activity coefficient. This fact is illustrated by figure 3.2. The green line expresses the real behaviour of the system (cf. [16]).

Activity and Fugacity The activity a_i (equation (3.24)) of liquid and the fugacity f_i (equation (3.24)) of gas mixtures is the real thermodynamic concentration in a liquid resp. the real thermodynamic partial pressure of a gas phase.
They are calculated from ideal characteristics by using their coefficients (cf. [20]).

$$a_i = \gamma_i \cdot x_i \qquad f_i = \varphi_i \cdot p_i \tag{3.24}$$

Activity and Fugacy coefficient method describes the vapour pressure above a real liquid mixture.
The fugacy coefficient φ_i (equation (3.25)) stands for the non-ideality of a gas. For technical gases at pressures lower than 5 bar it can be set to one ($\varphi_i = 1$). The reason is that gases at a low pressure can be handled as ideal gases (cf. [16]).
The activity coefficient γ_i (equation (3.26)) describes the deviation of real mixtures from ideality. Further, it is a measurement for the interaction between the components. For a pure component the activity coefficient is one.

$$\varphi_i \cdot p_i = \gamma_i \cdot x_i \cdot f_i^0 \tag{3.25}$$

In the equation above $\varphi_i = 1$ was set under the assumption of low pressures.

$$p_i = \gamma_i \cdot x_i \cdot f_i^0 \tag{3.26}$$

For high concentrations the activity coefficient is approximately constant. For average concentrations the activity coefficient has to be calculated by correlation models (see section 4.3).
Combined with Daltons law, equation (3.25), can also be written as:

$$\varphi_i \cdot y_i \cdot P = \gamma_i \cdot x_i \cdot f_i^0 \tag{3.27}$$

Finally, the correlations at interface equilibrium in technical systems with low pressure can be written as:

$$y_i \cdot P = \gamma_i \cdot x_i \cdot f_i^0 \tag{3.28}$$

As a result, the concentration of a component in the gas or aqueous phase depends just on the saturation vapour pressure f_i^0 (at high concentrations) or the Henry's constant (at low concentrations) and between the activity coefficient depending on the mole fraction $\gamma_i = f(x_i)$.

The temperature dependent saturation vapour pressure and Henry's constant are calculated by correlation models with adjustment parameters, for example the saturation vapour pressure by the Antione equation (equation (3.29)). The calculation of the Henry's constant is given in section 4.4.1. The calculation of the needed activity coefficent is explained in the following.

$$log f_i^0 = A_i - \frac{B_i}{C_i + T} \tag{3.29}$$

Calculation of the activity coefficient The activity coefficient calculation is based on the partial molar free excess enthalpy or partial molar excess Gibbs energy ($\overline{g}_i = \mu_i$).
The excess function (equation (3.30)) expresses the deviation from ideality. These deviations depend mainly on concentrations of components and on temperature. It can be defined by terms of concentrations and temperature-dependent coefficients (cf. [20]).

$$\overline{g}_i^E = \overline{g}_i - \overline{g}_i^{IM} = RT \cdot ln \frac{f_i}{f_i^{IM}} \tag{3.30}$$

In connection with Raoult's law (equation (3.23)) the fugacy can be written as:

$$f_i = x_i \gamma_i f_i^0 \tag{3.31}$$

for the real liquid and as

$$f_i^{IM} = x_i \cdot f_i^0 \tag{3.32}$$

for the ideal mixture.
These equations combined define the activity coefficient as a function of the partial molar free excess enthalpy (equations (3.33) and (3.34)).

$$\overline{g}_i^E = \overline{g}_i - \overline{g}_i^{IM} = RT \cdot ln \frac{f_i}{f_i^{IM}} = RT \cdot ln\gamma_i \tag{3.33}$$

$$ln\gamma_i = [\frac{\overline{g}_i^E}{RT}] \tag{3.34}$$

The partial molar excess Gibbs energy is derived from the excess Gibbs energy. Therefore, the relation of the activity coefficient and the excess Gibbs energy can be expressed in equation (3.35).

$$ln\gamma_i = [\frac{\partial(nG^E/RT)}{\partial n_i}]_{T,P,n_{j\neq i}} \tag{3.35}$$

This equation expresses the activity coefficient as function of the temperature, pressure and moles.

3.3.3 Vapour-Liquid Equilibria

The distribution of molecular species between the vapour and liquid phases is specified by the phase equilibria for the system at infinite dilution (cf. [17]). The calculation of the vapour phase composition is based on the extended Henry's law for the solute (CO_2):

$$y_i \varphi_i P = x_i \gamma_i H_i^{p0} exp(\frac{v_i^\infty (P - P^0)}{RT}) \tag{3.36}$$

In this equation H_i^{p0} and ν_i^∞ represent Henry's constant and partial molar volume at infinite dilution for molecular solute i in pure water at the system temperature (see [17]).
The partial molar volumes must be calculated by correlations, for example the correlation of Brelvi and O'Connell (1972) (cf. [17]).
Equation (3.36) determines the equilibrium between the vapour and liquid phases for supercritical species like CO_2 and N_2(cf. [18]).

For the pure components water and alkanolamine the vapour-liquid equilibria is given by

$$y_s \varphi_s P = x_s \gamma_s P_s^0 \varphi_s^0 exp(\frac{v_s (P - P_s^0)}{RT}). \tag{3.37}$$

This extension of the Raoult's Law is used for the solvents (H_2O, MEA, NH_3). The indices s declares the solvent species at the system temperature and saturation pressure. In this work, these mainly are the pure components H_2O and $MEA/\ NH_3$.
This equation is generally valid for non supercritical components.

The term $exp(\frac{v_i^\infty (P-P^0)}{RT})$ in the equations above represents the Poynting correction factor. It expresses the compression of the liquid phase at a pressure increase from P^0 to P.

3.4 Chemistry of Carbon Dioxide Absorption

3.4.1 Monoethanolamine

Equilibrium Reactions During the chemical absorption various reactions proceed. The main reaction mechanisms of the capture process are the formations of carbamate ($RNCHOO^-$) and bicarbonate (HCO_3^-).
The following equilibrium reactions (equations (3.38) - (3.42)) can be described as chemical dissociation.
Ionization of water

$$2H_2O \leftrightarrow H_3O^+ + OH^- \tag{3.38}$$

Dissociation of carbon dioxide

$$2H_2O + CO_2 \leftrightarrow H_3O^+ + HCO_3^- \tag{3.39}$$

Dissociation of bicarbonate

$$H_2O + HCO_3^- \leftrightarrow H_3O^+ + CO_3^{2-} \tag{3.40}$$

Dissociation of protonated monoethanolamine

$$H_2O + HOC_2H_4NH^+ \leftrightarrow H_3O^+ + HOC_2H_4N \tag{3.41}$$

Carbamate reversion to bicarbonate

$$HOC_2H_4NHCOO^- + H_2O \leftrightarrow HOC_2H_4NH_2 + HCO_3^- \tag{3.42}$$

The carbon capture step is in the formation of bicarbonate (reaction (3.39)) and carbamate (reaction (3.42)). These reactions of alkanolamines in aqueous solutions follow an acid-base buffer mechanism (cf. [17]).

Thermodynamic Equilibria By the law of mass action the following equilibrium constants of chemical reactions can be defined.

$$K_1 = \frac{[H_3O^+]^1 \cdot [HCO_3^-]^1}{[H_2O]^2 \cdot [CO_2]^1} \tag{3.43}$$

$$K_2 = \frac{[H_3O^+]^1 \cdot [CO_3^{2-}]^1}{[H_2O]^1 \cdot [HCO_3^-]^1} \tag{3.44}$$

$$K_3 = \frac{[H_3O^+]^1 \cdot [HOC_2H_4N]^1}{[H_2O]^1 \cdot [HOC_2H_4NH^+]^1} \tag{3.45}$$

$$K_4 = \frac{[HOC_2H_4NH_2]^1 \cdot [HCO_3^-]^1}{[HOC_2H_4NHCOO^-]^1 \cdot [H_2O]^1} \tag{3.46}$$

The dissociation equilibria of water:

$$K_w = [H_3O^+] \cdot [OH^-] \tag{3.47}$$

3.4.2 Aqueous Ammonia

Equilibrium Reactions The following equilibrium reactions are considered in the $CO_2 - NH_3 - H_2O$ system, according to [24].
The reaction mechanisms are classified in three equilibria types:
Vapour-liquid equilibria

$$CO_{2(g)} \leftrightarrow CO_{2(aq)} \tag{3.48}$$

$$NH_{3(g)} \leftrightarrow NH_{3(ag)} \tag{3.49}$$

$$H_2O_{(g)} \leftrightarrow H_2O_{(l)} \tag{3.50}$$

Speciation equilibria

$$NH_{3(aq)} + H_2O \leftrightarrow NH_4^+ + OH^- \tag{3.51}$$

$$CO_{2(aq)} + 2H_2O_{(l)} \leftrightarrow HCO_3^- + H_3O^+ \tag{3.52}$$

$$HCO_3^- + H_2O \leftrightarrow CO_3^{2-} + H_3O^+ \tag{3.53}$$

$$2H_2O_{(l)} \leftrightarrow H_3O^+ + OH^- \tag{3.54}$$

$$NH_{3(aq)} + HCO_3^- \leftrightarrow NH_2COO^- + H_2O_{(l)} \tag{3.55}$$

Liquid-solid equilibria

$$NH_4^+ + HCO_3^- \leftrightarrow NH_4HCO_{3(s)} \tag{3.56}$$

$$NH_4^+ + NH_2COO^- \leftrightarrow NH_2COONH_{4(s)} \tag{3.57}$$

$$2NH_4^+ + CO_3^{2-} + H_2O \leftrightarrow (NH_4)_2CO_3 \cdot H_2O_{(s)} \tag{3.58}$$

$$4NH_4^+ + CO_3^{2-} + 2HCO_3^- \leftrightarrow (NH_4)_2CO_3 \cdot 2NH_4HCO_{3(s)} \tag{3.59}$$

Reactions (3.55) and (3.56) describe the carbon dioxide capture step in the absorber.
In this reactive system solids are also formed at lower temperatures (mainly expressed by reaction (3.56)).

Thermodynamic Equilibria For the reactions (3.51) - (3.59) the following equilibrium constants can be declared.

$$K_1 = \frac{[NH_4^+] \cdot [OH^-]}{[NH_3] \cdot [H_2O]} \tag{3.60}$$

$$K_2 = \frac{[H_3O^+] \cdot [HCO_3^-]}{[CO_2] \cdot [H_2O]^2} \tag{3.61}$$

$$K_3 = \frac{[H_3O^+] \cdot [CO_3^{2-}]}{[HCO_3^-] \cdot [H_2O]} \tag{3.62}$$

$$K_4 = \frac{[H_3O^+] \cdot [OH^-]}{[H_2O]^2} \tag{3.63}$$

$$K_5 = \frac{[NH_2COO^-] \cdot [H_2O_{(l)}]}{[NH_{3(aq)}] \cdot [HCO_3^-]} \tag{3.64}$$

For the salt precipitation the following dissolution constants are defined:

$$K_6 = \frac{[NH_4HCO_{3(s)}]}{[NH_4^+] \cdot [HCO_3^-]} \tag{3.65}$$

$$K_7 = \frac{[NH_2COONH_{4(s)}]}{[NH_4^+] \cdot [NH_2COO^-]} \tag{3.66}$$

$$K_8 = \frac{[(NH_4)_2CO_3 \cdot H_2O_{(s)}]}{[NH_4^+]^2 \cdot [CO_3^{2-}] \cdot [H_2O]} \tag{3.67}$$

$$K_9 = \frac{[(NH_4)_2CO_{3(s)}] \cdot [NH_4HCO_{3(s)}]^2}{[NH_4^+]^4 \cdot [CO_3^{2-}] \cdot [HCO_3^-]^2} \tag{3.68}$$

3.5 Mass Transfer Models

3.5.1 Mass Transfer Rate - Film Theory

The stationary mass transfer due to diffusion is described by Fick's Law (3.69).

$$\dot{N}_i = D_i \cdot A \cdot (\frac{\partial c_i}{\partial \delta_i}) \tag{3.69}$$

Whereas, the mass transfer (3.70) from an interface area into a fluid phase is expressed by a mass transfer coefficient (β_i).

$$\dot{N}_i = \beta_i \cdot A \cdot \Delta c_i \tag{3.70}$$

Two Film Theory - Rate Based Physical Absorption In this model the component i is transported to the interface because of a concentration gradient between the bulk gas phase and the gas side film, which is seen as laminar. Then the component is solved in the liquid phase and diffuses in it (see figure 3.3).

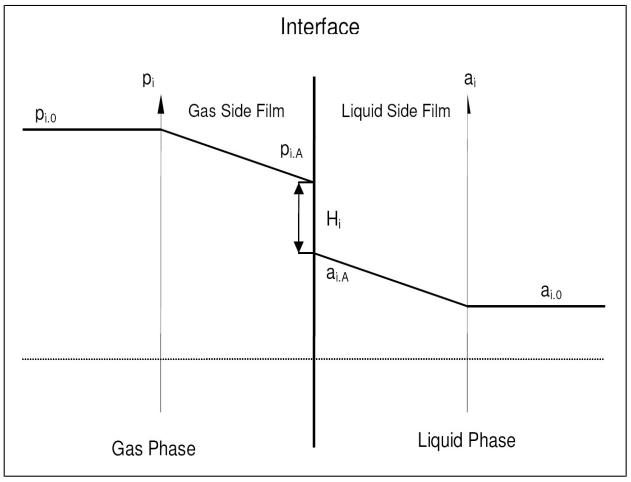

Fig. 3.3: Concentration profile in the two film theory

The interface is seen to be in equilibrium.

$$\dot{n}_i = \beta^g_{i,0} \cdot \frac{(p_{i,0} - p_{i,A})}{RT} = \beta^l_{i,0} \cdot (a_{i,A} - a_{i,0}) \tag{3.71}$$

Since a steady state is assumed the mass flux in the liquid and gas phase are equal. This leads to

$$\frac{\beta^l_{i,0}}{\beta^g_{i,0}} = \frac{(p_{i,0} - p_{i,A})/RT}{a_{i,A} - a_{i,0}} \tag{3.72}$$

$$a_{i,A} = a_{i,0} + \frac{\dot{n}_i}{\beta^l_{i,0}} \qquad\qquad p_{i,A} = p_{i,0} - \frac{\dot{n}_i \cdot RT}{\beta^g_{i,0}} \tag{3.73}$$

As a result, the interface concentration $a_{i,A}$ and the interface partial pressure $p_{i,A}$ cannot be calculated from this equation or barely measured.

Whereas, the relation between gas phase partial pressure and liquid phase concentration at the interface (equilibrium assumed, because of slow composition change resulting from diffusion) can be defined by Henry's Law.

$$p_{i,A} = H \cdot a_{i,A} \tag{3.74}$$

Equation (3.73) combined with Herny's Law (3.74) result in the next expression.

$$a_{i,A} = \frac{p_{i,A}}{H_i} = a_{i,0} + \frac{\dot{n}_i}{\beta^l_{i,0}} \tag{3.75}$$

By multipling Herny's constant, the partial pressure at the interface can be written in the following way.

$$p_{i,A} = a_{i,0} \cdot H_i + \frac{H_i \cdot \dot{n}_i}{\beta^l_{i,0}} \tag{3.76}$$

The only unknown variable in this equation is the mole flux, since the liquid bulk concentration can be seen as pre-given. Equation (3.76) was substituted into equation (3.73) to calculate the mole flux.

$$p_{i,0} - \frac{\dot{n}_i \cdot RT}{\beta^g_{i,0}} = a_{i,0} \cdot H_i + \frac{H_i \cdot \dot{n}_i}{\beta^l_{i,0}} \tag{3.77}$$

Finally, the mole flux from one phase into another could be expressed depending only on the bulk partial pressure and concentration, which had to be corrected by the ideal gas law.

$$\dot{n}_i = K_{o,g} \cdot (p_{i,0} - a_{i,0} \cdot H_i) \tag{3.78}$$

The overall mass transfer resistence between both phases is given as two serial resistence corrected by an equilibrium constant (Henry's constant).

$$\frac{1}{K_{o,g}} = \frac{H_i}{\beta^l_{i,0}} + \frac{RT}{\beta^g_{i,0}} \tag{3.79}$$

3.5.2 Mass Transfer with Chemical Reaction

The rate of reaction in the liquid phase r_{CO_2} is expressed in the following equation.

$$r_{CO_2} = k \cdot [CO_2] \cdot [NH_3] \qquad or \qquad r_{CO_2} = k \cdot [CO_2][MEA] \tag{3.80}$$

k is the second order rate constant (cf. [25]).

Tab. 3.2: Classification by Hatta number

$Ha < 0.02$	very low reaction rate
$0.02 < Ha < 0.3$	low reaction rate
$0.3 < Ha < 3$	average reaction rate
$3 < Ha << E_i$	high reaction rate
$E_i << Ha$	instantaneous reaction - very high reaction rate

Rate Enhancement Factor The rate enhancement factor E expresses the increase in mass transfer by chemical absorption compared to physical absorption.

$$\dot{N}_i = \beta^l \cdot (a_{i,A} - a_{i,0}) = E \cdot \beta_0^l \cdot (a_{i,A} - a_{i,0}) \tag{3.81}$$

The rate enhancement factor is defined by the reaction conditions. The faster and completer a reaction takes place, the more increases the enhancement factor and therefore the mass transfer.

$$E = \frac{\dot{N}_i}{\beta_0^l \cdot (a_{i,A} - a_{i,0})} = \frac{\dot{N}_i^{Overall}}{\dot{N}_i^{Diff}} \tag{3.82}$$

In other words, it is the ratio of rate of mass transfer in the presence of chemical reaction to the rate of mass transfer without chemical reaction (cf. [26]).
Some border cases can be defined:

- $E << 1$: The mass transfer is only carried out by physical absorption
- $E >> 1$: The mass transfer is dominated by the chemical reactions.

Hatta Number This dimensionless number compares the reaction rate of chemical absorption (r_{iA0}) to the reaction rate of physical absorpion ($r_{A0}{}^{phys}$). In other words, it is the ratio of the maximum mass transfer by chemical reactions compared to the maxium mass transfer based on diffusion.

$$Ha = \frac{r_{iA0}}{r_{A0}{}^{phys}} \approx \frac{\beta^l}{\beta_0^l} \tag{3.83}$$

According to [27] the Hatta number for a second order reaction can be calculated by the next correlation.

$$Ha = \frac{\sqrt{k_2 \cdot c_A \cdot D_i}}{\beta_0^l} \tag{3.84}$$

The connection between the Hatta number and the Enhancement factor is given by the following equation.

$$E = \frac{Ha}{\tanh Ha} \tag{3.85}$$

Furthermore, the Hatta number is a measurement for the reaction rate. The maximum value of Ha is achieved at an instantaneous reaction (cf. [23]).
By using the Hatta number different reaction regimes can be classified (see table 3.2).

HTU-NTU Concept The HTU (Height of Transfer Unit) - NTU (Number of Transfer Units) model is valid for one way mass transfer. This theory is based on a mass balance of an infinite volume with the height dz.
The transfered mole flow between the liquid and the gaseous phase matches the change in the loading of both phases.

$$d\,\dot{N}_i = \dot{G}_T \cdot dY = \dot{L}_T \cdot dX \tag{3.86}$$

The transfered mole flow can be expressed by the two film theory in the following way.

$$d\,\dot{N}_i = \dot{G}_T \cdot dY = \bar{\varrho}_g \cdot K_{o,g} \cdot (Y - Y^*) \cdot dA \tag{3.87}$$

The driving force dY is determined by the difference to the equilibrium loading Y^*. The related mass transfer area dA depends on the degree of wetting φ', which is the ratio between the wetted surface and the theoretical surface, the specific area of the packing a, the cross section of the column A_q and the differential height dz.

$$dA = \varphi' \cdot a \cdot A_q \cdot dz \tag{3.88}$$

This results in the following differential equation.

$$\dot{G}_T \cdot dY = \bar{\varrho}_g \cdot K_{o,g} \cdot (Y - Y^*) \cdot \varphi' \cdot a \cdot A_q \cdot dz \tag{3.89}$$

By separation of the variables and solving the integral $\int_0^H dz = H$, the height of the absorption column can be calculated.

$$H = \frac{\dot{G}_T}{K_{o,g} \cdot \varphi' \cdot a \cdot A_q \cdot \bar{\varrho}_g} \cdot \int_{Y_a}^{Y_e} \frac{dY}{Y - Y^*} = HTU_{o,g} \cdot NTU_{o,g} \tag{3.90}$$

The first term in equation (3.90) is the HTU and the second one the NTU value.

3.6 Washing solvents

In this section the basic requirements for washing solvents are declared. Afterwards, the selected solvents (MEA and Aqueous Ammonia) are discussed more detailed.

For the washing solvents of a chemical absorption process some requirements have to be met (cf. [5]). For solvents of a capture process these should be:

- Adequate solubility of gaseous component in the liquid phase
- High selectivity
- Adequate regeneration ability (Low regeneration heat duty)
- High mass specific loading of the solvent
- High reactivity
- Low thermal and oxidative degradation
- Low vapour pressure at absorption temperature
- Low viscosity
- Low corrosivity

- No toxicity
- Low costs.

For real washing solvents a compromise must be made.
Above all, the regeneration heat duty and the reactivity have a strong impact on the economic efficiency of the process. The regeneration heat is related to the steam consumption of the process and the reactivity to the absorber and desorber height.

3.6.1 Monoethanolamine

Monoethanolamine is an alkaline solvent with a strong chemical affinity to acid gases. Chemically seen, it is a primary amine and a weak base. Therefore, it forms a more stable carbamate than a secondary amine. In figure 3.4 the molecular structure of monoethanolamine is shown.
Monoethanolamine is already in use (e.g.: natural gas conditioning). For the absorption process of carbon dioxide from flue gas an approximately 30wt% aqueous solution of MEA is used (cf. [28]). The main properties of MEA are summerized in table 3.3. Additionaly, it must be mentioned, that MEA solutions start to polymerise at temperature of 125°C and pressure of 2.1 bar in the presence of carbon dioxide. This is a primary limiting factor for the conditions of the regeneration step.
The corrosive characteristics of the MEA solution depend on the concentration of aqueous MEA.

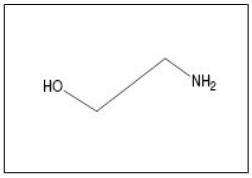

Fig. 3.4: Molecular structure of monoethanolamine

In the process the lean solvent has a typical loading of 0.1-0.15 mol CO_2/ mol MEA. Whereas, the rich solvent has a loading of 0.4 to 0.5. The maximum loading ($molCO_2$) of MEA is in the range between 0.5 to 0.6 mol CO_2/mol MEA. This follows from the carbamate reaction (see reaction (3.42): MEA + $HCO_3^- \rightarrow MEACOO^- + H_2O$), which defines the chemical absorption, and the formation of MEA^+ (see reaction (3.41)). It is obvious, that 1 mol MEA can only take 0.5 mol CO_2, since during the bicarbonate reaction (reaction (3.39): $2H_2O + CO_2 \rightarrow HCO_3^- + H_3O^+$) bicarbonate and H_3O^+ are formed, which both react with MEA to $MEACOO^-$ and MEA^+. In other words, for 1 mol CO_2 1 mol $MEACOO^-$ and 1 mol MEA^+ are formed, therefore 2 mol MEA can only take 1 mol CO_2.
Further, there are three main possibilities for the MEA degradation. These are:

- **Thermal degradation** is promoted by elevated pressure and temperature, since the rate of formation of these degradation products depends on temperature, CO_2 loading and MEA concentration [29]. These mechanism leads to higher solvent loss.
- **Oxidative degradation** takes place in the presence of oxygen and therefore in the absorber. It leads to fragmentation of the MEA, which results in solvent loss and internal corrosion from the degradation products. This has a negative effect on the overall process performance and process economics [30]. Besides, these degradation products form heat stable salts (HSS) with monoethanolamine. Some of those HSS can be regenerated by adding sodium hydroxide (NaOH) at higher temperatures in the so called reclaimer (for more details see [5]).

Tab. 3.3: MEA properties

Molecular Formula	C_2H_7NO	-
Molecular Weight	61.08	[g/mol]
Melting Temperature	10.5	[°C]
Boiling Temperature	171	[°C]
Density at 20°C	1.02	$[g/cm^3]$
Vapour Pressure at 20°C	0.5	[hPa]
Thermal Degradiation	205	[°C]

- **Degradation by sulfur and nitrogen oxides** In higher concentrations SO_x and NO_x can foul MEA [31].

According to [31] a MEA based process must obtain limits for SO_x and NO_x under 10 and 20 ppm. It should be mentioned that those limits are lower than the regulatory requirement (cf. [5]).

Summarized, the main advantages of MEA as a chemical solvent are:

- High reaction rate
- Industrial experience.

Whereas, the disadvantages are:

- High regeneration energy
- The reagent degrades in oxygen environment
- Degradiation of the solvent by SO_x and NO_x
- The solvent is highly corrosive
- Expensive compared to ammonia (cf. [5]).

3.6.2 Aqueous Ammonia

Ammonia is a weak base with also a strong chemical affinity to acid gases. Its molecular structure is illustrated in figure 3.5. It is widley spread in industrial systems (e.g.: denitrification).

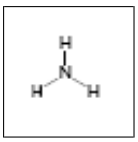

Fig. 3.5: Molecular structure of ammonia

Hence, it is produced in a large scale by the Haber-Bosch synthesis, it is cheap. Ammonia is colourless and attacks the mucous membrane at a concentration of 100 ppm and is therefore toxic. According to the acid-base metabolism, salts are formed in presence of acid gases. These dissociate at higher temperatures. Further, it is flammable (cf. [32]).
For the capture process solutions with 5-30wt% aqueous ammonia are used. One of the main differences to MEA is the coagulation of solids (ammonium bicarbonate), which are formed during the capture process. But at temperatures over 80°C ammonium bicarbonate is completely

dissolved (cf. [5]).
The main properties of ammonia are summerised in table 3.4.
The maximum mole ratio of NH_3/CO_2 is in the range of 1.0 to 4.0, according to [7]. This

Tab. 3.4: Ammonia properties

Molecular Formula	NH_3	-
Molecular Weight	17.03	[g/mol]
Melting Temperature	-77.7	[°C]
Boiling Temperature	-33	[°C]
Density at 0°C and 4.294 bar	0.639	$[kg/m^3]$
Vapour Pressure at 0°C	8573	[hPa]

cooresponds to mole loadings between 0.2 mol and 1.0 [CO_2/ mol NH_3], which can be achieved. The loading of the lean solvent is between 0.33 - 0.67 [mol CO_2/mol NH_3] and between 0.67 - 1 [mol CO_2/mol NH_3] for the rich aqueous ammonia solution (cf. [33]). The high loadings are achieved, since during the capture step one mole of ammonia is able to bond one mole carbon dioxide (see reaction (3.55): $NH_3 + HCO_3^- \rightarrow NH_2COO^- + H_2O$).
The main degradation products of NH_3 are ammonium sulfate or ammonium nitrate, which can be used as fertilizers [31].
The primary advantages are:

- Higher concentration gradient between liquid and gaseous phase because of the coagulation of solids
- Lower energy demand in the reboiler
- Lower corrosivity of the reagent
- Lower degradiation of the solvent by oxygen.

The main disadvantages of aqueous ammonia are:

- Deposits in the absorber and in heat exchangers because of the coagulation of solids at temperatures below 80°C
- High vapour pressure of ammonia leads to high ammonia slip
- High pressure for the regeneration, which can be seen as a disadvantage for the steam extraction, whereas it is an advantage for the carbon dioxide compression
- Lower pump ability because of higher viscosity (cf. [5])
- Toxicity.

3.7 Overall Process

In this section the overall process is shortly explained.
For both processes an upstream wet desulphurization system is assumed.

3.7.1 Monoethanolamine Process

Figure 3.6 illustrates a simplified Carbon Capture process based on chemical absorption by MEA.

The cooled flue gas and the cool lean solution enter the absorber in countercurrent flow. As the chemical solvent flows downward the CO_2 is absorbed.
In the washing section the vaporized monoethanolamine is captured. The circulating wash water is cooled to keep a neutral water balance. According to [34] a reflux of 3 % from the washing section to the absorber can be assumed. Make up water must be provided to avoid the build-up of solvent concentration. In this case, it is provided by recycling the condensate from the desorber overhead condenser.
The rich solvent exits the absorber bottom and is partially filtered to avoid soilds. The rich-lean heat exchanger transfers the sensible heat of the lean solvent to the rich solvent.
In the desorber the pre-heated solvent is regenerated. The overhead product of the desorber consists mainly of CO_2 and H_2O. It flows to a partial condenser, where the water is condensed. The remaining carbon dioxide stream flows to the compressor section. The desorber pressure is set in the range of 1 and 2.1 bar, according to [5]. The heat for the desorption of the CO_2 is provided by a reboiler. The reboiler is feed with condensing LP steam from the power plant (cf. [34]). In the reboiler the solvent is heat up to temperatures between 100 and 130°C depending on the desorber pressure.
The energy effort in the reboiler for the regeneration of the solvent consists of three contributions:

1. The thermal energy to separate the solute (CO_2) from the solvent
2. The latent heat of vaporisation to generate steam
3. The sensible heat to warm up the entering solvent to the temperature of the desorber (cf. [5]).

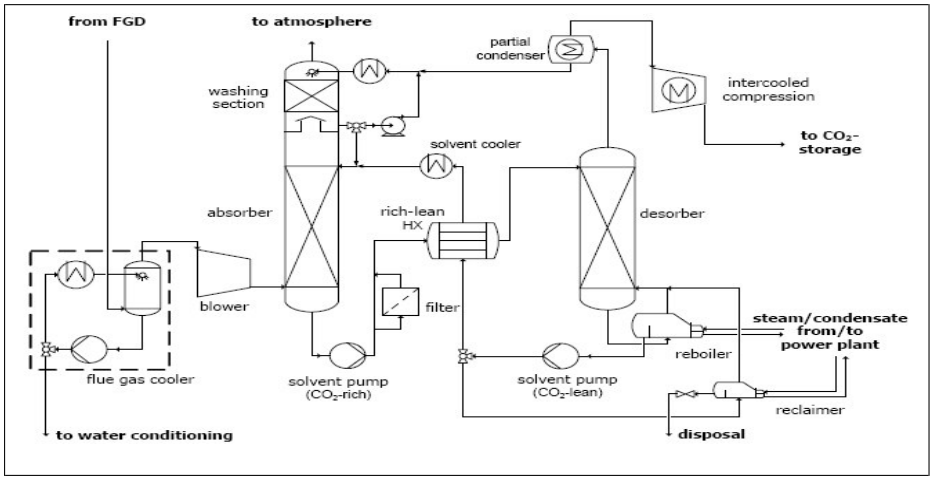

Fig. 3.6: Simplified flow sheet of the Monoethanolamine Process, [34]

The regeneration energy for MEA is in a range between 3.25 to 4 GJ/tCO_2 (cf. [5]). It depends on the ratio of solvent to gas and the desorber pressure (cf. [5]).
In the reclaimer the solvent is heated up to destroy formed salts and degradation products. Afterwards, the vapour solvent enters the desober.

3.7.2 Chilled Ammonia Process

The Chilled Ammonia Process is illustrated in figure 3.7. The capture process mainly consists of 4 subsystems:

- Gas cooling and cleaning
- Carbon dioxide absorption
- CO_2 Regeneration (Desorption)
- Treated flue gas and regenerated CO_2 wash.

The flue gas (red line) cooling is achieved by the cooling column and the dry cooler, where it is cooled down to apporximately 10°C. Hence the condensation of water, a booster fan is necessary (pressure loss).
In the absorption section the flow enters the absorption column at a temperature range of 0-20°C (according to [7]), where it encounters the lean solution (brown line). The rich solution (lime line) is chilled to counteract the exothermic reaction of the chemical absorption and to keep a moderate quantity of solid ammonium bicarbonate precipitating. Moreover, the low temperature is necessary because of the low vapour pressure. In the heat exchanger the rich solvent is heated up to the temperature range of 50-200°C (according to [7]), so that the precipitated salt dissolves, before it enters the desorber.
In the desorption column the washing solvent is regenerated at high pressure (2-140 bar, according to [7]). The sensible enthalpy, the reaction enthalpy and the enthalpy for the evaporation of water in the column are provided by an external reboiler fed with higher pressure steam.
In the washing section, the treated flue gas leaving the absorption column is washed with water (blue line) to minimize the ammonia slip to the atmosphere. The regenerated carbon dioxide is also washed to recover the ammonia from the vapour phase. Afterwards the carbon dioxide (green line) enters the compression subsystem (cf. [35]).

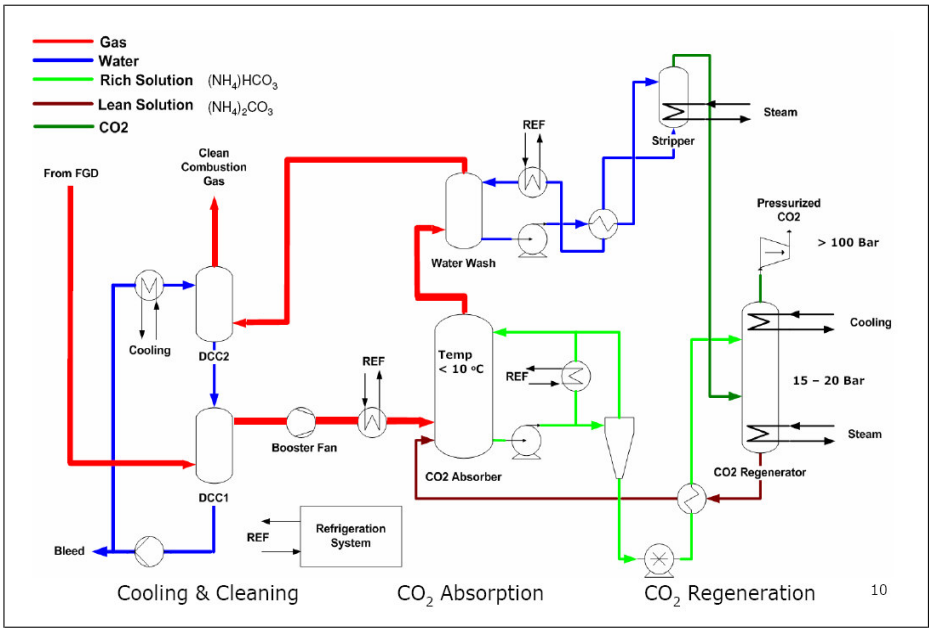

Fig. 3.7: Simplified flow sheet of the Chilled Ammonia Process

The main difference to the MEA process is the higher pressure and the lower temperature, because of the high vapour pressure of ammonia, to minimize the ammonia slip. Additionally, water washers are necessary, which bring higher investment and operating costs. Also cooling systems are needed. In contrast, lower temperatures and condensation result in lower flow rates (cf. [5]).
Besides, the CAP has a potential for selling the by-products, especially ammonium sulfate and ammonium nitrate as fertilizer (for more details see [31]).

4 Simulation Tool - Aspen Plus^{TM}

4.1 Configuration of ASPEN Plus^{TM}

ASPEN Plus^{TM} (**A**dvanced **S**ystem for **P**rocess **En**gineering) is a flowsheeting/ process simulation tool, which is used to quantitatively model the characteristic equations of a chemical process. The following equations can be solved:

- Coupled mass and energy balances
- Equilibrium relationships
- Rate correlations (reaction, mass-/ heat transfer).

These informations are used to predict stream flow rates, compositions, properties, operation conditions and equipment size. In ASPEN Plus^{TM} only steady state simulations, continuous processes at constant conditions, can be done. For a dynamic simulation programs like *ASPEN-dynamics*^{TM} are necessary.
In this work only steady state simulation is considered.

The structure of the ASPEN^{TM} software package and the relations between its subprograms are shown in figure 4.1.

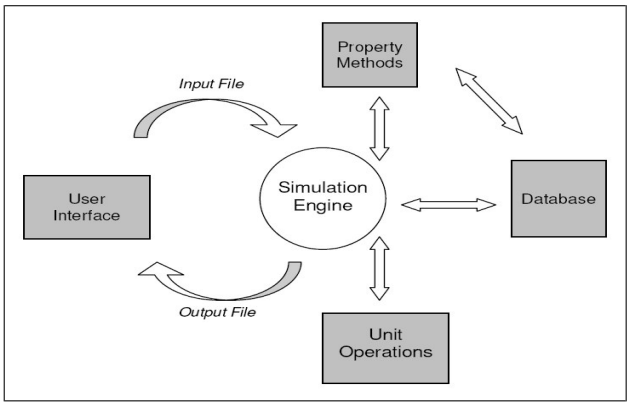

Fig. 4.1: Structure of ASPEN Plus^{TM} [19]

4.1.1 Manageable Systems

There is a wide group of components, which can be handled and calculated by ASPEN Plus^{TM}. In the following a short list of some manageable systems is given (cf. [19]).

- Petrochemical Systems
- Ideal or non-ideal organic and anorganic systems
- Aqueous or non-aqueous electrolyte systems
- Integration of solids
- Polymeres
- Pseudo-components (e.g.: cellulose).

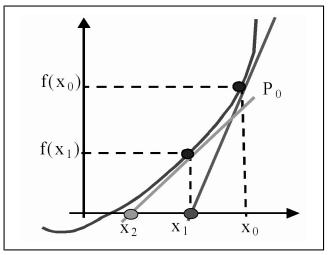

Fig. 4.2: Illustration of the Newton Method

4.1.2 Solving Methods

ASPEN Plus^{TM} has a modular sequencial solving approach. This means that the different unit operation blocks are solved in a certain order. Further, an equation oriented solving method is also possible. In this work, only the modular sequencial solving method was used.
The main advantages of this strategy are:

- Easy to follow the calculation
- Simple location of errors.

On the other hand, there are some disadvantages:

- Iterative solution necessary
- Long calculation time.

Convergence The iteration methods for convergence in ASPEN Plus^{TM} are mainly based on two methods:

- Direct Substitution (Direct Substitution, Wegstein-Method) or
- Newton's Method (Newton-Method, Secant-Method, Broyden-Method)

At the **Direct Substitution Method** a value must be estimated at first. It is replaced until the result fits the boundary conditions (equation (4.1)). The value r_i is calculated after executing the units around in the flow sheet and depends on the initial guess z_i.

$$z_{i+1} = r_i \tag{4.1}$$

The *Wegstein method* is a variation of this principle. In this model an acceleration/ attenuation factor q is added (equation (4.2)). This approach makes the direct substitution more controlable.

$$z_{i+1} = s \cdot z_i + (1 - s) r_i \tag{4.2}$$

$$s = \frac{l}{l-1} \qquad\qquad l = \frac{r_i - r_{i-1}}{z_i - z_{i-1}} \tag{4.3}$$

The **Newton's Method** is a numerical solving approach for nonlinear equations. The principle is illustrated by figure 4.2 and equation (4.4).

$$z_{i+1} = z_i - \frac{f(z_i)}{f'(z_i)} \tag{4.4}$$

For a system of equations equation (4.4) can be written as

$$z_{i+1} = z_i - J^{-1} \cdot f(z_i) \qquad J_i = \frac{\partial f}{\partial z_i} \tag{4.5}$$

where J is called Jacobi matrix.
This iteration method converges quickly, if the iteration begins near the desired root. Therefore, a good initialisation is necessary.
The *Secant* and the *Broyden method* are variations of the Netwon's method. At the Secant method the derivation of the function is linearised (equation (4.6)).

$$\frac{\partial f}{\partial z_i} = \frac{f(z_i) - f(z_{i-1})}{z_i - z_{i-1}} \tag{4.6}$$

The Broyden method uses a system of equations with a linearized Jacobi matrix.

$$z_{i+1} = z_i + t_i \overline{J_i} f(z_i) \tag{4.7}$$

$$\overline{J_{i+1}} = \overline{J_i} - (t_i R_{1,i} + \overline{J_i} R_{2,i}) \frac{s^T \overline{J_i}}{s^T \overline{J_i} R_{2,i}} \tag{4.8}$$

$$R_{2,i} = f(z_{i+1}) - f(z_i) \qquad R_{1,i} = z_{i+1} - z_i \qquad s^T = R_{1,i} \tag{4.9}$$

For both methods no adjustment of the convergence parameters is possible. This methods should only be used for non monotone functions (cf. [19]).

4.2 Vapor Phase Models - Equations of State

In the following the equations of state, which were used for gases in the simulation with ASPEN Plus^{TM}, are described.

4.2.1 Van-der-Waals Equation

The Van-der-Waals equation (equation (4.10)) expresses the deviation of a non-ideal gas from the ideal gas law ($pV = nRT$)(cf. [20]).

$$p = \frac{RT}{(v-b)} - \frac{a}{v^2} \tag{4.10}$$

This cubic equation of state describes the characteristics of non-ideal gases. The first parameter b (expressed by equation (4.18)) describes the covolume of molecules. It is a measurement for the repulsion force between molecules. The second correction parameter a expresses the attraction between molecules and depends on the critical temperature and pressure (see equation (4.17). The calculation of these parameters is given by equation (4.14) to equation (4.18).

4.2.2 Extended Van-der-Waals Equations

Soave Redlich Kwong Model (4.11) is an extension of the Van-der-Waals equation (4.10) by adding the b parameter in the second fraction.

$$p = \frac{RT}{v-b} - \frac{a(T)}{v(v+b)}. \tag{4.11}$$

$$a(T) = a_c \alpha(T) \tag{4.12}$$

$$\alpha(T) = (1 + m(1 - \sqrt{T_R}))^2, \qquad m = 0.48 + 1.574\omega - 0.176\omega^2 \tag{4.13}$$

In this equation a is a function of the temperature, pressure at the critical point and the acentric factor ω, which considers the vapour pressure at 70% of the critical temperature (cf. [36]).
The most important difference is the generalization of the temperature-dependent term $a(T)$ (cf. [37]).

4.2.3 Mixing Rules

The different impact of particular species on the thermodynamic variables of the mixture is considered by using mixing rules. In the following some of the most important rules are shortly mentioned.

Van-der-Waals Mixing Rule To describe non-ideal gas mixtures in an apropriate manner mixing rules, like the Van-der-Waals mixing rule (equation (4.14)), have to be used. This is a quadratic mixing rule. The adjustment parameter for the attraction parameter a for mixtures is given by equation (4.14).

$$a = \sum_{i=1}^{n} \sum_{j=1}^{n} x_i x_j a_{ij} \tag{4.14}$$

$$a_{ij} = \sqrt{a_i a_j}(1 - k_{ij}) \tag{4.15}$$

k_{ij} has to be measured or set to zero.
The covolume adjustment parameter for mixtures is calculated by:

$$b = \sum_{i}^{n} x_i b_i \tag{4.16}$$

The attraction parameters for every single component in the mixture ($a_{i/j}$) can be calculated with the following equations.

$$a_{i/j} = \frac{27R^2T_c^2}{64P_c} \tag{4.17}$$

$$b_{i/j} = \frac{RT_c}{8P_c} \tag{4.18}$$

These depend only on two characteristic values for each components i. e. the temperature and pressure at the critical point.

g^E Model Mixing Rules This rule has to be used for strongly polar systems.
Generally, the free excess Gibbs energy of a mixture is calculated as

$$g^E(T, p, x) = RT(ln\varphi(T, p, x) - \sum_{i}^{n} x_i ln\varphi_i(T, p)). \tag{4.19}$$

Under the assumption/ simplification that the molar volume v_m equates the covolume parameter b and that the excess volume v_m^E is zero, a linear mixing rule can be formulated.

$$\frac{a}{b} = \sum_{i}^{n} x_i \frac{a_i}{b_i} - \frac{g_\infty^E}{ln2} \tag{4.20}$$

The free excess Gibbs energy at infinite pressure g_∞^E is determined by a modified NRTL equation (for more details see [20]).

Density Dependent Mixing Rules This theory is based on the quasichemical approach for mixtures by Guggenheim (see [38]).

4.3 Liquid Phase Models - Activity Coefficient Models

Aspen Plus^{TM} uses various models for the interpolation and extrapolation of thermodynamic data for liquid mixtures.
The calculation of the activity coefficient is based on the excess Gibbs energy. The following models were used in the simulations.

The Wilson Equation (see [39]) showed that liquid mixtures could be expressed by an algebraic function of local composition. This theory is based on the quasichemical theory by Guggenheim (cf. [40]).

4.3.1 NRTL Models

In this method interactions with ions in solutions are modeled.

The Nonrandom, Two-Liquid Equation uses the local compositions for representating excess Gibbs energies of liquid mixtures. Therefore, they are called local composition theories.

In this theory the nonrandomness of mixing, expressed by the equation of Wilson ([39]), is modified to get the relation between the local mole fractions x_{21} and x_{11}. The basic approach of Wilson is that the local concentration around a molecule differes from the bulk concentration. The mole fraction x_{21} stands for molecules that are in the immediate neighborhood of molecule 1. This correlation is illustrated in figure 4.3.
The basic assumption of the NRTL model is that the local mole fraction around a molecule 1 is independent from the mole fraction around molecule 2.

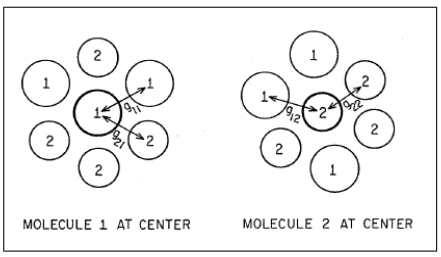

Fig. 4.3: Two types of cells according to Scott's Two-Liquid Theory of Binary Mixtures, [40]

In the NRTL theory the discrepancy to the bulk concentration results from the interaction energy, declared by the molar Gibbs energy, from a molecule in the center to molecules of its own species 11/22 and to molecules of different species 12/21 (see figure 4.3). This approach is given in equation (4.21). Therefore, α_{12} is a constant characteristic of the nonrandomness of the mixture.

$$\frac{x_{21}}{x_{11}} = \frac{x_2}{x_1}\frac{exp(-\alpha_{12}g_{21}/RT)}{exp(-\alpha_{12}g_{11}/RT)} \qquad \frac{x_{12}}{x_{22}} = \frac{x_1}{x_2}\frac{exp(-\alpha_{12}g_{12}/RT)}{exp(-\alpha_{22}g_{11}/RT)} \tag{4.21}$$

Furthermore, the relations between the local mole fractions are expressed by

$$x_{21} + x_{11} = 1 \qquad x_{12} + x_{22} = 1 \tag{4.22}$$

These equations say that the sum of the mole fraction of the molecules 2/ 1 in the immediate neighbourhood to the molecule 1/ 2 (x_{21}/x_{12}) and the mole fraction of the molecule 1/ 2 (x_{11}/x_{22}) in the immediate neighbourhood to 1/ 2 is constant (=1).
From the equations (4.21) and (4.22) the local mole fractions can be calculated.

$$x_{21} = \frac{x_2 exp(-\alpha_{12}(g_{21} - g_{11})/RT)}{x_1 + x_2 exp(-\alpha_{12}(g_{21} - g_{11})/RT)} \tag{4.23}$$

$$x_{12} = \frac{x_1 exp(-\alpha_{12}(g_{12} - g_{22})/RT)}{x_1 + x_2 exp(-\alpha_{12}(g_{12} - g_{22})/RT)} \tag{4.24}$$

It should be noted that $g_{12} = g_{21}$.
According to the two-liquid theory of Scott [41] two kind of cells (see figure 4.3) in a binary mixture must be distinguished.
"*For the first type, cells containing molceules 1 at their centers, the residual Gibbs energy can be calculated as the sum of all residual Gibbs energies for two-body interactions expierenced by the center molecule*", according to [40].
As a result, the Gibbs energy $g^{(1)}$ for a cell containing molceule 1 at its center is

$$g^{(1)} = x_{11} g_{11} + x_{21} g_{21}. \tag{4.25}$$

For pure liquids ($x_{11} = 1, x_{21} = 0$) the residual Gibbs energy is

$$g^{(1)}_{pure} = g_{11}. \tag{4.26}$$

For the second type of cells the equations are

$$g^{(2)} = x_{12} g_{12} + x_{22} g_{22} \qquad\qquad g^{(2)}_{pure} = g_{22}. \tag{4.27}$$

In a binary solution the change of the Gibbs energy is the sum of two changes in the residual Gibbs energy:

1. Transfer of x_1 molecules from a cell of the pure liquid 1 into a cell 1 of the solution
2. Transfer of x_2 molecules from a cell of the pure liquid 2 into a cell 2 of the solution

This correlation is given in the following equation

$$g^E = x_1(g^{(1)} - g^{(1)}_{pure}) + x_2(g^{(2)} - g^{(2)}_{pure}). \tag{4.28}$$

To get the former indices we substitute equations (4.22) and (4.24)-(4.27) into (4.28).

$$g^E = x_1 x_{21}(g_{21} - g_{11}) + x_2 x_{12}(g_{12} - g_{22}) \tag{4.29}$$

Finally, equation (4.29) coupled with x_{21} and x_{12} from equation (4.23) and (4.24) is called the NRTL (non-random, two liquid) model (cf. [40]).

The activity coefficients can be callculated by differentiation of equation (4.29) according to equation (3.35).

$$ln\gamma_1 = x_2^2(\tau_{21}\frac{exp(-2\alpha_{12}\tau_{21})}{x_1 + x_2 exp(-\alpha_{12}\tau_{21})^2} + \tau_{12}\frac{exp(-\alpha_{12}\tau_{12})}{x_2 + x_1 exp(-\alpha_{12}\tau_{12})^2}) \tag{4.30}$$

$$ln\gamma_2 = x_1^2(\tau_{12}\frac{exp(-2\alpha_{12}\tau_{12})}{x_2 + x_1 exp(-\alpha_{12}\tau_{12})^2} + \tau_{21}\frac{exp(-\alpha_{12}\tau_{21})}{x_1 + x_2 exp(-\alpha_{12}\tau_{21})^2}) \tag{4.31}$$

To simplify the notation the following abbrevations are used.

$$\tau_{12} = (g_{12} - g_{22})/RT \qquad \tau_{21} = (g_{21} - g_{11})/RT \tag{4.32}$$

$$g_{12} = g_{21} \tag{4.33}$$

$$G_{12} = \rho_{12} exp(-\alpha_{12}\tau_{12}) \qquad G_{21} = \rho_{21} exp(-\alpha_{12}\tau_{21}) \tag{4.34}$$

Now the expressions for the Gibbs energy of a binary mixture and the activity coefficients can be written in a simplified and shortened way.

$$\frac{g^E}{RT} = x_1 x_2 [\frac{\tau_{21} G_{21}}{x_1 + x_2 G_{21}} + \frac{\tau_{12} G_{12}}{x_2 + x_1 G_{12}}] \tag{4.35}$$

$$ln\gamma_1 = x_2^2 [\frac{\tau_{21} G_{21}^2}{(x_1 + x_2 G_{21})^2} + \frac{\tau_{12} G_{12}}{(x_2 + x_1 G_{12})^2}] \tag{4.36}$$

$$ln\gamma_2 = x_1^2 [\frac{\tau_{12} G_{12}^2}{(x_2 + x_1 G_{12})^2} + \frac{\tau_{21} G_{21}}{(x_1 + x_2 G_{21})^2}] \tag{4.37}$$

The adjustable parameters in this model are $(g_{12} - g_{22})$ and $(g_{21} - g_{11})$. α_{12} can be seen as a third adjustable parameter or a predetermined value. Another possible way is to take G_{12} and G_{21} as temperature-dependent adjustable parameters (cf. [40]).

The Electrolyte-NRTL equation modifies the non-random, two liquid model of Renon for mixed solvent electrolyte solutions. This model is based on the theory that the excess Gibbs energy of a mixed solvent electrolyte system can be written as the sum of two contributions. These contributions are

1. The local ion-molecule, ion-ion and molecule-molecule interactions in the immediate neighborhood of any species
2. The long-range ion-ion interactions beyond the immediate neighborhood of a centeral ionic species (cf. [17]).

Drafted as an equation, this statement can be written as

$$g^E = g^E_{LR} + g^E_{local}. \tag{4.38}$$

The Long range ion-ion interactions are considered by Pitzer's reformulation of the Debye-Huckel formula (equation 4.40).

$$g^E_{LR} = g^E_{Pitzer} + g^E_{Born} \tag{4.39}$$

$$g^E_{Pitzer} = -RT(\sum_k^n x_{kk})\sqrt{(\frac{1000}{M_s})}(\frac{A_\phi I_x}{\rho})ln(1 + \rho\sqrt{I_x}) \tag{4.40}$$

Whereas, A_ϕ is a function of the mixed solvent dielectric constant D_s and the mixed solvent density ρ_s.

$$A_\phi = A_\phi(D_s, \rho_s) \tag{4.41}$$

To transfer this equation from infinite dilution in the mixed solvent to infinite dilution in the aqueous phase, the Born equation (eq. (4.42)) must be included. This correction term is needed

to represent the change in reference state of the dielectric constant of the mixed solvent and of water.

$$g^E_{Born} = RT(\frac{e^2}{2kT})(\frac{1}{D_s} - \frac{1}{D_w})(\sum_i^n \frac{x_i z_i^2}{r_i})10^{-2} \tag{4.42}$$

In this equation D_w represents the dielectric constant of pure water and D_s of the solvent.

For local interactions the NRTL model by Renon and Prausnitz (see section 4.3.1) is used (equation (4.29)).

Finally, the following equation describes the ElecNRTL model.

$$g^E = (g^E_{Pitzer} + g^E_{Born}) + g^E_{NRTL} \tag{4.43}$$

The activity coefficient is again calculated by derivation of the partial molar free excess Gibbs energy (cf. [17], [42], [43]).

$$ln\gamma_i = [\frac{\partial(n_i G/RT)}{\partial n_i}]_{T,p,n_{j\neq i}} = [\frac{\partial(g^E/RT)}{\partial n_i}]_{T,p,n_{j\neq i}}. \tag{4.44}$$

4.3.2 UNIQUAC Models

The UNIQUAC model is used for the calculation of non-electrolyte VLE or liquid-liquid equilibria. The extension (electrolyte UNIQUAC NRF Equation) can be used for electrolytic solutions. It is also a local composition model.

The UNIQUAC Method stands for **UNI**versal **QUA**si**C**hemical Method.
The basic approach of UNIQUAC model is, that a set of bonded segments (number of segments per molecule r_1) represent a molecule of a component 1. These segements are defined as same size. They are only distinguished by their external contact area. Further, the system is seen as a lattice. The number of external nearest neighbours is expressed by zq_1 where z is the lattice coordination number and q_1 proportional to the molecule's external surface area.

At first, the molar excess Gibbs energy is set equal to the molar Helmholtz energy of mixing (a^E, A), which is a function of the configurational partition function $Z = Z_{lattice} \cdot Z_{cell}$.

$$g^E \approx a^E = \frac{\Delta A}{n_1 + n_2} - RT(x_1 lnx_1 + x_2 lnx_2) \tag{4.45}$$

The configurational partition function Z for the lattice refers to the situation where the center of every segment is coincident with a lattice site. Z_{cell} is the impact of motions of a segment about this central position.
$Z_{lattice}$ is a function of the interaction energies (U) and the number of possible configurations for a mixture (ω).
Similar to the NRTL approach the lattice energy U_0 is calculated as function of the composition of a region in the immediate vincity of molecule 1 and 2. It is expressed as the sum of all interaction energy between pairs of nonbonded segments.

$$\theta_{11} + \theta_{21} = 1 \qquad\qquad \theta_{12} + \theta_{22} = 1 \tag{4.46}$$

$$-U_0 = q_1 N_1(\theta_{11} u_{11} + \theta_{21} U_{21}) + q_2 N_2(\theta_{22} u_{22} + \theta_{12} u_{12}) \tag{4.47}$$

u_{ij} stands for the interaction energy between sites i and j. It is defined as $u_{ij} = \frac{z}{2}U_{ij}$. Equation (4.47) is zero, since the potential energy of the ideal gas state is taken as zero.
The number of configurations is given by a function of numbers of configurations that are associated with a site occupied by a segment of molecule i (ω_i) and the number of molecules (N_i).

$$\omega = \omega_1 \cdot \omega_2 h(N_1, N_2) \tag{4.48}$$

The h function is defined by the athermal case ($u_{ij} = 0$).

All these approaches together, equation (4.45) can be written as the sum of a combinatorial and a residual contribution.

$$g^E = g^E_{comb} + g^E_{res} \tag{4.49}$$

For binary and multicomponent systems these terms are calculated by equations (4.50) and (4.52).

$$(\frac{g^E}{RT})_{comb} = \sum_i^n x_i ln\frac{\Phi_i}{x_i} + \frac{z}{2}\sum_i^n q_i x_i ln\frac{\theta_i}{\Phi_i} \tag{4.50}$$

Where Φ_i and θ_i are expressed by

$$\Phi_i = \frac{x_i r_i}{\sum_j^n x_j r_j} \qquad\qquad \theta_i = \frac{q_i x_i}{\sum_j^n q_j x_j}. \tag{4.51}$$

The combinatorial expression contains two composition variables. This contribution is calculated exclusively from pure component structural parameters (r_i, q_i). An important fact is that in equation (4.50) these are no binary adjustment parameters.
The residual contribution contains only one composition variable. However, there is an additional adjustable binary parameter.

$$(\frac{g^E}{RT})_{res} = -\sum_i^n q_i x_i ln(\sum_j^m \theta_j \cdot \tau_{ij}) \tag{4.52}$$

The binary adjustmant parameter

$$\tau_{ij} = \exp -[\frac{u_{ij} - u_{ii}}{RT}] \tag{4.53}$$

is derived from experimental or estimated activity coefficients (cf. [44]).

The electrolyte UNIQUAC NRF Model is an extension of the UNIQUAC model for electrolyte solutions, since the UNIQUAC model is only valid for non-electrolyte solutions. The NRF stands for Non Random Factor. The modification of the UNIQUAC model consists of three parts:

1. Adoption of the combinatorial contribution to solvents
2. Additional long-range interaction contribution term
3. Modification of the residual contribution by using a Non Random Factor Γ_{ii}

The combinatorial contribution explained in the UNIQUAC model is adopted for solvents. Moreover, a contribution for long-range interactions and one for short-range interactions are added. Those two terms substitute the residual part of the excess Gibbs energy.
The basic equation of the electrolyte UNIQUAC NRF Model is

$$\frac{g^E}{RT} = (\frac{g^E}{RT})_{comb} + (\frac{g^E}{RT})_{LR} + (\frac{g^E}{RT})_{SR} \tag{4.54}$$

The long range interaction contribution is given by a modification of the Pitzer's reformulation of the Debye-Huckel formula.

$$(\frac{g^E}{RT})_{LR} = -A\frac{Z_i^2\sqrt{I}}{1+B\sqrt{I}} \tag{4.55}$$

Where $I = \frac{1}{2}\sum_i m_i z_i^2$ is the ionic strength and A, B are the usual Debye-Hückel Parameters.
The short range interaction contribution is an extension of the UNIQUAC residual contribution based on local area fraction.

$$(\frac{g^E}{RT})_{SR} = \sum_i^n q_i x_i [ln\Gamma_{ii} + \sum_j^m \theta_j ln\tau_{ji}] \tag{4.56}$$

The main difference to the long range term is the definition of a local area fraction between two components i and j.

$$\theta_{ij} = \theta_i \Gamma_{ij} \qquad \Gamma_{ij} = \tau_{ij}\Gamma_{jj} \tag{4.57}$$

Therefore, the additional Non Random Factor (τ_{ji}) is defined as follows (cf. [45]).

$$\sum_j^m \theta_j \tau_{ji} \Gamma_{ii} = 1 \qquad \Gamma_{ii} = {}^1/_{\sum_j^m \tau_{ji}} \tag{4.58}$$

4.3.3 Vapor Phase Fugacity Coefficients

In this case, a model for the calculation the vapour phase fugacity coefficient is not compulsory necessary, since it can be set to 1 for most technical gases.
Besides, the real characteristics of the gas phase are determined by equations of state modelling the vapor phase (see section 4.2).

4.4 Property Calculations

Property calculations are the essential part of every simulation. The quality and significance of the simulation depend on the quality of the used properties.
In this section the main calculation methods are described.

4.4.1 Physical Properties

In the following the property calculation methods for the main properties are mentioned.

Pure Components

Dielectricity Constant is the ratio of the amount of the stored electrical energy when a voltage is applied, relative to the permittivity of a vacuum. The definition is

$$\epsilon_r = \frac{\epsilon}{\epsilon_0} = \frac{C}{C_0} \qquad \epsilon_0 = 8.85410^{-12}\frac{A\cdot s}{V\cdot m}. \tag{4.59}$$

A more practical definition is the fraction of two capacitance (same distance) one with vacuum and one with the dielectric between its plates.
This means that the dielectric constant relates a component's ability to stabilize an ionic solution. The tendency for ions to form or remain as ionic species increases as the dielectric constant increases (cf. [18]). According to [18] it is related to the square of the refractive index.

Aqueous Ammonia: The dielectric constant is expressed by a polynomial temperature-dependent function.

$$D_i = A_i + B_i \cdot (\frac{1}{T} - \frac{1}{C_i}) \tag{4.60}$$

where $C_i = T_{ref}$ is.
For pure ammonia this parameter was regressed by experimental data (see 6.1.1).
Monoethanolamine: For aqueous Monoethanolamine it is calculated by the following temperature-dependent equation, according to [17].

$$D_{MEA} = 35.76 + 14836[1/T - 1/273.15] \tag{4.61}$$

According to [18], the temperature dependent dielectric constant for water is represented by:

$$D_{H_2O} = 78.65 + 31989[1/T - 1/298.15] \tag{4.62}$$

For the mixed solvent the dielectric constant is calculated by

$$D_m = \sum_i w_{mi} \cdot D_i. \tag{4.63}$$

The UNIQUAC Parameters r_i and q_i for pure components can be adopted in ASPEN Plus^{TM}. Whereupon, r_i represents the relative Van der Waals volumes and q_i the surface areas.

Heat capacity at infinite dilution The heat capacity of a pure component is given by the derivation of the inner energy and the enthalpy.

$$(\frac{\partial U}{\partial T})_V = c_v \qquad\qquad (\frac{\partial H}{\partial T})_p = c_p \tag{4.64}$$

Therefore the liquid enthalpy is calculated by the following expressions in ASPEN Plus^{TM}.

$$H_m^l(T) = \sum_i x_i H_i + \sum_k x_k H_k^\infty + H_m^E \tag{4.65}$$

The liquid enthalpy for solvents and solutes (H_i) is expressed by deviations of ideality. The excess enthalpy of the mixture (H_m^E) and the infinite dilution aqueous phase enthalpy (H_k^∞) are calculated by deviations of standards. For detailed informations it is referred to [18].
The calculation of the temperature-dependent infinite dilution aqueous phase heat capacity is declared in the following equation.

$$c_{p,i}^\infty = C_1 + C_2 T + C_3 T^2 + \frac{C_4}{T} \tag{4.66}$$

Further, the solid heat capacity is modeled by a polynomial function, called *CPSP01* (equation (4.67)). It is used for calculating enthalpy, entropy and free energy of components.

$$C_p^{0,s} = C_1 + C_2 T + C_3 T^3 + \frac{C_4}{T} + \frac{C_5}{T^2} + \frac{C_6}{T^3}. \tag{4.67}$$

Extended Antione equation This extended vapour pressure (extension of equation (3.29)) correlation is used to calculate the vapour pressure of pure components (cf. [18]).

$$ln f_i^0 = A + \frac{B}{T + C} + D \cdot T + E \cdot lnT + F \cdot T^G \tag{4.68}$$

Standard Enthalpy of Vaporization The Watson heat of vapourisation equation (4.69) is used in ASPEN Plus^{TM} for the calculation of H_2O and MEA (cf. [18]).

$$\Delta H_i(T)^{vap} = C_{1i}(1 - T_{ri})^{C_{2i}+C_{3i}T+C_{4i}T^2} \tag{4.69}$$

where $T_{ri} = T/T_{ci}$ is the reduced temperature of component i. In this equation the heat of vaporization of a pure liquid component at any temperature is estimated from a known value of a single temperature ($\Delta H_i(T_1)$).

Binary Parameters

NRTL and GMELC (τ_{ij}) are assumed to be temperature dependent and can be calculated by a temperature dependent function with adjustment constants (cf. [17]).
For molecule-molecule interaction (*NRTL*) it is given by

$$\tau_{ij} = A_{ij} + B_{ij}/T + C_{ij}ln(T) + GT. \tag{4.70}$$

Moreover, the nonrandomness parameter α can be set by $\alpha_{ij} = C_{ij}$.
For electrolyte-molecule interaction (*GMELC*) the adjustment parameter is

$$\tau_{ij}^{'} = A_{ij}^{'} + B_{ij}^{'}/T + C_{ij}^{'}(\frac{(T_{ref} - T)}{T} + ln\frac{T}{T_{ref}}). \tag{4.71}$$

The UNIQUAC Parameters (τ_{ij}) can be expressed as a polynomial function with fitting parameters.

$$ln(\tau_{ij}) = A_{ij} + B_{ij}/T + C_{ij} \cdot ln(T) + D_{ij} \cdot T^2 + E_{ij}/T^2 \tag{4.72}$$

Liquid Molar Volume is defined as

$$v_m = \frac{M}{\varrho}. \tag{4.73}$$

For mixtures the molar volume is calculated using

$$v_m = \frac{\sum_i x_i M_i}{\rho_{mix}} \tag{4.74}$$

In the simulation it is calculated with the Clarke model. For the solvent the quadratic mixing rule was used.
For solids the molar volume is calculated by the following polynomial model, which is used to calculate density (named *VSPOLY*).

$$v_m^s = C_1 + C_2T + C_3T^2 + C_4T^3 + C_5T^4. \tag{4.75}$$

Activity Coefficients The calculation method for the activity coefficient is explained in chapter 4.3.

4.4.2 Reactive System

Equilibrium constants The temperature-dependency of equilibrium constants for the chemical reactions is calculated by using the following polynomial equation (cf. [17]).

$$\text{ln K}=\text{C}_1 + \tfrac{C_2}{T} + C_3 \cdot lnT + C_4 \cdot T \tag{4.76}$$

Henry Parameters The correlation for the temperature-dependent Henry's coefficient at the interface is also given by a polynomial equation (cf. [17]).

$$\ln k_i^H = A + \frac{B}{T} + C \cdot lnT + D \cdot T + \frac{E}{T^2} \tag{4.77}$$

In ASPEN Plus^{TM} a volume weighted mixing rule is utilized to describe the Henry's constant of CO_2 in a mixed solvent (cf. [18]).

$$ln(\frac{k_i^H}{\gamma_i^\infty}) = \sum_A w_A ln(\frac{k_{i,A}^H}{\gamma_{i,A}^\infty}) \tag{4.78}$$

4.5 Simulation System

4.5.1 RADFRAC Module

The RADFRAC Module by ASPEN Plus^{TM} is a rigorous model and used for simulating all types of multistage vapour-liquid fraction operations (cf. [46]).
In this work, the module is used for the simulation of chemical absorption and stripping processes.
The RADFRAC Module was chosen because of its suitability for systems with strong liquid phase nonideality and the option to handle soilds on every stage of the column.

Moreover, chemical reactions that occure in the column can also be modeled by the RADFRAC module. Three different reaction types can be handled:

- Equilibrium
- Rate-based
- Electrolytic.

Salt participations can also be modeled (cf. [46]).

Equilibrium Method - RADFRAC This model treats separations as equilibrium problems. The RADFRAC equilibrium method is suitable for circumstances with stable tray and/ or Murphree efficiencies. In this model all reactions are handled as chemical equilibrium reactions, which includes dissociation and the participation of solids (cf. [15]).
The equilibrium model was chosen to model the absorption and desorption process for both capture technologies in this work. The reason is, that no realized absorption or desorption column was simulated and therefore no design variables were given.

Pressure Drop In the RADFRAC module using the equilibrium method the stage or column pressure drop can be included as a pre-given value by the user. Thus, it is not calculated and seen as a constant (cf. [15], [47]).

Part II
Realization

5 Specifications

5.1 Flue Gas Specifications

In this work, the flue gas from a super critical CFB power plant, using coal as fuel, with a design capacity of 600 MWe is used as entry stream for the downstream capture process. These flue gas specifications of [48] were used for the sake of comparison. The HP steam temperature is 600°C with a pressure of 270 bara. Further the condenser pressure is 35 mbara and the sea water temperature is set to 15.7°C. The net efficiency of the simulated power plant is around 44.9 % (see [48]).
The composition of the flue gas produced by the power plant is listed in table 5.1.

Tab. 5.1: Fluegas specifications

Flow rate	1750000	Nm^3/h
Temperature	120	$°C$
Pressure	1.01	bar
Composition:		
N_2	74.1	$v\%$
CO_2	13.5	v%
H_2O	7.1	v%
O_2	4.4	v%
Ar	0.9	v%

5.2 Carbon Dioxide Recovery

The CO_2 recovery rate for both scrubbing processes was fixed to 90wt% removal of the flue gas carbon dioxide component flow rate. This was necessary to make the capture processes comparable to each other.
Since the flue gas flux was pre-given, the following CO_2 flow rates were defined (see table 5.2).

Tab. 5.2: Carbon dioxide removal

CO_2-Removal	90	$wt\%$
Inlet CO_2 Flow	407033.4	kg/h
Pure CO_2 Flow	366330.4	kg/h
Outlet CO_2 Flow / Slip	40703.3	kg/h

5.3 Washing solvents

In the following the used washing solvents for the capture process are specified.

5.3.1 Monoethanolamine

For the chemical absorption of CO_2 from flue gas an aqueous MEA solution with an initial value of 30wt% MEA was selected. This selection is on the basis of the work by *Oexmann J* (cf. [5]). Hence the chemical equilibrium reactions, the concentration changed during the capture process. In the steady state simulation a solvent with the operating data and composition listed in table 5.3 was used. The initial carbon dioxide loading (5.1) results from the cyclic process and was calculated to 0.33 mol CO_2/ mol MEA.

$$X = \frac{(n_{CO_2} + n_{MEACOO^-} + n_{HCO_3^-} + n_{CO_3^{2-}})}{(n_{MEA} + n_{MEA^+} + n_{MEACOO^-})} \tag{5.1}$$

The selection of this specific solvent stream is based on the results in section 6.3.

Tab. 5.3: Aqueous Monoethanolamine solution - specifications

Flow rate	6200000	kg/h
Temperature	40	$°C$
Pressure	1.01	bar
Composition:		
H_2O	0.565	kg/ kg solution
MEA	0.216	kg/ kg solution
MEA^+	0.139	kg/ kg solution
$MEACOO^-$	0.016	kg/ kg solution
CO_2	$2.54E^{-08}$	kg/ kg solution
N_2	$8.40E^{-09}$	kg/ kg solution
O_2	$1.02E^{-09}$	kg/ kg solution
HCO_3^-	0.0001	kg/ kg solution
CO_3^{2-}	0.0629	kg/ kg solution
H_3O^+	$5.16E^{-12}$	kg/ kg solution
OH^-	$1.66E^{-06}$	kg/ kg solution
Ar	$4.12E^{-08}$	kg/ kg solution

5.3.2 Aqueous Ammonia

The aqueous Ammonia solvent had an initial concentration of 12 wt% Ammonia. This value was chosen, because it was recommended by by [49] for minimal voltilization from the solution and represents an optimum according to [35].
Due to the proceeding equilibrium reactions, the composition of the solvent also changed. In table 5.4 the steady state composition and operating data is given. The initial loading of 0.2 [mol CO_2 / mol NH_3] is resulting of the pump-around.
The reason for the selection of this specific solvent stream is given in section 7.3.

Tab. 5.4: Aqueous Ammonia - solvent specifications

Flow rate	3 200 000	kg/h
Temperature	30	$°C$
Pressure	1.01	bar
Composition:		
H_2O	0.872	mol / mol Solvent
NH_3	0.078	mol / mol Solvent
NH_4^+	0.025	mol / mol Solvent
NH_2COO^-	0.022	mol / mol Solvent
$NH_4HCO_{3,s}$	0	mol / mol Solvent
HCO_3^-	0.002	mol / mol Solvent
CO_3^{2-}	0.001	mol / mol Solvent
CO_2	$2,90E^{-08}$	mol / mol Solvent
N_2	$1.70E^{-07}$	mol / mol Solvent
O_2	$5.09E°{-}06$	mol / mol Solvent
H_3O^+	$3.74E^{-13}$	mol / mol Solvent
OH^-	$2.51E^{-06}$	mol / mol Solvent
Ar	$9.37E^{-07}$	mol / mol Solvent

5.4 Packing Specification

The absorption and desorption columns were designed as random packing columns. As packing material metal *Raschig* rings with data from [50] were chosen. The main input data is listed in the next table.

Tab. 5.5: Packing specifications

Type	Raschig Rings	50-50 mm
Material	Metal	
K_3	0.088	-
K_4	0.077	-
a	110	m^2/m^3
ϵ	0.95	m^3/m^3
d_p	50	mm

A random packing column is actually not predestinated for an absorption problem of this kind, because of its high pressure drop, material pollution problems, wall effect and investment costs strongly increasing with the column diameter. Thus, stacked packing or perform-contact columns would fit better. Nevertheless, the random packing column was selected, since for the other types special data by manufacturers would be necessary.

6 Monoethanolamine Process

6.1 Modeling of the Capture Process

In this section the modeling of the monoethanolamine absorption and desorption process is discussed.

6.1.1 Properities

At first, the used properties, on which the simulation is based, are mentioned.

Chemistry The calculation of the thermodynamic properties of a system depends on it's chemistry.
The chemistry of the $CO_2 - MEA - H_2O$ system is based on equilibrium reactions. These reactions and their equilibrium constants were explained in section 3.4.1.
For the calculation of the equilibrium constants a polynomial expression was used (equation (4.76)). Therefore, the constants $C_1 - C_4$ had to be adjusted.
The equilibrium constants for the reactions (3.38) - (3.42) were adopted by data from [17]. The used adjustment parameters are listed in table 6.1.
These values are valid for systems with temperatures up to 120°C and amine concentrations up to 50 wt% (according to [17]).

Tab. 6.1: Equilibrium constants for MEA

Reactions	C_1	C_2	C_3	C_4	**T [°C]**
K_1 (3.43)	231.456	-12092.1	-36.7816	0	0-225
K_2 (3.44)	216.049	-12431.70	-35.4819	0	0-225
K_3 (3.45)	2.1211	-8189.38	0	-0.007484	0-50
K_4 (3.46)	2.8898	-3635.09	0	0	25-120
K_5 (3.47)	132.899	-13445.9	-22.4773	0	0-225

This property data set for the equilibrium constants was taken from [17].

Property Base Method The choosing of the basic property method for the calculations was done by using the guidelines according to [46]. The procedure is represented in figure 6.1.
As a result, the ElecNRTL model, explained in section 4.3.1, had been choosen as basic method. The ASPEN Plus^{TM} notation of the chosen method is ELECNRTL-RK model, since the Soave Redlich Kwong Equation is used for the calculation of the vapour phase.
In other words, this base methode uses the ELECNRTL model for calculating the activity coefficient (equation (4.43)) and the Soave-Redlich-Kwong (equation (4.11)) equation of state for modeling the vapour phase.
This ASPEN Physical Property System contains binary and pair interaction parameters, which are mainly taken or calculated from ASPEN's included data base. The data set for *NRTL* adjustment parameter τ_{ij} for molecule-molecule interaction (equation (4.70)) and the *GMELC* adjustmentparameter $\tau_{ij}^{'}$ for electrolyte-molecule interaction (equation (4.71)) were adopted from the *emea* template (cf. [15]).

The main property insert for the ELECNRTL method is the Dielectric constant of the pure component. Thus, equations (4.61) and (4.62) according to [17] and [18] were entered in the

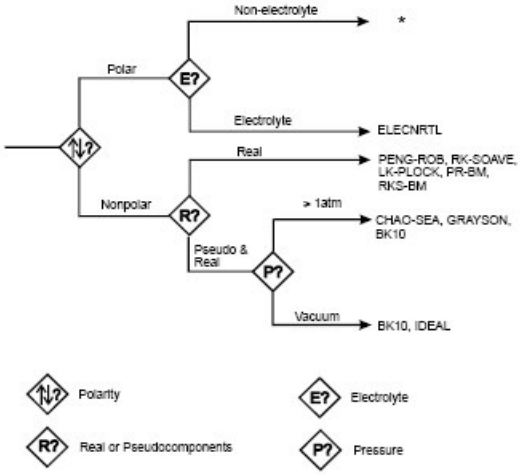

Fig. 6.1: Guidelines for choosing a property method, [46]

ASPEN Plus^{TM} property system.

The by the ELECNRTL model calculated $T(x, y)$ diagrams at constant pressure are shown in figure 6.2 for 1.01 bar and in figure 6.3 for 1.9 bar. The comparison between the experimental data from the *"DECHEMA Chemistry Data Series"* [51] and the calculated the vapour-liquid equbilibria is also given by figure 6.2.
The comparison of both figures shows an average agreement between the calculated and the measured data. For high MEA concentrations the deviation is very high. For a mole fraction H_2O of 0.9 (30 wt% MEA) the temperature deviation between the calculated and measured data is 7.5 K for the gaseous phase and 0.4 K for the liquid phase.
Unfortunatly no experimental data for the VLE of H_2O and MEA at 1.9 bar could be found.

One of the main issues of this model is that no valdidation of the ternary system $H_2O - MEA - CO_2$ could be done, because of missing data.

Property inserts The property inserts of the modeling are based on an ASPEN Plus^{TM} property template called *emea*. It uses the ELECNRTL property method and is indicated for systems containing CO_2, H_2S, MEA and H_2O. According to [52] the data package is valid for temperatures up to 120°C and MEA concentrations up to 50 wt%.
This data set was uptdated with property data by [18].

The properties for pure components, that were fitted to [18] are mentioned in the following:

- The extended Antoine Equation (equation (4.68)) for the pure components H_20, CO_2 and ions
- Henry's constant of CO_2 in H_2O (equation (4.77))
- The infinite dilution aqueous phase heat capacity (equation (4.66)).

All these properties - equations were explained in 4.4.1 - were adjusted to the data by [18]. The used parameters are listed in the following tables 6.2 to 6.4.

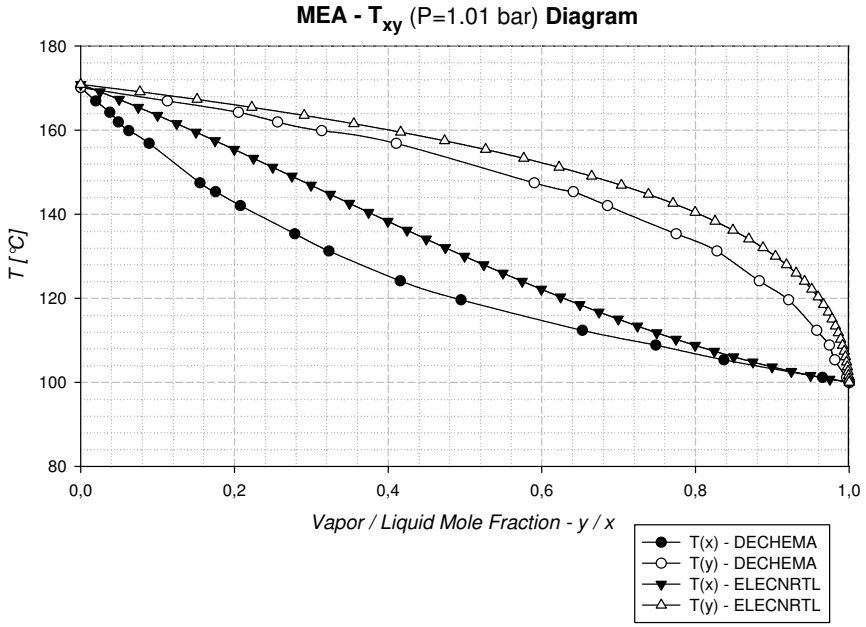

Fig. 6.2: Experimental data of Vapour-Liquid Equilibrium for the $MEA - H_2O$ system at 1.01 bar pressure against calculated VLE

Tab. 6.2: Antoine equation parameters

Parameters	H_2O	CO_2	MEA	$Ions$
A	65.64	72.83	165.87	-1.00E+20
B	-7207	-3403	-13492	0
C	0	0	0	0
D	0	9.49E-03	0	0
E	-7.139	-8.560	-21.9	0
F	4.045E-06	2.91E-16	1.38E-05	0
G	2	-13445.9	2.00	0

The ASPEN Plus^{TM} program code for the extended Antione Equation is *PLXANT*.

Tab. 6.3: Henry's constant [Pa] for CO_2 in H_2O

A	B	C	D	E
170.7126	-8477.711	-21.95743	0.005781	0.0

Tab. 6.4: Infinite dilution aqueous phase heat coefficients

CPAQ0	H^+	OH^-	$MEAH^+$	$MEACOO^-$
C_1	0	0	-1700443	-2408071
C_2	0	-497.9	7093	17268
C_3	0	0	-8.49	-26.0
C_4	0	0	1.51E+08	0

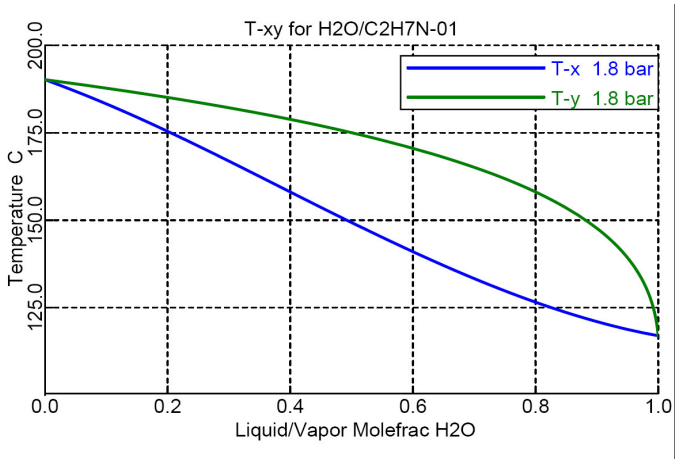

Fig. 6.3: Vapour-Liquid Equilibrium for the $MEA - H_2O$ system at 1.9 bar pressure

CPAQ0 is the ASPEN Plus^{TM} program code for the infinite dilution aqueous phase heat capacity, which is needed to calculate the specific heat capacity.

6.1.2 Components

In this section the used components and their operating data for modeling the capture process are explained shortly (visualisation see flowsheet 6.4).

Columns The absorber (*A-1* in flowsheet 6.4) of the scrubbing process was modeled with the RadFrac module in ASPEN Plus^{TM}. Nevertheless, this equilibrium based module is disadvantaged compared to the RateFrac module (according to [15]). For example, the pressure profile of the column can not be considered as detailed as by the rate based calculation approach.
The RateFrac module is a rate-based approach for modeling colums with chemical reactions. Thus, the reaction kinetics of the chemical system can be considered. As an example, in the RadFrac module a good separating capacity can be already achieved with 6 steps. Whereas, in reality at least 20 steps are necessary. The reason is, that the reaction kinetics have an strong impact on the mass transfer and therefore on the separation capacity. The RadFrac module is based on the Two-Film Theory (see 3.5.1)
On the other hand, this model needs lots of design specifications. Since no existing absorber was treated, these data were not available. Besides, in this work a comparison of the overall process for the capturing in general should be considered.
The desorber column (*D-1* in flowsheet 6.4) was also represented by the RadFrac module. For the desorber the use is not as critical as for the absorber, since for the separation and there for the mass transfer the absorption is the leading process step.

The basic operation conditions for the absorber and desorber column are summerized in table 6.5. The stripper pressure of 1.9 bar was selected, because this operation parameter was realized in some industrial projects (eg. the CASTOR Project, see section 6.4.1).

Tab. 6.5: Absorber and Desorber operation conditions - MEA

	A-1	**D-1**
Average Temperature [°C]	66	96
Pressure [bar]	1.01	1.9
Pressure drop [mbar]	100	0
Reboiler	No	External
Condensator	No	External
Theoretical separation stages	6	5

Heaters and Coolers in the simulation were modeled by the ASPEN Plus^{TM} unit operation model *heater*. It is suitable for single or multiphase calculation with one outlet stream and an optional water decant stream (cf. [46]).
The simulation contains 3 coolers. These are the pre-cooler for the absorption step (*C-1*), the solvent cooler for the lean solvent (*C-3*) and the condenser (*C-2*) of the desorber. Further, there is just one real heater, which is the desorber reboiler (*R-1*).
The operating data of those is listed in table 6.6.

Tab. 6.6: Heaters operation conditions - MEA

	C-1	**C-2**	**C-3**	**C-4**	**C-5**	**R-1**
Temperature [°C]	40	75	40	15	17	122
Pressure [bar]	1.01	1.9	1.01	1.01	1.01	1.9
Pressure drop [mbar]	0	0	0	0	0	0
Cooling/ Heating Duty [MW]	−132.5	−27	−129.8	−51.9	−28.6	328.9

The cooler *C-4* for the recooling of the water, which was used for the quenching of the flue gas, and the pure CO_2 product gas cooler *C-5* were only added to the optimum process to make both process easier comparable.
A pressure of zero expresses no pressure drop in ASPEN Plus^{TM}.

Heat exchanger As heat exchanger the *MHeatX* model was selected for the heat exchanger between the rich and the lean solvent, called *HX-1* in the flowsheet.
MHeatX performs multiple heat transfer between various hot and cold streams. It represents multiple heaters, which are connected together by heat streams. The main advantage of this calculation model is the fast convergence and therefore leads to a faster flowsheet convergence. On the other hand, this model does not calculate any heat transfer coefficient.

For the calculation the difference between cold inlet stream and hot outlet stream was hold constant to approximately $\Delta T = 5K$. Further, no pressure drop was inserted. The main problem of the *MHeatX* model is that the temperature difference can not be set constant by the model itself. As a result, the temperatures had to be corrected manually by the user to keep a more or less constant temperature difference.

Flashs The *Flash2* unit operation model by ASPEN Plus^{TM} was used for simple vapor-liquid separation steps. By this model one vapour outlet and one liquid outlet stream are produced. Additionally, optional water decant streams can be used. This model is suitable for flashes and single-stage separators (cf. [46]).

In the simulation 4 of them were needed. These were the fluegas cooling column (*DCC-1*), the condensated water separator (*S-1*), the final head-washer for the clean gas (*W-1*) and the vapour-liquid separator for the reflux (*S-2*).
The operating data is mentioned in table 6.7.

Tab. 6.7: Flashs operation conditions - MEA

	SEP-1	**SEP-2**	**DCC-1**	**W-1**
Temperature [°C]				
Pressure [bar]	1.9	1.9	1.01	1.01
Pressure drop [mbar]	0	0	0	0
Water flow [t/h]	0	0	1000	10
Water Temparture [C°]	–	–	15	15

Pumps, Blowers and Valves For the rich solvent pump (*P-1*) the unit operation model *Pump* was selected. By this model only the power requirement at a given outlet pressure specification can be calculated. The fluegas blower (*B-1*) was modeled by *Compr*, where a compressor was modeled. The pressure difference between desorber and absorber was released by using the *Valve* model (*VALVE*) (cf. [46]).
Table 6.8 gives an overview of the operation data.

Tab. 6.8: Pump, blower and valve operation conditions - MEA

	P-1	**B-1**	**VALVE**
Pressure Increase/ Decrease [bar]	0.7	0.1	0.8
Pump Efficiency	-	0.86	–
Type	-	*Polytropic*	–
Power [MW]	0.09	7.9	0

Mixers and Spliters For the combination of different material streams into one outlet stream the ASPEN Plus^{TM} Unit Operation model *Mixer* was taken. This module is based on an adiabatic phase equilibrium flash calculation. The Unit Operation model *Splitter* is the counterpart operation based on the same basics (cf. [46]). In other words, these unit operation model splits the resulting stream.
Summarized 4 mixers and one spliter were used in the simulation.

6.1.3 Overall Mass Balance

Since the vaporization of MEA and water and therefore the loss in the cleangas and CO_2 outlet stream, make-up MEA must be added to the overall process to keep a neutral mass balance. Further, it is necessary because by various sources (fluegas, head wash water,...) water is added to the cycle and therefore the MEA solution is diluted. As a result, a certain amount of water must be drawn off the system and MEA had to be added.
This fact was realized by using the design specification function of ASPEN Plus^{TM}.

Water The water mass balance is necessary, since additional water is brought into the system by the flue gas.
The primary loss of water is due to condensation and evaporization of the water during the

process. The ingoing streams in the system are the flue gas water ($\dot{m}^W_{fluegas}$), the cooling column water ($\dot{m}^W_{DCC}$) and the water of the washing column ($\dot{m}^W_{wash-water}$), whereas the outgoing streams are the cooling coulmn water mixed with the condensated water of the fluegas ($\dot{m}^W_{DCC+Kond}$), the vaporized water in the cleangas ($\dot{m}^W_{cleangas}$) and in the outlet carbon dioxide stream ($\dot{m}^W_{co2,out}$) and finally the separated water ($\dot{m}^W_{sep}$). The final water separation was varied during the simulation to keep a neutral balance.

$$\dot{m}^W_{makeup} + \dot{m}^W_{fluegas} + \dot{m}^W_{DCC} + \dot{m}^W_{wash-water} - \dot{m}^W_{DCC+Kond}$$

$$- \dot{m}^W_{wash-water} - \dot{m}^W_{cleangas} - \dot{m}^W_{co2,out} - \dot{m}^W_{sep} = 0 \tag{6.1}$$

In the MEA Process water had to be added, because of the higher clean gas temperatures.

MEA Because water was added, a balance for MEA to keep the amount must also be done. The amount of make up MEA was fixed by an overall material balance of the capture process. The main loss of MEA is in the outlet carbon dioxide stream ($\dot{n}^{MEA}_{co2,out}$) and the clean gas stream ($\dot{n}^{MEA}_{cleangas}$), additionally the separated MEA ($\dot{n}^{MEA}_{sep}$) in the splitter (*S-1*). Further, the dissociation of MEA into $MEACOO^-$ ($\dot{n}^{MEA^-}_{sep}$) and MEA^+ ($\dot{n}^{MEA^+}_{sep}$) had to be included. Therefore not a mass balance but rather a material balance was set up. The amount of the MEA make up stream was varied to keep the balance neutral.

$$\dot{n}^{MEA}_{makeup} - \dot{n}^{MEA}_{cleangas} - \dot{n}^{MEA}_{co2,out} - \dot{n}^{MEA}_{sep} - \dot{n}^{MEA^+}_{sep} - \dot{n}^{MEA^-}_{sep} = 0 \tag{6.2}$$

6.2 Simulation of the Capture Process

This section shows the developed simulation model and its flow sheet.

6.2.1 Simulation

Basic Design Approach The first step in simulating a thermodynamic system with computers, is manual pre-estimation.
Therefore, for a low partial pressure of the solute, the physical absorption has been estimated by using Henry's law. The Henry coefficient of CO_2 in H_2O was calculated from the data by [18] to $706.5bar$. With an ambient pressure of $1.01bar$ the minimum solvent ratio for the physical absorption of carbon dioxide in water is given in the next equation, according to equation (3.22).

$$m = \frac{706.47}{1.01} = 699.47 \approx 700 \tag{6.3}$$

In other words, for the absorption of CO_2 in water at ambient pressure 700 times of the gas flow for the solvent flow ($\dot{L}_{min} = 700 \cdot \dot{G}$) would be needed. This expression shows very well, that the pure water at ambient pressure is not suitable for carbon capture.

The chemical absorption can be estimated by using the Enhancement factor E. The Enhancement factor for the aqueous MEA solution was estimated from [26] to approximatly $E \approx 450$ for a CO_2 partial pressure of $13kPa$ and a CO_2 Loading of $0.1kmol/kmol$ (for higher loadings the the Enhancement factor decreases and therefore the solvent ratio increases) to calculate the

minimum solvent ratio. As a result, the solvent ratio for chemical absorption can be estimated by the following simplified equation.

$$\frac{\dot{L_{min}}}{\dot{G}} = \frac{700}{450} \approx 1.5 \tag{6.4}$$

The minium solvent ratio for the MEA absorption process is around 1.5. For smaller loadings the ratio would even be lower.

Discription of the Process A short description of the capture process has already been given in section 3.7.1. In the following flow sheet this process has been adopted to the flow sheeting tool ASPEN Plus^{TM}.

Here, just a short description of the main differences in the simulation is given. The flue gas cooler in the simulation consists of the *DCC-1* cooling column and the precooler *C-1*. Additionally, a water separator was added to separate the condensed water. The cooling and the condensed water are combined in the mixer *M-1*.
The washing section was modeled by an external single-stage washer *W-1*. The MEA loaded washing water was recycled to the solvent.
The filter in the rich solvent stream was ignored, since no solids were incorporated in the model.
The heat exchanger was replaced by the *MHeatX* model (*HX-1*). The reclaimer was also not necessary, because of the missing modeling of solids. The mixers *M-2, M-3* were added to build an external reflux and the stripp water inlet. The partial condenser was modeled by an condenser (*C-2*) and a separator (*S-2*).
The most important difference is the mixer (*M-4*) for adding the make up water and MEA to simulate a steady state.
Further, the cyclic condensed solvent stream from the desorber was not recirculated to the desorption column because of convergence issues. Hence, the solvent stream was cooled down further and mixed to the lean solvent to decrease the solvent loss due to evaporization.

Flow Sheet Figure 6.4 shows the flow sheet in ASPEN Plus^{TM} of the post-combustion capture process based on aqueous monoethanolamine solution (larger flow sheets are given in the appendix).

6.3 Results

Now, a short overview of the simulation results is given.
At first the main characteristics and operating parameters of the process were varied to find the optimal operating point.

6.3.1 Optimisation of the Process

Reboiler Duty At an approximately constant CO_2 recovery rate between 89-91 wt%, the needed reboiler duty per ton removed carbon dioxide depending on the ratio between solvent stream (L) and flue gas stream (G) was simulated. The result is given in figure 6.5.

Figure 6.5 shows that an optimum of the solvent ratio in the absorber can be found. In this case, the optimum is at a solvent ratio of $L/G = 2.8kg/kg$. At this point an energy demand of 3.23 GJ per ton carbon dioxide is necessary to achieve an approximately 90% recovery rate.

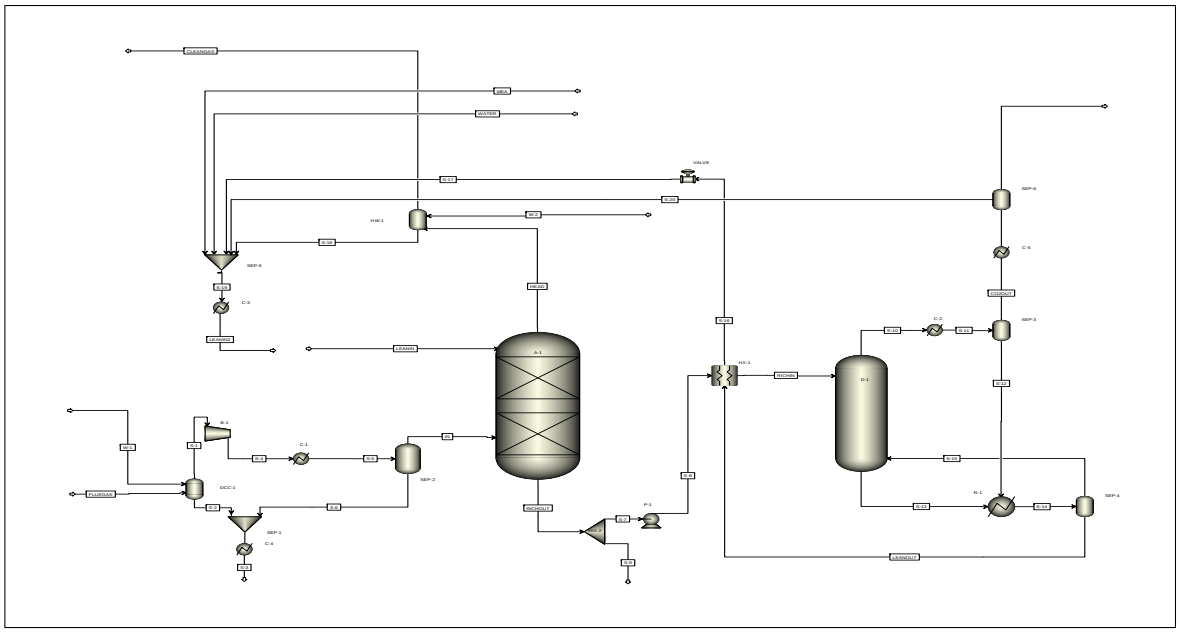

Fig. 6.4: Flow sheet of the MEA Capture process

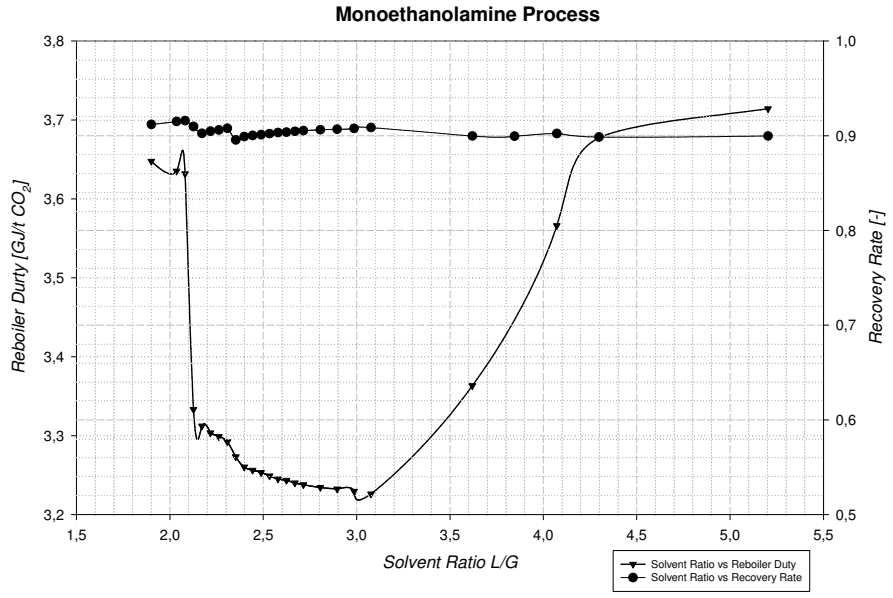

Fig. 6.5: Reboiler duty plot against absorber $\dot{L}/\dot{G}$ ratio

The energy requirement increases for higher or lower solvent ratios. For the lower ratio it must be mentioned that the minimum value (estimated in section 6.2.1) can't be under-run to keep a stable simulation. In this specific simulation the minimum is around $1.7 kg/kg$. The up- and downturns of the reboiler curve are the result of a not completely constant temperature difference between the in and outgoing streams in the heatexchanger.
Further, it appears that the process can be run between a solvent ratio of 2.3 to $3 kg/kg$ with a constant steam consumption of approximately $3.3 GJ/tCO_2$.
The minimum of the energy requirement in the reboiler curve results from the fact, that for low solvent ratios the solvent must be better regenerated to achieve the same capture efficiency. For high solvent ratios the reboiler duty also increases, because more energy is need for the change in the latent heat.

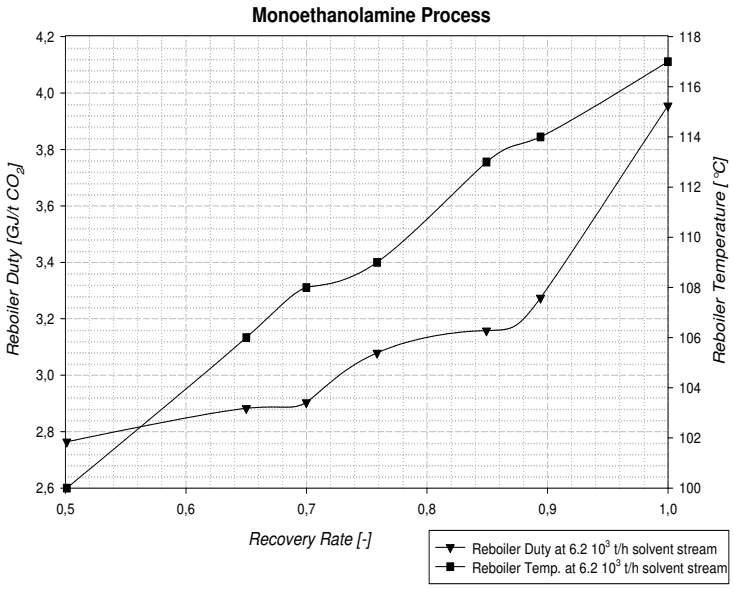

Fig. 6.6: Reboiler duty plot against carbon dioxide removal at constant $\dot{L}/\dot{G}$ ratio

Figure 6.6 shows the fact that a carbon dioxide recovery rate over 90% needs a huge energy amount, which is provided by steam. Therefore, a hundred percent recovery rate with a MEA process is highly inefficient. In this figure the ratio between solvent and flue gas is set to the optimum of 2.8. The second line in figure 6.6 shows the reboiler temperature increase resulting from the higher heating duty.
Finally, figure 6.7 summarizes the former results into one plot. Additionally the change in the loading of the aqueous solution is shown, which will be described further in section 6.3.2.

Operating Point Hence, an operating point with the optimum solvent ratio of 2.8 kg solvent per kg flue gas ($6.2 \cdot 10^3 t/h$), a reboiler duty of 1193 GJ/h and a carbon dioxide recovery rate of 90.6 wt% was fixed as reference state for the simulation.

6.3.2 Stream Results

In the following the main stream results of the simulation are presented.

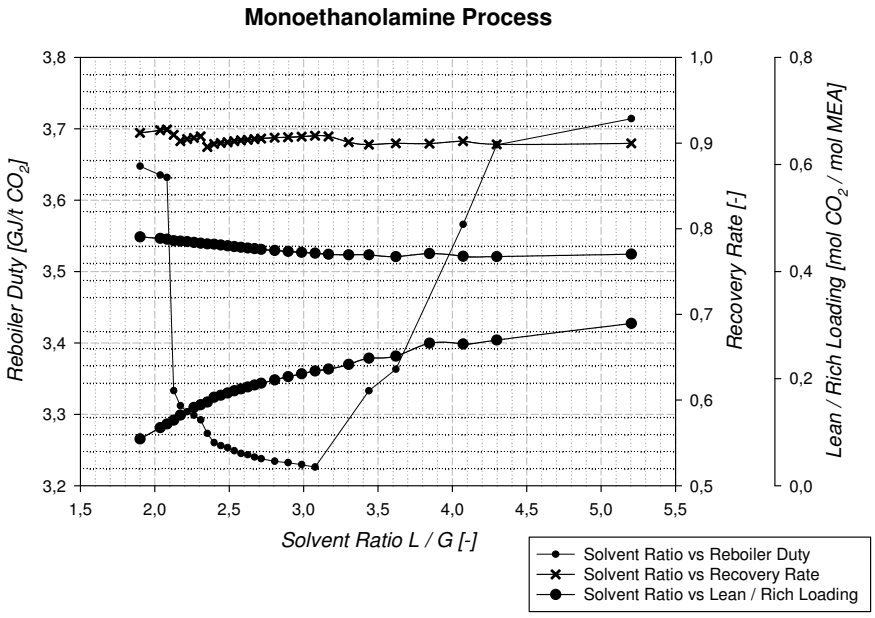

Fig. 6.7: Reboiler duty, recovery rate and solvent loading plot against absorber $\dot{L}/\dot{G}$ ratio

CO_2 Removal The capture rate of the gas stream leaving the power plant was fixed to 90 wt%. The purified flue gas stream has the following composition (see table 6.9). Because of the capture process and the assumed SO_2 and NO_x removal mainly contains nitrogen.
The MEA slip to the environment is around 0.2 PPM-wt and therefore very low, since a head washing section was added.

Tab. 6.9: Clean gas composition

Flow rate	1851112.96	kg/h
Temperature	63	$°C$
Pressure	1.01	bar
Composition:		
N_2	76.8	$wt\%$
H_20	14.6	$wt\%$
O_2	5.2	$wt\%$
CO_2	2.1	$wt\%$
MEA	$2.11E^{-03}$	$wt\%$
Ar	1.3	$wt\%$

CO_2 Recovery The composition of the pure carbon dioxide product stream based on the operating point is given by table 6.10. This is the composition of the gas stream leaving the stripper condenser. By using further cooling and seperation steps, where the gas can be cooled down to around 30°C an almost pure CO_2 stream can be produced (not treated in this work).

Tab. 6.10: Product Gas Composition

	At desorber		At final cooling	
Flow rate	405364.29	kg/h	369324.7	kg/h
Temperature	75	$°C$	30	$°C$
Pressure	1.9	bar	1.9	bar
Composition:				
N_2	3.48E^{-03}	$wt\%$	3.85E^{-03}	$wt\%$
H_20	9.6	$wt\%$	0.95	$wt\%$
O_2	4.27E^{-04}	$wt\%$	4.72E^{-04}	$wt\%$
CO_2	90.4	$wt\%$	99.03	$wt\%$
MEA	1.91E^{-05}	$wt\%$	2.25E^{-14}	$wt\%$
Ar	0.02	$wt\%$	0.02	$wt\%$

Washing solvent - MEA The composition of the solvent at the operating point has already been given in table 5.3 in section 5.3. The initial concentration of the solution was set to 30 wt%, since this value for the process parameter is most referred in literature (e.g.: [53] and [5])
Figure 6.8 shows the lean and rich solvent loading of the aqueous MEA solution at different liquid to gas ratios and at a constant capture rate of 90%. It illustrates the fact, that for a lower solvent flux a higher regeneration of the MEA solution, and therefore lower loadings of the lean solvent, are needed to achieve the same capture efficiency.
In the selected optimum operation point the lean solvent loading is around 0.2 [mol CO_2/ mol MEA] and for the rich loading 0.44 [mol CO_2/ mol MEA].

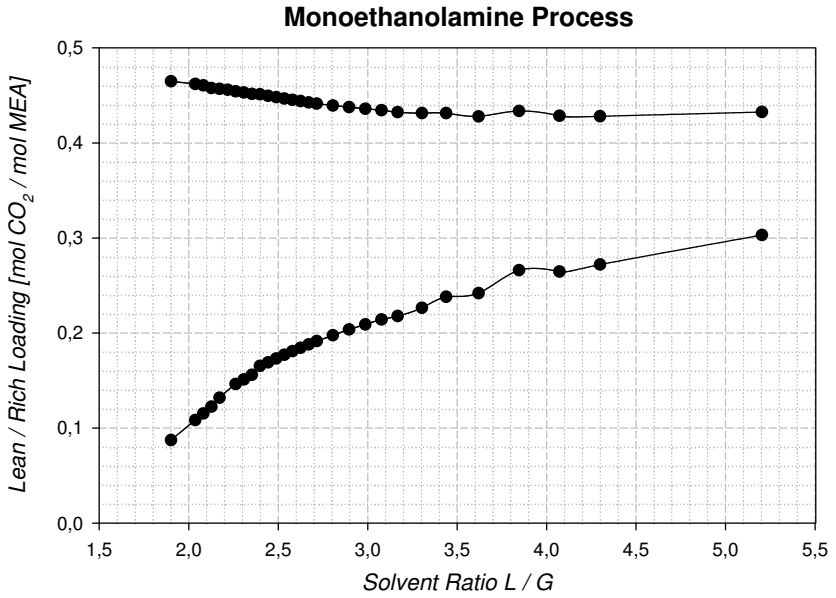

Fig. 6.8: Solvent Loading plot against Absorber L/G Ratio

6.4 Validation of the Model

To verify the model for the capture process by monoethanolamine in section 6.1, the simulation results are compared to experimental results and results by simulations in other publications.

6.4.1 The CASTOR Project

Besides the application of the MEA Process for natural gas purification, some industrial projects for flue gas treating have been realized. An example for those is the CASTOR Project, which was carried out in public and private partnership.

The Project The CASTOR (CO_2 from Capture to Storage) project was funded by the EU with aims at developing new technologies for post-combustion capture and aims at studing European storage sites. The project was handled between Feb. 2004 and Feb. 2008 with a total budget of 16 mio. €.
The project dealed with the building of a pilot plant for post-combustion capture in an existing coal-fired power planted operated by *ELSAM* in Denmark (cf. [54]).

The pilot plant is based on the design of a standard industrial amine-based carbon dioxide recovery plant with some modifications. The scheme of the pilot plant is described in figure 6.9 (cf. [55]). Moreover the operating data is given in table 6.11.

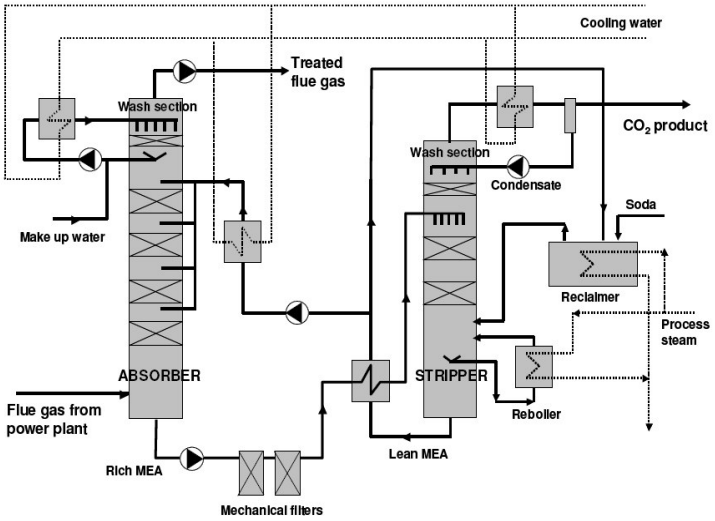

Fig. 6.9: Flow sheet of the CASTOR pilot plant [10]

Tab. 6.11: Operating data of the CASTOR pilot plant [10]

Parameter	Design value	
Flue gas capacity	5000	Nm^3/h
CO_2 removal (at 12% CO_2)	1000	kg/h
Capture percentage	90	%
Max solvent flow	40	m^3/h
Max reboiler steam flow	2500	kg/h at 2.5 bar
Max stripper pressure	2	bar
Flue gas conditions	45 °C,	<10 ppm SO_2
	<65 ppm NO_x,	<10mg/Nm^3 dust

The pilot plant was operated for 2000 hours on the reference solvent (30 wt% MEA). Afterwards, two new solvents (CASTOR 1, 2) were operated.
In this work, only the results of the MEA solvent are discussed (for further information see [55]).

Project Results Above all, the steam consumption of the reboiler in the desorption step was considered. Therefore, the heat duty in dependence to the liquid-to-gas ratio ($\dot{L}$ / $\dot{G}$) at 90% recovery and the carbon dioxide recovery at optimal $\dot{L}$ / $\dot{G}$ ratio were measured. The results are visualized in diagram 6.10 from [55].
The tests were performed at a constant desorber pressure of 1.9 bar (according to [55]).

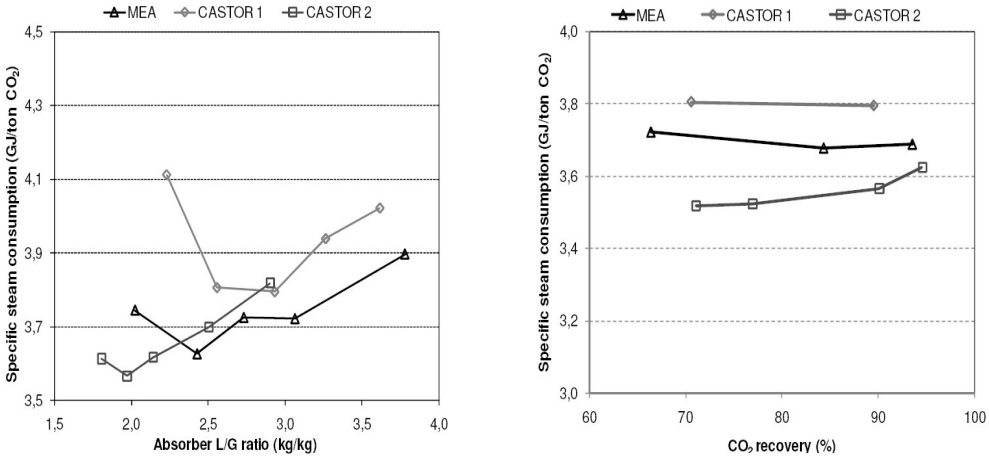

Fig. 6.10: Steam consumption Plot against liquid-to-gas ratio at 90% recovery - Steam consumption plot against recovery at optimum liquid-to-gas ratio [10]

6.4.2 Other Simulations

Simulation by Abu-Zahra et al. In the work by [53] the results for the optimum process are listed in table 6.12.

Tab. 6.12: Optimum process results by [53]

30 wt% MEA	
CO_2 Removal [%]	90
Stripper operating pressure [bar]	2.1
Amine lean solvent loading [mol CO_2/mol MEA]	0.32
Amine rich solvent loading [mol CO_2/mol MEA]	0.49
Reboiler heat requirement [GJ/t CO_2]	3.29
Solvent flow rate [m^3/t CO_2]	27.8
Lean solvent temperature [°C]	30
Cooling water:	
Feed cooling water [m^3/t CO_2]	9
Condenser [m^3/t CO_2]	24
Lean cooler [m^3/t CO_2]	57
Scrubber [m^3/t CO_2]	0.03
CO_2 product compressor intercooling [m^3/t CO_2]	13
Total cooling water required [m^3/t CO_2]	103

Simulation by Oexmann et al. The following figure (fig. 6.11) shows the reboiler curve (Reboiler duty and solvent loading plot against solvent ratio) presented by [5].

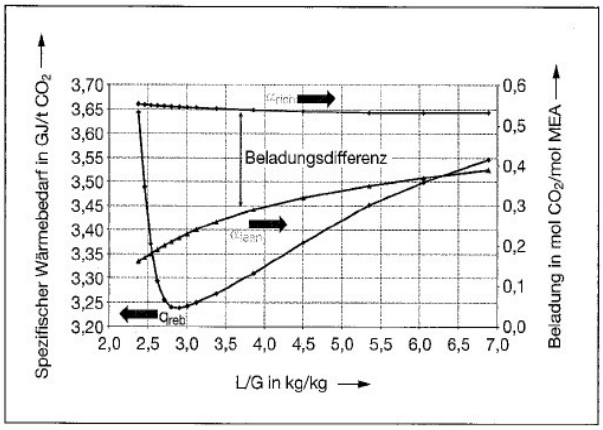

Fig. 6.11: Specific heat duty and loading at constant CO_2 carbon dioxide removal [5]

6.4.3 Validation

In this section an approximate validation between the simulation model explaind in section 6.1 and the realized CASTOR plant or other simulations was done.
Since no detailed data was available, most parameters were estimated from various diagrams.

Comparison with the CASTOR Project The results of the CASTOR project, explained in section 6.4.1, were compared to the simulation results in section 6.3.

The reboiler heat demand depending on the solvent ratio of the simulation model (expressed in figure 6.5) and the results of the CASTOR project (given in section 6.10) agree in the main points.

The minimum reboiler duty of the simulation is at a ratio of 2.8 kg/kg and around 3.3 GJ/t CO_2. At the CASTOR project results the lowest specific steam consumption is 3.6 GJ/t at $\dot{L}/\dot{G}$ ratio of approximately 2.5 kg/kg according to [55].
Thereby, it must be mentioned that the simulation uses an equilibrium based (chemical and phase equilibria) calculation approach. This fact could be a reason for the difference of approximately 0.3 GJ/t in steam consumption.
In the plant a fixed flue gas flow of $5000 Nm^3/h$ was fixed during the measurement. In the simulation a very high flue gas flow of $1750000 Nm^3/h$ was treated. Nevertheless this fact cannot be a reason for the different solvent ratio, since it is not considered in the equilibrium model.

The reduction of the reboiler steam at the optimum L/G ratio in the CASTOR project (figure 6.10) and in the simulation (figure 6.6) did not fit so well.
While in the CASTOR results the specific steam consumption increases at a lower recovery rate, it has a decreasing trend in the simulation. A reason for this could be effect of the desorber height, which was not considered in the simulation.

Comparison with other Simulations For further validation of the simulation the results of this work were compared to other simulations.

The simulation results by [53] treat a similiar fluegas and the therefore the reboiler duty matches well. The lean loading difference between the simulations is around around 0.1 [mol/ mol solvent]. One possible reason could be the different desorber pressure. Nevertheless the loading of the rich solvent compares very well. The deviation here is just around 0.05 [mol/ mol solvent].
Figure 6.11 by [5] shows a similiar tendency as our simulation results. The specific reboiler duty at a certain solvent to flue gas flow ratio agrees quite well.
The loadings for the lean and rich solvent differ from each other at approximately 0.1 $[molCO_2/molMEA]$. One possible reason for the deviation could be again the higher desorber pressure in [5] of 2.1 bar.

All in all we conclude that the simulation gives a realistic description of the energetic desorber performance. At least enough for an approximate, overall energetic comparision of the capture process with others.

7 Chilled Ammonia Process

7.1 Modeling of the Capture Process

This section shows the modeling of the post-combustion capture process based on an aqueous ammonia solution.

7.1.1 Properities

The properties used in the model are given in the following.

Chemistry The chemistry of the $NH_3 - CO_3 - H_2O$ system and its related equilibrium constants are listed in table 7.1. The modeling is based on the approach by recommended [56].

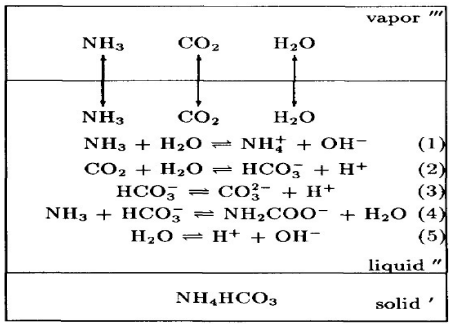

Fig. 7.1: Precipitating Reactions in the $NH_3 - H_2O - CO_2$ System [57]

The dissociation constants for the reactions (3.63) (the dissociation of water), (3.61) (the dissociation of carbon dioxide) and (3.62) (dissociation of bicarbonate) were adopted from the MEA chemistry section and therefore from [17], since these reactions take place in both systems.
The temperature-dependency of the solubility constant of ammonium bicarbonate ($NH_4HCO_{3(s)}$) was taken from an expression given by [57].

$$lnK = 8.3413 - \frac{2465.32}{T} \tag{7.1}$$

The temperature-dependent dissociation constant for ammonium bicarbonate is listed in equation (3.65) of table 7.1.
The equilibrium constant for the formation of the ammonium carbamate ion (NH_2COO^-) (reaction (3.64)) is given by [58]. Further, the equilibrium constant for the dissociation of ammonia (reaction (3.60)) was adopted by the ASPEN Plus template *nh3co2* or rather imported with the *ElecWizard* tool by ASPEN Plus^{TM}. According to [59], the only additional solid that can be formed at these process conditions is $(NH_4)_2CO_3 \cdot H_2O$ in the chilled lean solvent to the absorber. By pre-giving a fixed CO_2 initial concentration, it can be ensured that ammonium carbonate does not precipitate.
Also the formation of the other solids at these process conditions was neglected. As a result, the dissociation constants for equations (3.66) to (3.68) were set to zero.
Finally, the considered reactions can be summarized in figure 7.1.

Tab. 7.1: Equilibrium Constants for Aqueous Ammonia

Reactions	C_1	C_2	C_3	C_4	**T [°C]**
K_1 (3.60)	-1.256563	-3335.7	1.4971	-0.037057	-
K_2 (3.61)	231.465439	-12092.1	-36.781601	-	0-225
K_3 (3.62)	216.050446	-12431.7	-35.481899	-	0-225
K_4 (3.63)	132.89888	-13445.9	-22.477301	-	0-225
K_5 (3.64)	-4.583437	2900	0	0	-
K_6 (3.65)	8.3413	-2465.32	0	0	36 - 200
K_7 (3.66)	0	0	0	0	-
K_8 (3.67)	0	0	0	0	-
K_9 (3.68)	0	0	0	0	-

Property Base Method As base property method the UNIQUAC-NRF model proposed in [45] would be predestined, since lots of data are given by [24]. The main property insert for the UNIQUAC-NRF model are the r_i and the q_i parameters for pure chemicals i.

Unfortunately, the UNIQUAC-NRF model is not yet available in ASPEN Plus^{TM} (cf. [46]). As a result, the ELECNRTL-RK model was again selected as base property method.
Therefore, the adjustment parameters *NRTL* for molecule-molecule interaction (τ_{ij}) and *GMELC* for electrolyte-molecule interactions were adopted from the *nh3co2* template by ASPEN Plus^{TM}, especially from the ASPEN Plus^{TM} intern data bank *ENRTL-RK*.
The property data package *nh3co2* is valid up to pressures of 17 atm, 23 mol/kg NH_3, 9 mol/kg CO_2 and temperatures of 110°C (according to [52]). Nevertheless, some operation parameters do not fit the validity of the data package, the data set was used in the simulation due to the lack of other suitable property data sets or experimental results. But the optimum process parameters were selected in the range of the validity of the property insert as good as possible to limit the uncertainty of the simulation results.
For further validation of the simulation results the phase diagrams for the binary mixture were calculated and showed good agreement.
The data set for the VLE was compared with data from the *"DECHEMA Chemistry Data Series"*. The phase diagram at a constant pressure (T_{xy}) of 1.01 bar is given in figure 7.2. The calculated and measured data agree quite well. Besides, it has to be mentioned that measured data were only available at low concetrations of ammonia and therefore the data set results into a straight line with the boiling temperature of ammonia as final point.

The phase diagrams at constant temperatures of 60°C and 147°C were calculated and compared to the data from [51]. At the lower temperature the agreement is also very good, shown in figure 7.3. At the higher temperature and therefore at higher pressure the deviation increases. For example at NH_3 mole fraction of 0.3 the deviation is around 0.5 bar, see also figure 7.4. But the deviation of the experimental and calculated date in the operation point with a mole fraction of 0.08 mole NH_3 per mole H_2O is almost zero.
Figures 7.2 to 7.4 give an overview of the good fit of the binary data between NH_3 and H_2O. On the other hand, one of the main issues of this model is the improper valdiation of the ternary $NH_3 - H_2O - CO_2$ system and the solid-liquid equilibria, because of the more complicated modeling approach and missing specific experimental data at operating conditions for the validation. Another main property parameter for the ELECNRTL method is the dielectric constant. This parameter was regressed by experimental data for Ammonia (see next paragraph).

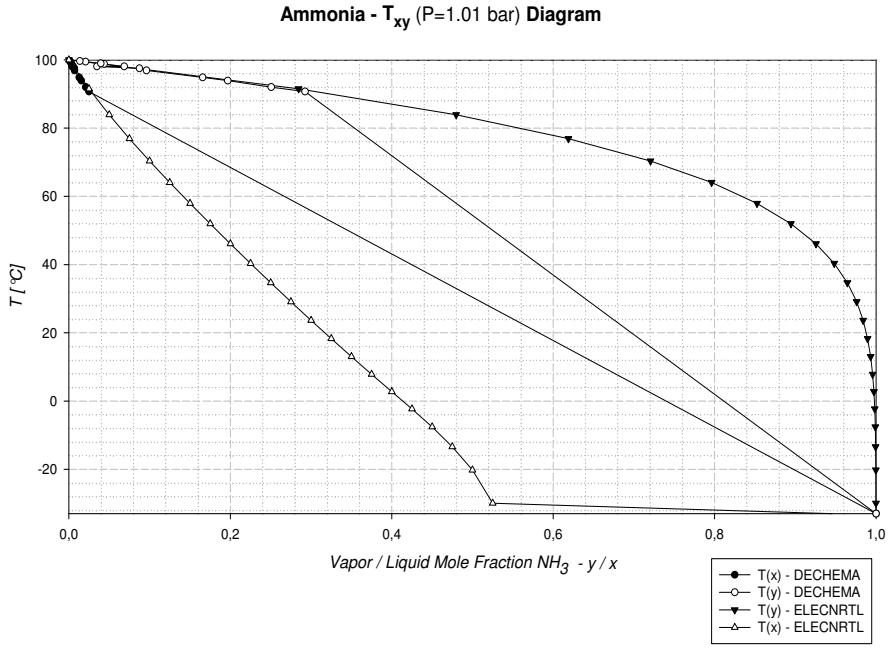

Fig. 7.2: Vapor Liquid Equilibria of the system $NH_3 - H_2O$ at 1.01 bar

Property Inserts The property inserts are based on an ASPEN Plus^{TM} propertiey template named *nh3co2*.

This data set was updated with property data correletations from various sources. Especially, pure component data were added.

Because of the importance of the dielectric constant in the ELECNRTL model, this pure component parameter was regressed from a polynomial function by [60] and compared to an experimental data set from *clippercontrols.com* [61] (given in table 7.2).

Tab. 7.2: Dielectric constant experimental data for ammonia

Dielectric constant of Ammonia	Temperature in °C
26	-80
25	-59
22	-40
20	0
17	20
16.5	20.5

From the polynomial function (equation (7.2)) and the data set a temperature-dependent and suitable for ASPEN Plus^{TM} function was regressed (equation (7.3)) according to equation (4.60).

$$\epsilon_r(T) = 66.756 - 0.24696 \cdot T + 0.00025913 \cdot T^2 \tag{7.2}$$

The reference temperature for this function is 293.2°K with $\epsilon_r(293.2K) = 16.61$. Although, this

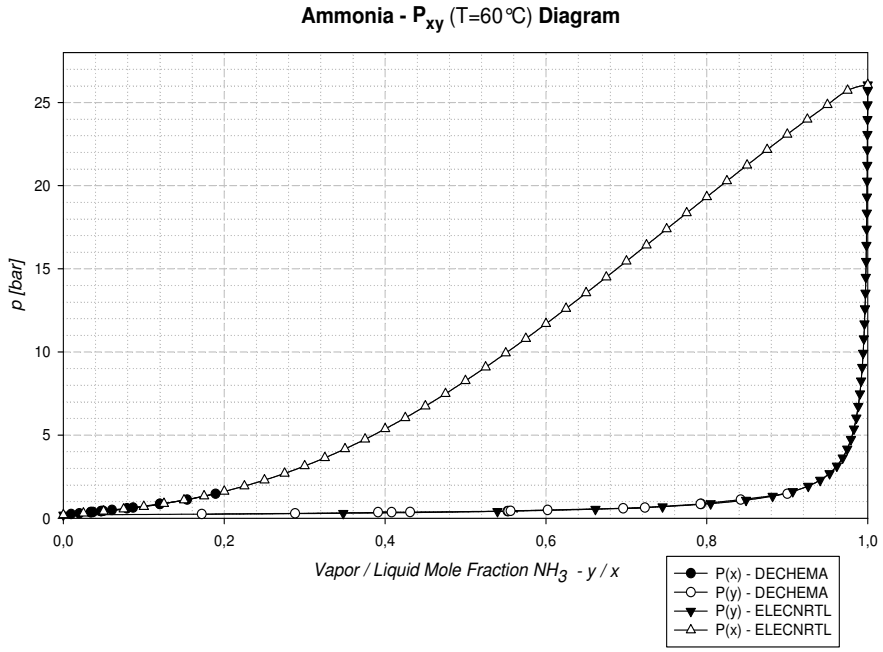

Fig. 7.3: Vapor Liquid Equilibria of the system $NH_3 - H_2O$ at 60°C

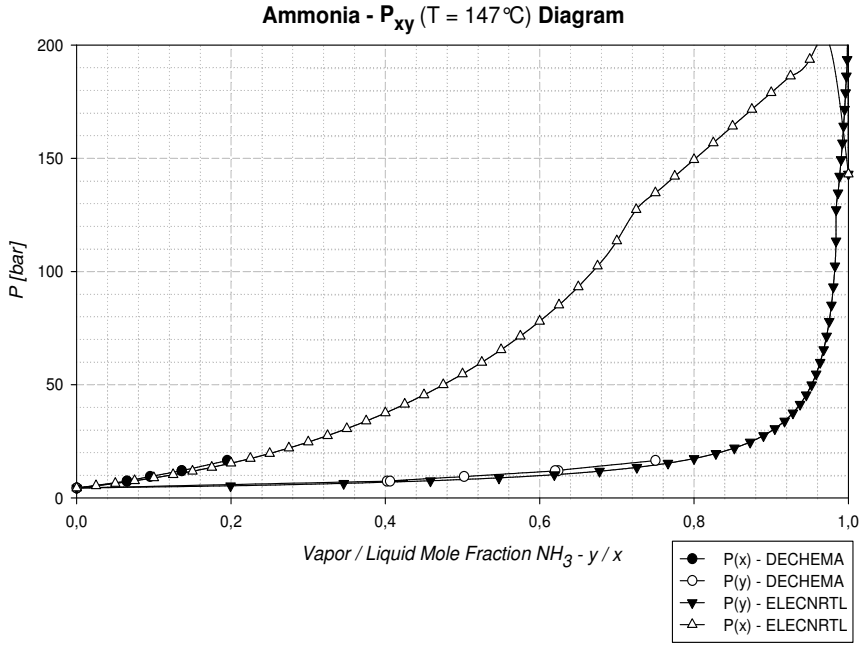

Fig. 7.4: Vapor Liquid Equilibria of the system $NH_3 - H_2O$ at 147°C

function is just valid in a temperature range between 238°K / -35.14°C and 323°K / 50°C it was used for the simulation. The regression procedure is illustrated in figure 7.5.

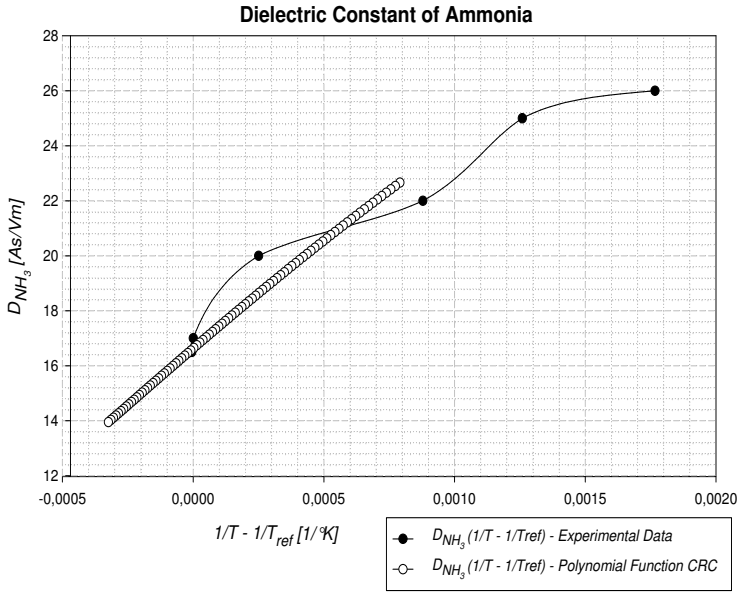

Fig. 7.5: Regression of the Dielectric Constant of ammonia from experimental data

$$D_{NH_3} = 16.595 + 7870.1 \cdot (\frac{1}{T} - \frac{1}{293.2}) \tag{7.3}$$

The property data set for the infinite dilution aqueous phase heat capacity *CPAQ0* for the $NH_3 - H_2O - CO_2$ system was taken from the *nh3co2* property template of ASPEN Plus^{TM}. Henry's constant for CO_2 in water was fitted again to the data by [17].

For the modeling of the solid ammonium bicarbonate (NH_4HCO_3) property data from [24] were used. According to the assumption by [24], the solid heat capacity for species was taken as constant for ammonium bicarbonate. The value of C_1 in the calculation model (given in equation (4.67)) was set to $32.20\frac{kJ}{mol \cdot K}$.

The solid molar volume was also assumed to be constant and was calculated by the molar weight and density of NH_4HCO_3. The molar weight for ammonium bicarbonate $M = 79.06g/mol$ and ammonium carbamate $M = 78.07g/mol$ were take from the *National Institute of Standards and Technology* (NIST).

$$v_m^s = \frac{M_s}{\varrho_s} = \frac{79.06g/mol}{1.59g/cm^3} = 49.72cm^3/mol \tag{7.4}$$

This value was used for the constant C_1 in equation (4.75).
Remaining pure component property data were taken from the ASPEN Plus^{TM} databanks *ASPENPCD, SOLID, INORGANIC, PURE11* from [52].

7.1.2 Components

In this section the used components and their operating data for modeling the capture process are explained shortly (visualisation see flowsheet 7.6).

Columns For the absorber and desorber columns the RadFrac model was selected again for the simulation approach, because of the same reasons described in section 6.1.2. The number of the separation steps are not representative for a real absorption column because of the equilibrium based calculation approach of the RadFrac model (more details to the column height are given in section 8.2.1).
The operating data of the columns in the optimum point are given in table 7.3.

Tab. 7.3: Absorber and desorber operation conditions - CAP

	A-1	**D-1**
Average temperature [°C]	37.5	162
Pressure [bar]	1.01	20
Pressure drop [mbar]	100	100
Reboiler	No	External
Condensator	No	External
Theoretical separation stage	5	6

At this point, it should be mentioned, that the cooled head washing section (described in section 6.2.1) can be seen as an additional indermediate cooled separation stage.

Heaters and Coolers These were modeled by the heater model in ASPEN Plus^{TM}, which is described in section 6.1.2.
There are 4 coolers and 2 heaters in the simulation: the solvent cooler (*C-1*), the flue gas direct cooler (*C-2*), the condenser (*C-3*), the overhead cooler (*C-4*) and as heaters the desorber reboiler (*R-1*) and the heater (*H-1*), which was supposed to maintain a constant solvent temperature. A constant solvent temperature at this point was necessary for manual data transfer to the ingoing lean solvent stream into the absorber. The additional cooler (*C-4*) compared to the MEA Process was necessary to cool down the outgoing head product of the absorber and limit therefore the ammonia slip to the atmosphere.
The operation conditions of the heaters and coolers in the selected optimum operation point are summarized in table 7.4.

Tab. 7.4: Heaters operation conditions - CAP

	C-1	**C-2**	**C-3**	**C-4**	**R-1**	**H-1**
Temperature [°C]	10	10	145	15	187	30
Pressure [bar]	1.01	1.01	1.01	20	20	1.01
Pressure drop [mbar]	0	0	0	0	0	0
Cooling/ Heating Duty [MW]	−63.2	−210.5	−6.9	−188.9	234.4	60.5

The cooler *C-5* for the recooling of the water, which was used for the quenching of the flue gas, and the pure CO_2 product gas cooler *C-6* were only added to the optimum process to make both processes easier comparable. In *C-5* the quench water was cooled down to 17°C, which resulted in a cooling duty of -30.3 MW. For the cooling of the product gas to 30°C at a pressure of 20 bar -45.6 MW were necessary.

Heat exchanger As heat exchanger the *MHeatX* model in the ASPEN Plus^{TM} simulation program was selected again because of its good convergence characteristics. The temperature

difference between the ingoing rich solvent stream and the outgoing lean solvent stream was hold constant to approximately $T \approx 10K$, which is already very hard to achieve with solvents containing solids (slurry).

Flash Several *Flash* units (explained in section 6.1.2) were needed in the simulation. The fluegas cooling column *DCC-1*, the separation unit for the condensed water in the fluegas *SEP-1*, the vapor-liquid separators for the solvent reflux in the desorber *SEP-3* and *SEP-4*, and finally the head washing column *HW-1* to minimize the ammonia slip. In all of them the pressure drop was set to zero and no heating or cooling duty was fixed.

Pumps and blowers The solvent pump *P-1* was modeled again by the ASPEN Plus^{TM} model *Pump* and the flue gas blower *B-1* by the *Compr* model. The pressure change from desorber to absorber was simulated by the *Valve* model called *VALVE* in the simulation. Additionally, a compressor for the refigeration system was necessary (*B-2* not shown in the flow sheet). The operating data in the optimum is given in table 7.5.

Tab. 7.5: Pump, Blower and Valve operation conditions - CAP

	P-1	**B-1**	**B-2**	**VALVE**
Pressure Increase/ Decrease [bar]	19	0.2	9.5	19
Pump Efficiency	–	0.86	–	–
Type	-	*Polytropic*	*Polytropic*	–
Power [MW]	2.1	15.3	67	0

Mixers and Spliters In the simulation 3 mixers and splitters were used (*M-1*, *M-2* and *SEP-2*).

7.1.3 Overall Mass Balances

Because of the ingoing water in the flue gas and the loss of ammonia and water in the clean gas and CO_2 product streams, at least the two main balances had to be calculated to achieve a neutral mass balance and avoid the building up of the streams.

Water Balance The ingoing water in the system is the make-up water, which is needed because of the separation of condensed water, the gaseous water in the flue gas, the water used to cool the flue gas and the water for the head wash. Whereas water goes out with the separation of the condensed water in the flue gas, the water in the clean gas stream, the water in the product stream and the water brought out by the additional separator, which is needed if too much water gets into the system.

$$\dot{m}^W_{makeup} + \dot{m}^W_{fluegas} + \dot{m}^W_{DCC} + \dot{m}^W_{wash-water} - \dot{m}^W_{DCC+Kond}$$

$$- \dot{m}^W_{cleangas} - \dot{m}^W_{co2,out} - \dot{m}^W_{sep} = 0 \tag{7.5}$$

The balance was realized in the simulation by implementing a design specification by which water was added using the make up stream, if the balance was negative, or separating water by the separation block *SEP-2*, if the balance was positive.
In the case of the CAP water had to be separated from the system. The reason is, that because of the low outgoing clean gas temperature more water is going in the system as leaving it. By

the design specification in ASPEN Plus^{TM} an amount of 8500 kg/h water was calculated, which had to be separated by the separation block.
Since a separation of just water was not possible, also ammonia and all its ions were separated and had to be added to the system by the make-up stream. This fact contributed to the make-up amount.

NH_3 Balance Because of the change in the amount of water and the loss of NH_3 due to evaporation in the product or clean gas stream also ammonia had to be added to the system. When the solvent stream was separated in the splitter unit *SEP-2*, all of the ionic forms of NH_3 were also removed. Therefore an equivalent amount of ammonia had to be added for them. Thus, a mole flow balance was chosen instead of a mass balance.

$$\dot{n}_{makeup}^{NH_3} - \dot{n}_{cleangas}^{NH_3} - \dot{n}_{co2,out}^{NH_3} - \dot{n}_{sep}^{NH_3}$$

$$- \dot{n}_{sep}^{NH_4^+} - \dot{n}_{sep}^{NH_2COO^-} - \dot{n}_{sep}^{NH_4HCO_3} = 0 \tag{7.6}$$

This fact was realized again by a design specification. The results for the make-up amount are given in section 8.1.5.

7.2 Simulation of the Capture Process

In this section the simulation and its flow sheet are presented.

7.2.1 Simulation

Discription of the Process A short overview of the process has already been given in section 3.7.2.
Some of the main changes to this explanation are the additional separator (if too much water gets into the system) *SEP-2*, the head cooler *C-4* to minimize the ammonia slip, the quench water stream *W-1* to cool down the flue gas and therefore the cooler *C-5* to avoid heating up. The condensed water stream in the desorber was added directly to the reboiler unit *R-1* to benefit the convergence of the model.
The cooled head stream washing section (head cooler *C-4* and single stage separator *HW-1*) can be seen as an additional intermediate cooled stage of the absorber.
The cyclic condensed solvent stream from the desorber was not recirculated to the desorption column because of convergence issues. Hence, the solvent stream was cooled down further and mixed to the lean solvent to decrease the solvent loss due to evaporization.
The final cooling system of the product gas was necessary to get the same output streams for both processes.

Flow Sheet The flow sheet of the simulated Chilled Ammonia Process is given in figure 7.6 (larger flow sheets are given in the appendix).
The refrigeration system is not visulaized in the flow sheet.

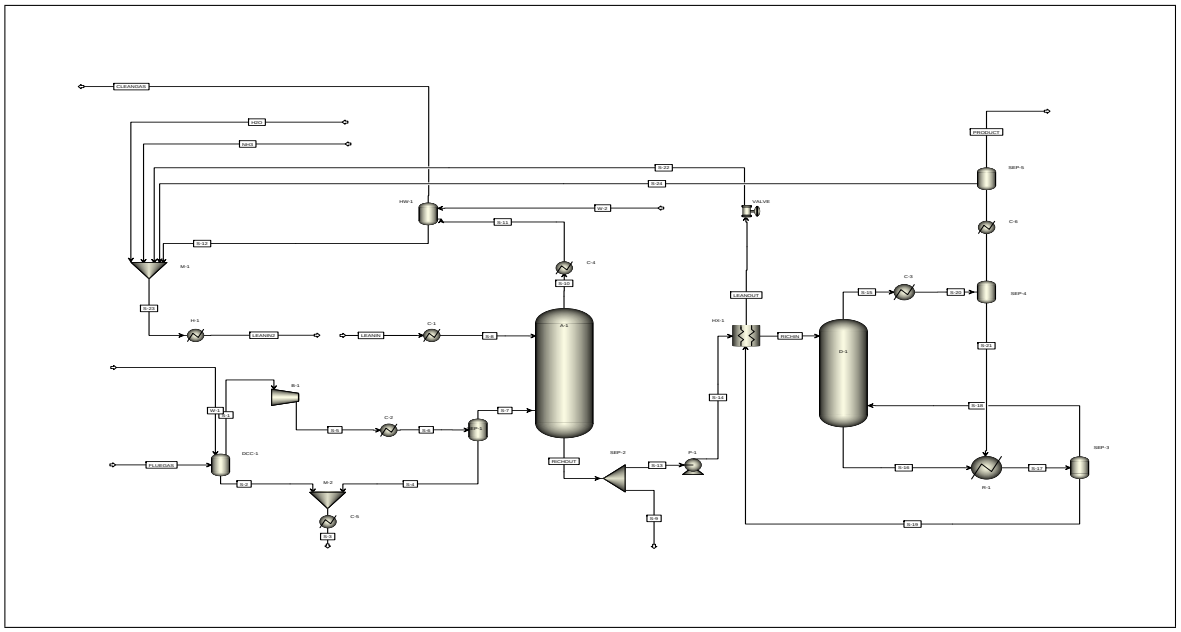

Fig. 7.6: Flow sheet of the Chilled Ammonia Process

7.2.2 Refrigeration System

To provide the coolers, which work under the fixed river temperature of 15°C, with cooling water a classical chilling system was used (not shown in the flow sheet).
As cycle medium ammonia was selected, because of its availability in the system. The ammonia was cooled at a pressure of 14 bar down to 20°C (vapor fraction zero) with river water, which was heated from 15 to 21°C. Afterwards NH_3 was expanded to a pressure of 5.5 bar in an expansion valve. Therefore, the Joule-Thomson effect (adiabatic expansion) lead to the further down cooling of the agent to 7°C. The 7°C ammonia was used for the coolers and thereby heated up until vaporization (vapor fraction equal one). Finally, NH_3 was brought back to the initial pressure of 14 bar by using a compressor. Thus the cycle could be closed.
The results for the compressor energy demand and the necessary river water flow for the first heat exchanger are given in table 7.5 and 8.3.

7.3 Results

In this section the main simulation results are given.

7.3.1 Optimisation of the Process

A representative process with optimum process parameters had to be created to carry out a comparison of the two process.
The main process parameters as solvent ratio, reboiler duty and pressure were varied to find the optimum process conditions.

Effect of the Desorber Pressure At first, the influence of the desorber pressure on the reboiler duty and the fraction of ammonia in the pure CO_2 product gas stream was simulated.
The reboiler curve in figure 7.7 shows that an optimum of the needed reboiler duty is around 20 bar. For higher pressures the heat requirement increases. Moreover the reboiler temperature

increases almost linear with the desorber pressure. At this point it must be mentioned again, that the used property data package in this model is just valid up to 17 bar (according to [52]), hence these simulation results should be seen as critical. Since the difference between the valid model pressure and the optimum pressure was not so far, it was selected nevertheless for further calculations.
Figure 7.7 shows that by increasing the pressure in the desorption column the slip of NH_3 in the product gas can be minimized further.

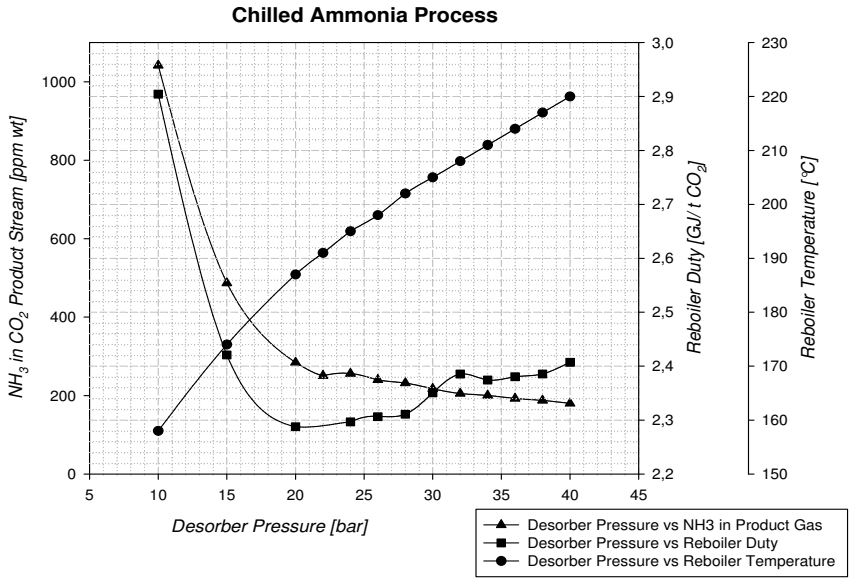

Fig. 7.7: Influence of the desorber pressure

Effect of the Solvent Cooler Temperature Since the absorption column in this simulation model had no itermediate cooling system, the solvent and flue gas cooler were the only possiblity to influence the absorber temperature. The ammonia slip to the head gas stream of the absorption column depends primary on the absorber temperature. Figure 7.8 shows clearly, that with increasing solvent temperature the ammonia slip to the absorber head stream increases in-line. For the optimum simulation a solvent cooler temperature of 10°C was selected, since it is a compromise between cooling duty and ammonia slip. Besides, the slip to the head gas stream could not be reduced under 100 PPM even at 1°C cooler temperature. Thus, the head cooler was necessary.
The impact of the temperature on the chemical absorption of carbon dioxide into ammonia can be seen in figure 7.9, which gives the absorber parameters in the optimum operation point. It shows that the largest difference in the composition of CO_2 in the vapor phase and the composition of the physically solved CO_2 in the liquid phase and therefore the largest mass transfer flux (see equation (3.70)) is at low temperatures on stage 4, above the entering flue gas.
The conversion in the concentration difference at stage 5 results from the used scale. In addition, the constant liquid composition of carbon dioxide in the liquid phase from stage 4 to 5 indicates the fully loaded solvent.

Effect of the Desorber Condenser Temperature Another operating parameter, which effects the quality of the product gas is the condenser temperature of the desorber. Since in this

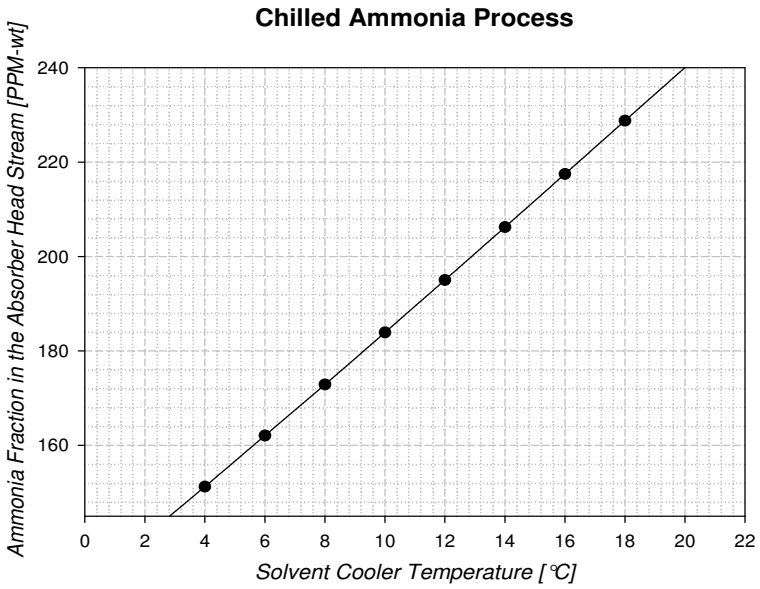

Fig. 7.8: Influence of the solvent cooler temperature

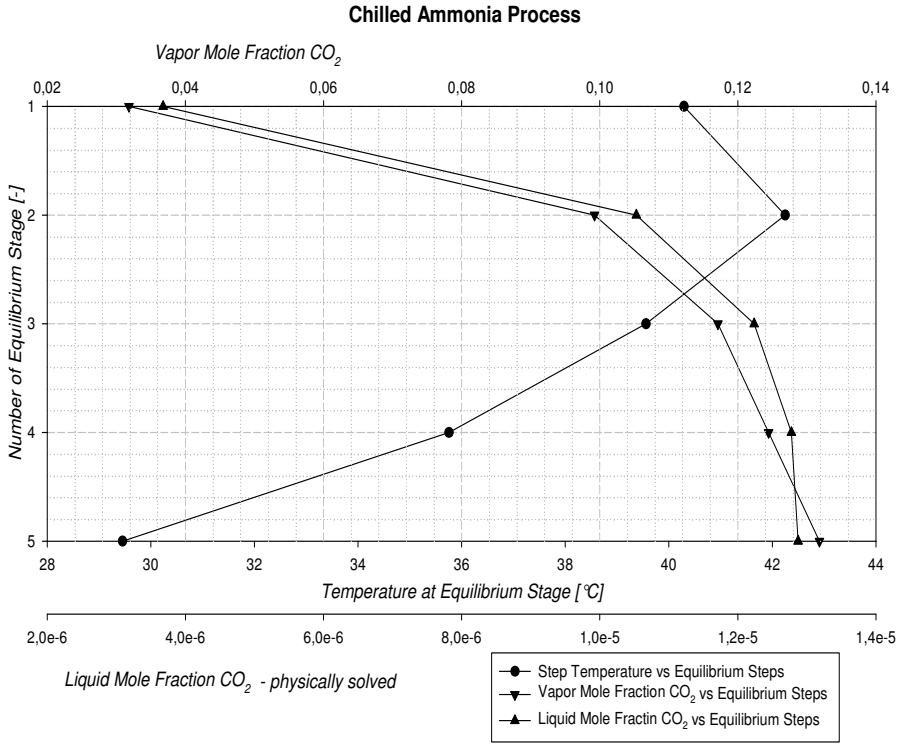

Fig. 7.9: Absorber Temperature, Vapor/ Liquid Composition of carbon dioxide on each equilibrium stage

simulation the condensed solvent was recirculated to the stripper, the condenser temperature effected the reboiler duty. In real columns this amount would be probably added to the absorber. But this will lead to further cooling duty of the lean solvent.
For comparability reasons approximately the same temperature difference between reboiler and condenser temperature as in the MEA Process (50 K) was fixed.
Because no specific requirements for the product gas were made, the condenser temperature was set to 145°C to optimize the heat requirement in the reboiler.

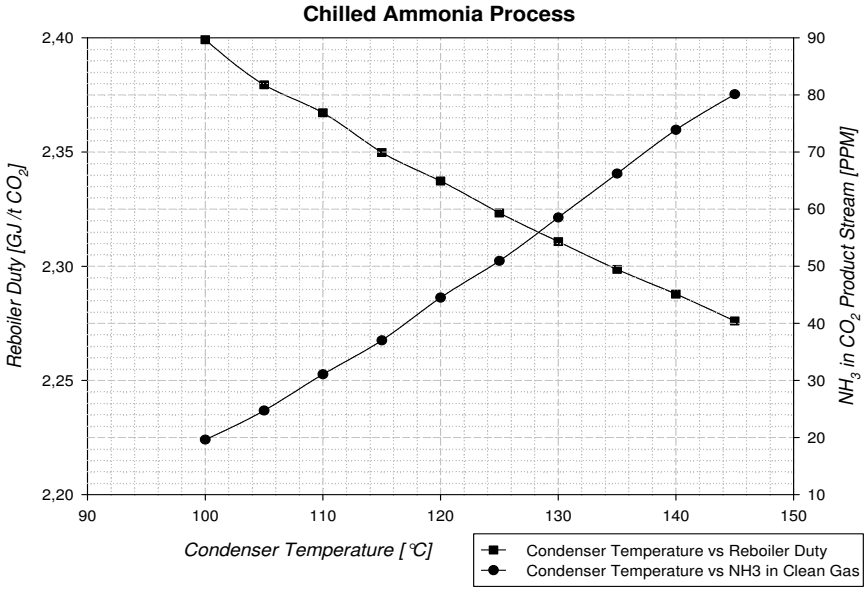

Fig. 7.10: Influence of the condenser temperature

Reboiler Duty One of the main parameters of the capture process is the heat/ steam requirement in the reboiler. At constant pressure the reboiler duty depends on the liquid to gas flow solvent ratio. This fact is expressed in figure 7.11. This figure shows clearly, that there is an optimum reboiler duty at a specific solvent ratio. It expresses the fact, that on the one hand a smaller amount can be regenerated more or on the other hand a larger amount can be less regenerated to generate the same capture efficiency.
The carbon dioxide removal rate from the flue gas was set constant to approximately 90% by using a design specification in ASPEN Plus^{TM}. By fixing the reboiler duty, the lean loading of the solvent is also fixed.
In this simulation the lowest heating requirement (2.23 GJ/t CO_2) was achieved at a solvent ratio of 1.45.
Figure 7.11 shows that the ammonia slip into the clean gas depends hardly on the solvent ratio or on the reboiler duty. The ammonia slip to the atmosphere after the additional head wash is always around 40 PPM-wt.

Lower ammonia concentrations in the clean gas could be achieved by better cooling of the absorption column, the lean solvent and the fluegas. In this simulation, the lean solvent and flue gas temperature were set to 10°C, which lead to an average column temperature of 37.5 °C. Lower solvent and flue gas temperatures were not seen as reasonable, because of the increasing cooling requirement and the more difficult realization.
A more detailed presentation of the temperature in the desorption column is given by figure 7.12. It shows the temperature, vapor and liquid composition of carbon dioxide on each equilibrium

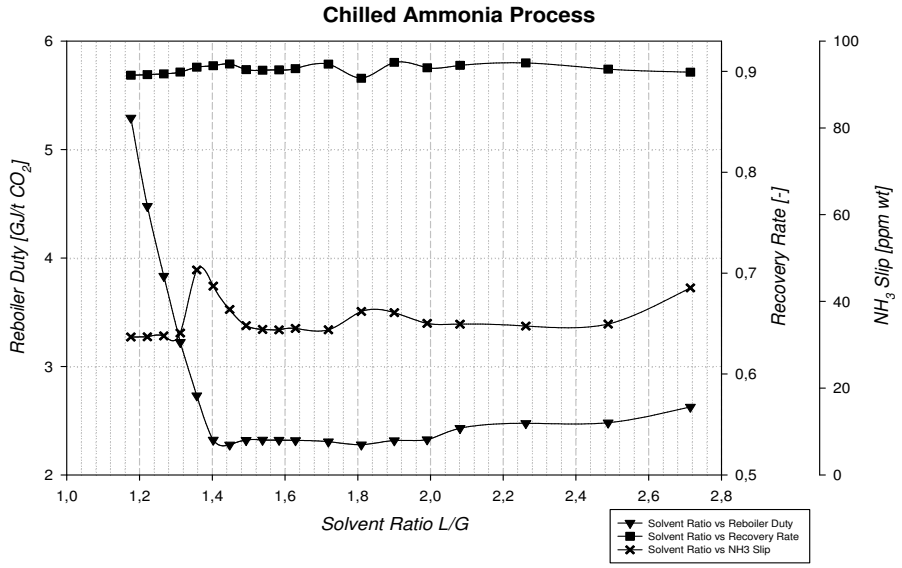

Fig. 7.11: Reboiler Duty plot against absorber $\dot{L}/\dot{G}$ ratio

stage in the simulated process.

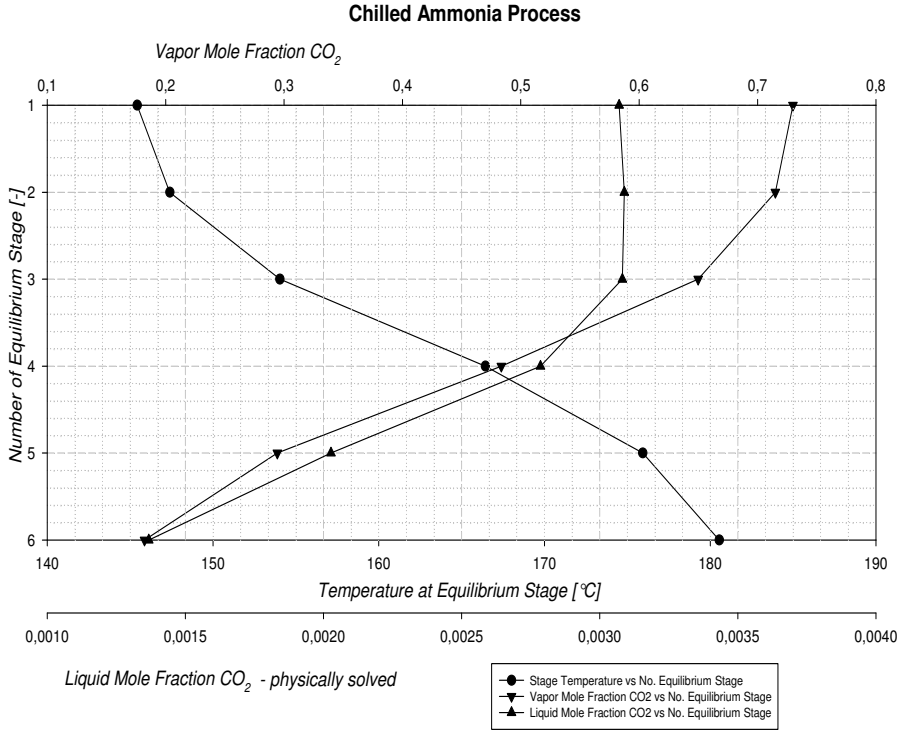

Fig. 7.12: Desorber temperature, vapor/ liquid composition of carbon dioxide on each equilibrium stage

As visualized in figure 7.12 the desorber temperature decreases from the bottom (stage 6 reboiler stream) towards the top. The energy is necessary for the evaporation of water, the back

reaction of the capture step and the sensible heat. Whereas the liquid mole fraction of carbon dioxide from stage 1 (ingoing rich solvent) to stage 6 (outgoing lean solvent). The composition of the vapor phase increases in the contrary direction. The approximately constant liquid composition of the physical solved carbon dioxide from stage 1 to 3 indicates, that the temperature is too low for the desorption of the CO_2.

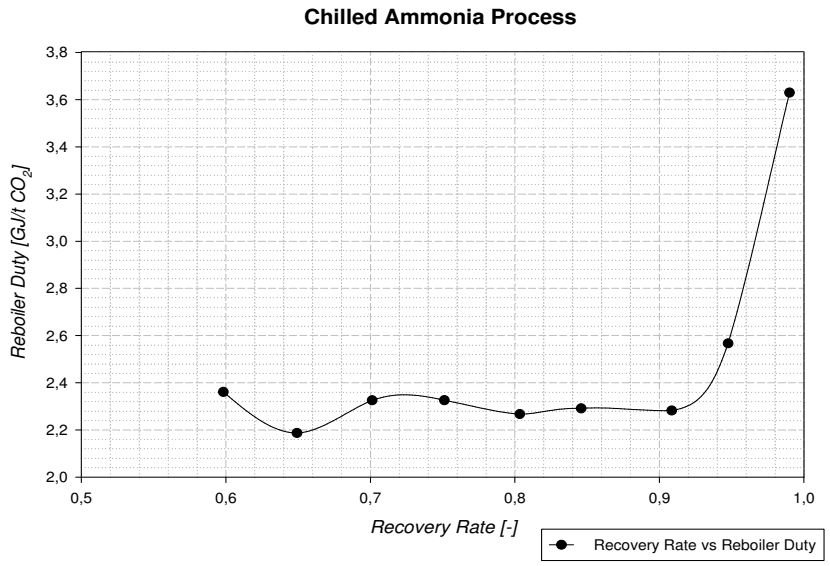

Fig. 7.13: Reboiler duty plot against recovery rate

Figure 7.13 expresses that for carbon dioxide removal or recovery rates over 95 wt% the reboiler duty requirement increases up to 3.6 GJ/t CO_2.

Figure 7.14 summarizes the main process parameters including the lean and rich solvent loading, which is mentionend in the next section 7.3.2.

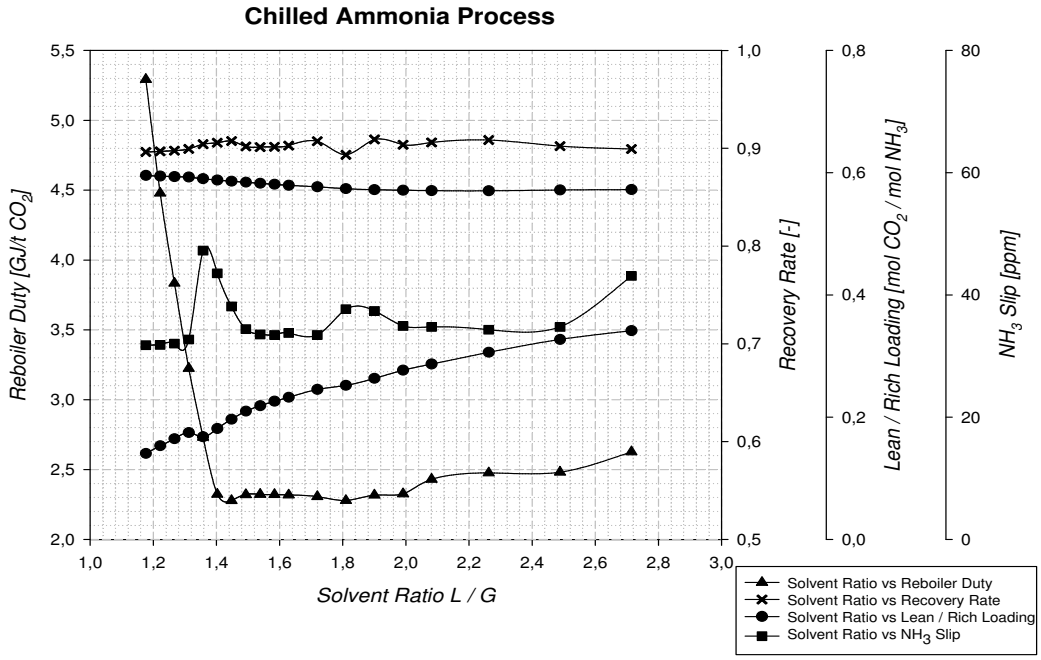

Fig. 7.14: Reboiler duty, recovery rate, solvent loading and ammonia slip plot against absorber $\dot{L}/\dot{G}$ ratio

Optimum Operating Point The optimum operating point for the Chilled Ammonia Process was set to a solvent ratio of 1.45 [kg solvent/ kg flue gas] with a specific reboiler duty of 2.23 GJ/t CO_2. Further a desorber pressure of 20 bar and a lean solvent and flue gas temperature entering the absorption column of 10°C were selected.

7.3.2 Stream Results

In this section the results for the main streams calculated in the simulation are shortly summarized.

CO_2 Removal The purified flue gas stream had the following composition (see table 7.6). For the minimization of the ammonia slip to the atmosphere a head cooling system with a constant temperature of 15°C was chosen. This cooling step from 40°C to 15°C is necessary to reduce the otherwise immense water requirement of the downstream water-ammonia scrubber. Hence the outgoing amount of ammonia to the atmosphere was fixed to approximately 40 PPM-wt by implementing the head cooler.

Tab. 7.6: Clean gas composition

Flow rate	1597477.96	kg/h
Temperature	14	$°C$
Pressure	1.01	bar
Composition:		
N_2	89.0	$wt\%$
H_20	0.9	$wt\%$
O_2	6.0	$wt\%$
CO_2	2.2	$wt\%$
NH_3	0.4	$wt\%$
Ar	1.5	$wt\%$

CO_2 Recovery The composition of the pure carbon dioxide product stream based on the operating point is given in table 6.10. This is the composition of the gas stream leaving the desorber condenser. By using further cooling and separation steps the gas can be cooled down to around 30°C and an almost pure CO_2 stream can be produced (not treated in this work).

Tab. 7.7: Product gas composition - CO_2 stream

At condenser			At final cooling	
Flow rate	405364.29	kg/h	337116.8	kg/h
Temperature	140	$°C$	30	$°C$
Pressure	20	bar	20	bar
Composition:				
N_2	6.21E^{-03}	$wt\%$	7.63E^{-04}	$wt\%$
H_20	8.0	$wt\%$	0.1	$wt\%$
O_2	0.2	$wt\%$	0.24	$wt\%$
CO_2	88.9	$wt\%$	99.6	$wt\%$
NH_3	2.8	$wt\%$	1	$PPM - wt$
Ar	0.04	$wt\%$	0.05	$wt\%$

Washing solvent -Ammonia The composition of the solvent in the operating point has already been given in table 5.4 in section 5.3.
Figure 6.8 shows the lean and rich solvent loading of the aqueous MEA solution at different liquid to gas ratios. It shows the fact, that for lower solvent ratios a higher regeneration in the desorption column and therefore lower lean loadings of the solvent are necessary to achieve the

same carbon dioxide capture rate.
For the selected operation point the loading of the lean solvent is around 0.2 mol CO_2/ mol NH_3 and around 0.6 mol CO_2/ mol NH_3 for the rich solvent.

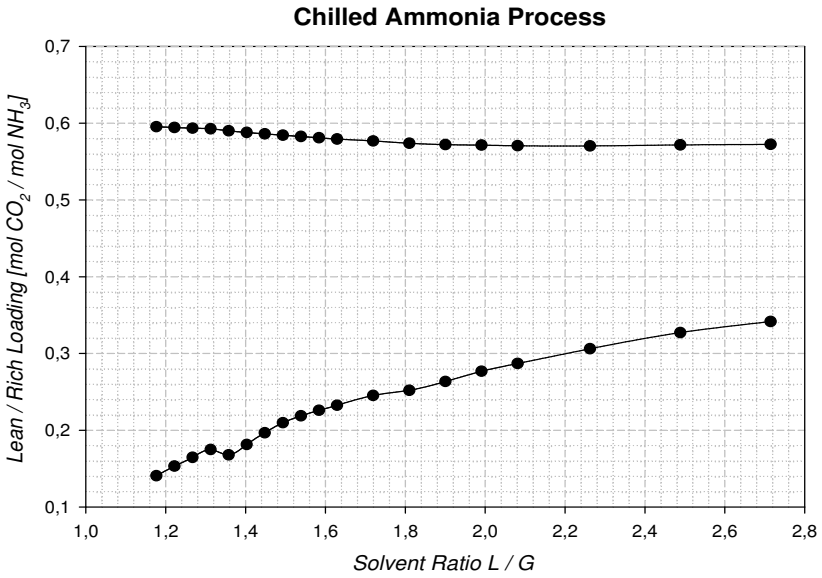

Fig. 7.15: Solvent loading plot against absorber $\dot{L}/\dot{G}$ ratio

7.4 Validation of the Model

In this section an approximate validation of the developed process model and its results was attempted.

7.4.1 The Chilled Ammonia Process by Alstom Power

In 2006 Alstom Power established a 5 year program for the commercialization of the CAP. The development program had 4 main steps:

- Small bench scale testing at SRI Int.
- Large bench scale testing at SRI Int.
- Field pilot testing at We Energies
- Commercial Demonstration at AEP Mountaineer coal plant (shown in figure 7.16)

Fig. 7.16: Chilled Ammonia Pilot Plant by Alstom Power at AEP [62]

Some issues in the development program are the demonstration of the low ammonia emission and the handling of the bicarbonate solides. According to [63] the main issues could be solved (e.g.: an acid wash was added to reduce the emissions to extremly low levels). Further, in [64] it is mentioned that the ammonia slip was reduced to lower levels as it was indicated by former experimental results. Figure 7.17 gives a 3-D views of the field pilot plant of the CAP at We Energies. Unfortunately no detailed results of the field pilot plant or first results of the commercial demonstration (started in the third quater of 2009) are yet available to the public.
As explained in the patent [7] the carbon dioxide is absorbed at ambient pressure and a temperature of 0-20°C. Thereby the slurry containig ammonium bicarbonate is generated. In the desorber the ammonium bicarbonate is turned into ammonium carbonate at temperatures moderately above 100°C and pressures around 20-40 bar.

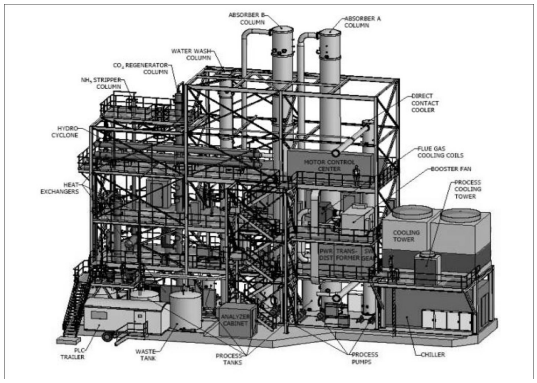

Fig. 7.17: We Energies Field Pilot Plant [64]

7.4.2 Other Simulations

Due to the lack of detailed public experimental data for the CAP, the results of this work's simulation were compared to simulation results by other authors. In the following the authors and their results are shortly mentioned.

Simulation by Valenti et al. [35] made a simulation of the CAP based on an extended bibliographic review. Their approach is not based on a specific simulation tool. The main results of the work by Valenti et al. is summerized in table 7.8.

Tab. 7.8: Process Results by [35]

11.5 wt% NH_3	
CO_2 Removal [%]	90
Stripper operating pressure [bar]	40
Stripper operating temperature [°C]	120
Lean solvent loading [kg CO_2/kg solvent]	0.1
Reboiler heat requirement [GJ/t]	1.5

Simulation by Darde et al. The detailed simulation by [33] is based on the extended Uniquac model. This makes a detailed description of the solid-liquid equilibria possible.
In [33] the energy requirement in the reboiler is calculated to approximately 2.25 GJ/t CO_2 for a solvent with an ammonia initial mass fraction of 12 wt% (from [65]). The ammonia solvent temperature was set to 8°C in this simulation approach.
As optimum process an ammonia solvent with an initial mass fraction of 28 wt% was found. Thereby a reboiler heat requirement of 2.05 GJ/t CO_2 could be achieved.

Simulation by Mathias et al. [59] used the the ELECNRTL model in ASPEN Plus^{TM} to simulate the CAP. The maximum ammonia slip was set to 10 ppmv NH_3 in this simulation. Further, the CO_2 loading of the lean solvent stream was fixed to ensure that ammonium bicarbonate and $(NH_4)_2CO_3.H_2O$ do not precipitate. The CO_2 loading for an ammonia solution with an initial mass fraction of 15 wt% was calculated to approximately 0.4 for the lean solvent and 0.8 for the rich solvent at a constant absorber temperature of approximately 10°C. The reboiler duty for an initial mass fraction of 26 wt% ammonia was calculated to approximately 2.3 GJ/t CO_2.

7.4.3 Validation

In this section an approximate validation approach of the simulation results of this work is attempted.

Comparison to Alstom's CAP Since no experimental results or data from the pilot or demonstration plant are available, a validation of this simulation with a real plant was not possible.
The main deviation between the patented CAP (see [7]) and this simulation is the reboiler temperature. In the patent it is set in the range of 50-200°C and preferable in the range of 100-150°C and in most simulations a value around 120°C is mentioned (e.g.: [35], [33]). In this work the reboiler temperature is around 185°C. One possiblity for the large difference of these values could be the lack in the modeling of the ternary $NH_3 - H_2O - CO_2$ system and the solid liquid equilibria.

Comparison to other Simulations The difference between results by Valenti et al. [35] for the reboiler duty and the results of this work differ from each other by around 0.75 GJ/t CO_2. Even though, almost the same inital mass fraction for the ammonia solution was used. The reason for the deviation could be in the higher desorber pressure of 40 bar and the different thermochemical model used by Valenti et al.
Otherwise the results by [33] for the reboiler requirement fit very good the results of this work. Darde et al. calculated a reboiler duty of approximately 2.25 GJ/t CO_2 for a 12 wt% inital mass fraction ammonia solution. Unfortunately no information about the desorber pressure could be found.

The work by Mathias et al. [59] gives the highest reboiler duty for the regeneration step compared to the other simulations. The lean and rich loadings from [59] and this work differ in approximately 0.2 mol CO_2/ mol NH_3 for both values. Possibilities for the deviation could again be the different thermochemical model and the different initial mass fraction.

All in all, the model and simulation presented in this work produced values similar to other simulations. Hence this simulation model should be valid enough for an approximate comparison of the two simulated processes (MEA and CAP).

8 Comparison of Monoethanolamine Process and Chilled Ammonia Process

In this chapter the considered post combustion capture processes are opposed to each other in an energetic, economic and ecological way.

8.1 Energetic Comparison

At first, the several energy requirements during the capture process are considered.
All considerations were made at the optimum process point given in section 6.3 and section 7.3.

8.1.1 Reboiler Duty

One of the most important energy entry parameters in the system is the reboiler duty for the desorption column, since it effects directly the power loss of the power plant.
Table 8.1 contrasts the specific energy requirement in the reboiler for the Monoethanolamine Process and the Chilled Ammonia Process. It shows that the specific reboiler heat requirement

Tab. 8.1: Comparison of the specific reboiler duty

	MEA Process	**CAP**
Reboiler temperature [°C]	122	187
Reboiler duty [GJ/t CO_2]	3.25	2.25

for the desorption step is approximately 1GJ/t CO_2 higher for the MEA Process than for the CAP. This results from the lower heat of reaction in the ammonia solution.
Concerning the reboiler duty the CAP is advantaged compared to the MEA Process. The quality (temperature) of the CAP reboiler energy is higher than the quality of the MEA Process. At this point it has to be mentioned again that this fact could result from the improperties of the ternary ($NH_3 - H_2O - CO_2$) system (see section 7.1.1).

8.1.2 Cooling Duty

Another important energy parameter is the cooling requirement for both processes. The several specific cooling duties in the process are listed in table 8.2. In this table the solvent heater is also listed, although it expresses no real energy entry. This component was just necessary for the simulation to transfer the lean solvent stream.
The lower cooling duty for the lean solvent results from the higher head wash water stream, which was mixed to the lean solvent before entering the absorption column. Since for the head wash river water with a temperature of 15°C was used, it helped cooling the lean solvent.

The comparison in table 8.2 shows, that for the Chilled Ammonia Process the overall specific cooling duty is approximately -1.15 GJ/t CO_2 larger than for the MEA Process.
To estimate the difference in the cooling water consumption, river water with an inlet temperature of 15°C and an maximum outlet temperature of 21°C was selected for all coolers with a required cooling temperature above 15°C. These are all coolers in the MEA Process, but in the CAP two coolers need 10°C and the head cooler 15°C as cooling temperature. Thus, a refrigeration system was necessary. Here, a refigeration system based on ammonia was chosen (more details see section 7.2.2). This system had an additional water and energy consumption. The necessary

Tab. 8.2: Comparison of the specific cooling duty

	MEA Process	**CAP**
Lean solvent cooler [GJ/t CO_2]	−1.28	−0.62
Flue gas cooler [GJ/t CO_2]	−1.28	−2.05
Desorber condenser [GJ/t CO_2]	−0.26	−0.07
Quench water cooler [GJ/t CO_2]	−0.51	−0.44
Product gas cooler [GJ/t CO_2]	−0.28	−0.29
Head cooler [GJ/t CO_2]	-	−1.84
Solvent heater [GJ/t CO_2]	-	0.59
Sum [GJ/t CO_2]	−3.61	−4.73

amount of river water with a temperature of 15°C for the ingoing and 21°C for the outgoing stream due to the refrigeration system was added to the river water needed for the other coolers in the CAP.
The results from the simulation are listed in the next table.

Tab. 8.3: Comparison of the specific cooling water consumption

	MEA Process	**CAP**
T_{in} | T_{out} [°C]	Specific cooling water [$m^3/t\ CO_2$]	Specific cooling water [$m^3/t\ CO_2$]
15 | 21	122	204

The calculations showed, that the specific cooling water consumption for the CAP is around 60% higher than for the MEA Process.

8.1.3 Power Duty

The next energy parameter, which is representive for a capture process, is the electric power requirement because of the pumps, blowers and compressors implemented in the process.
In these simplified simulation models just one blower for the flue gas (to overcome the absorption column pressure drop, which was set to 100 mbar for both columns) and one pump for the rich solvent stream were necessary. Their specific energy requirements are listed in table 8.4. Because

Tab. 8.4: Comparison of the specific power duty

	MEA Process	**CAP**
Blower *B-1* [GJ/t CO_2]	0.08	0.08
Rich solvent pump *P-1* [GJ/t CO_2]	0.001	0.02
Pressure increase [bar]	0.1/0.8	0.2/19
Refrigeration system compressor *B-2* [GJ/t CO_2]		0.65
Sum [GJ/t CO_2]	0.081	0.75

of the higher pressure in the CAP stripper column the electric power requirement for the rich solvent pump is larger in the CAP compared to the MEA. The auxiliary power demand of the CAP is around 8 times larger than the power demand of the MEA Process.
Nevertheless, this brings some advantages, since it lowers the energy effort for the carbon dioxide compression step. The relatively low energy consumption of the rich solvent pump in the CAP results from the smaller solvent streams.

8.1.4 Solvent Flow

A further parameter, which strongly effects the costs of a capture plant, is the size of the solvent stream. Because of the higher capture efficiency of the ammonia solution this process is capable with a smaller solvent flow. The optimum solvent flow ratio was fixed in section 6.3. Table 8.5 lists the specific solvent flow of each process to achieve the required specific reboiler duty given in table 8.1.

Table 8.5 shows that for the CAP almost half of the solvent flow compared to the MEA Process

Tab. 8.5: Comparison of the specific solvent flow

	MEA Process	**CAP**
Specific solvent flow [t/t CO_2]	17	9

is necessary. This leads to smaller equipment and therefore lower equipment costs.

8.1.5 Water and Solvent Consumption

The water consumption for the head washing system to minimize the solvent slip and the water used by the quench cooling system for precooling the flue gas are listed in table 8.6. Further the solvent loss (MEA or NH_3) and therefore the amount of make-up solvent are also given in this table. Table 8.6 shows, that the make-up water consumption for the MEA Process is much

Tab. 8.6: Comparison of the specific make-up streams

	MEA Process	**CAP**
Specific water flow for the quench cooling system [t/t CO_2]	2.7	2.7
Specific water flow for the head wash system [t/t CO_2]	0.03	0.03
Make-up water [t/t CO_2]	0.5	0
Make-up MEA/ NH_3 [kg/t CO_2]	0.12	26.8

larger than for the CAP. This follows from the higher temperature of the purified flue gas leaving the MEA capture plant (no head cooler as in the CAP). Table 6.9 and 7.6 in section 6.3.2 and 7.3.2 give the same result.

The low temperatures in the CAP lead to the fact that not only no water has to be added but also water and therefore solvent has to be removed from the system.

8.1.6 Power Plant Integration

Another important energetic aspect for every post combustion capture system is the implementation in the power plant and therefore the loss of power due to the capture step. The following calculation of the specifc power loss was done according to [**?**]

The specific loss of electric power can be calculated by the following formulas given in [66].

$$p_{loss} = \frac{P_{loss}}{\dot{m}_{CO_2,cap}} \tag{8.1}$$

$$P_{loss} = P_{reg} + P_{cap} + P_{comp} + P_{cw} \tag{8.2}$$

The auxiliary power demand for the pumps and blowers P_{cap} was taken from the simulation (8 MJ/s for MEA Process and 77 MJ/s for CAP). The specific power demand for the carbon

dioxide compression was estimated from [53] to 0.079 kWh/kg CO_2 for the MEA Plant. The power demand due to the compression for the CAP was estimated to be around 40% of the power needed in the MEA plant because of the higher desorber pressure.
The power decrease due to the extraction of the low pressure steam could be calculated by the following equations.

$$P_{reg} = \eta_{eff} \cdot \eta_{carnot} \cdot \dot{m}_{CO_2} \cdot \epsilon^{'} \cdot q \tag{8.3}$$

q is the specific reboiler duty of the capture plant.

$$\eta_{carnot} = 1 - \frac{T_{cond}}{T_{ext}^{sat}(p_{ext})} \tag{8.4}$$

$$\eta_{eff} = 0.7855 + 0.01485 \cdot p_{ext} \tag{8.5}$$

Thereby the condenser temperature of the power plant was assumed to $T_{cond} \approx 300K$, the temperature and pressure of the extracted steam to $T_{ext} \approx 403.15K$ for MEA and $T_{ext} \approx 468.15K$ for CAP, thus the steam pressure was determined (Gibb's Phase law) to $p_{ext} \approx 2.7$ bar respectively $p_{ext} \approx 13.98$ bar.

The calculated specific power loss for the power plant due to the MEA capture process is 0.272kWh/kg CO_2 and 0.441kWh/kg CO_2 for the CAP.
The power loss for solvent regeneration is around 0.172kWh/kg CO_2 for the MEA Process and 0.201kWh/kg CO_2 for the CAP. The reason is the higher quality of the required energy (steam temperature) in the CAP reboiler. The power demand for the carbon dioxide compression is 0.079kWh/kg CO_2 for the MEA Process (taken from [53]) and 0.031kWh/kg CO_2 for the CAP. The power demand for the capture process is 0.022kWh/kg CO_2 for the MEA Process and 0.208kWh/kg CO_2 for the CAP.
Although the specific reboiler duty is lower in the CAP than in the MEA Process, the power loss of the power plant is higher because of the immense energy requirement in the refrigeration system resulting from the cooling agent compressor and because of the higher quality of the reboiler energy demand.

8.2 Economic Comparison

In this section an approximate calculation of the equipment and operating costs for both capture plants is done to make a qualitative economic comparison of the processes possible.
At this point, it should be me mentioned that the detailed and exact estimation of the costs was not a main task of this thesis.

8.2.1 Equipment Costs

To estimate the investment costs for both capture plants the equipment size of the main components had to be estimated at first.

Estimation of the equipment size For an approximate estimation of the main equipment the absorber/ stripper column diameter and height were calculated according to [66]. The principle of the design approach for the column diameter and height is based on the work by [50] and [66] and visualized in figure 8.1.

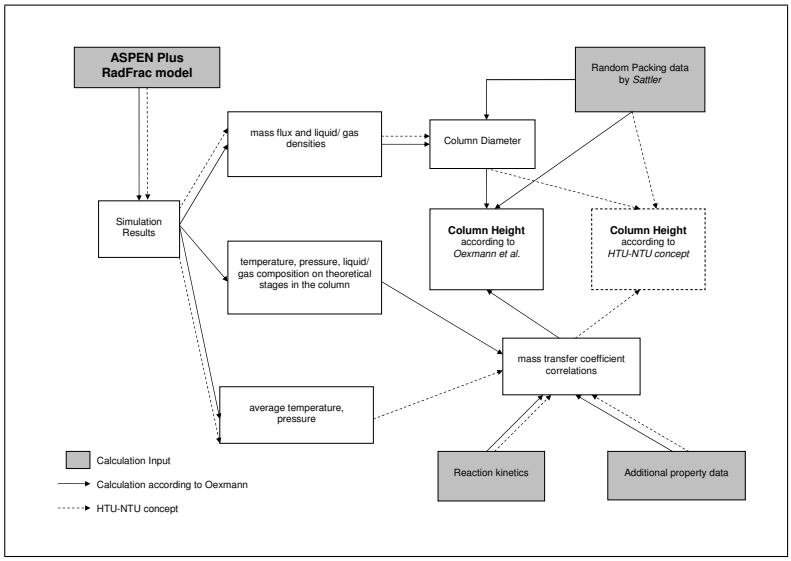

Fig. 8.1: Principle of the height calculation

Column diameter The calculation for the column diameter followed [50]. A random packing was chosen for the absorber. For the packing material 50 mm metal *Raschig* Rings were selected. The needed packing parameters (K_3 and K_4) were also taken from [50] (also see section 5.4).
The maximum column diameter was limited to 14 m, which expresses the upward limit for a column due to transport according to [16]. To achieve this value the number of coloums n was varied in the calculation ($\dot{V}_g$=$\dot{V}_{fluegas}$ /n, $\dot{m}_l$=$\dot{m}_{solvent}$ /n).
The calculation of the diameter of random packing was done according to [50].

The liquid loading/ liquid velocity was calculated, which depends primary on the liquid mass flux. For the calculation the absorber diameter D_K had to be estimated at first and was solved afterwards in an iterative way.

$$w_l = \frac{\dot{m}_{l,max} \cdot 4}{\rho_l \cdot \pi \cdot D_K^2} \tag{8.6}$$

The necessary mass/ volume stream and density data were taken from the simulation results done in ASPEN Plus^{TM}.

The maximum surface gas velocity was determined by an expression given in [50].

$$w_{g,0} = K_3 \cdot (\frac{\rho_l}{\rho_g})^{0.5} \cdot [1 - K_4 \cdot f(\nu_l) \cdot w_l^{0.5}] \tag{8.7}$$

Therefore the specific packing parameters were selected from [50] (see table 5.5). The empiric viscosity function $f(\nu_l)$ is given in the next equation and must be used for viscosities higher than 1 mPa s.

$$f(\nu_l) = 0.8 + 0.225 \cdot \nu_l^{0.25} \tag{8.8}$$

By using the maximum surface gas velocity the column diameter was fixed with the following formula.

$$D_K = \sqrt{\frac{4 \cdot \dot{V}_g}{w_{g,0} \cdot \pi}} \tag{8.9}$$

Column height The calculation of the column height is on the one hand based on the HTU/NTU concept (see section 3.5.2) and on the other hand based on a modified concept implementing the simulation results explained in [66].

For the calculation of the column height (following the **HTU-NTU concept**), the mass transfer coefficient (based on gas phase for HTU concept and based on liquid phase for the calculations according to [66]) had to be determined.
The modified mass transfer coefficient based on the liquid film was extended by the enhancement factor (see section 3.5.2) to accommodate the chemical reaction.

$$K_{o,g} = \frac{1}{1/\beta_g + m/\beta_l \cdot \bar{\varrho}_g \,/\, \bar{\varrho}_l} \qquad K'_{o,l} = \frac{1}{1/\beta_g + 1/(m \cdot E \cdot \beta_l)} \tag{8.10}$$

$K_{o,g}$ is the coefficient based on the gas phase used in the HTU-NTU concept, whereas $K'_{o,l}$ was used by [66]. $K'_{o,l}$ is not exactly the mass transfer coefficient based on the liquid phase, but it was used in [66] and [53] for the estimation of the column heights.
The temperature dependent solubility is given by Henry's constant and the total pressure in the columns $m = H_i/P$. It was calculated with the empirical equation explained in section 4.4.2 with data from [18] for carbon dioxide in water.
The enhancement factor was determined by the following equation (according to [27]), since a fast reaction $3 < Ha << E_i$ (see section 3.5.2) was assumed.

$$E = Ha = \frac{\sqrt{k_{MEA/NH_3} \cdot D_{CO2} \cdot C_{MEA/NH_3}}}{\beta_l} \tag{8.11}$$

D_{CO_2} is the binary diffusivity coefficient of CO_2 in the gas phase.
The rate constant for the second order reaction between CO_2 and MEA based on the Arrhenius law was adopted by [53]. The reversible reaction in the desorber k'_{MEA} was also taken from [53].

$$k_{MEA} = 4.4 \cdot 10^8 \cdot \exp -5400/T \qquad k'_{MEA} = 3.9 \cdot 10^{10} \cdot \exp -6863.8/T \tag{8.12}$$

For the ammonia system reaction kinetics were adopted from [56] (0.1 mole frac NH_3 concentration) to

$$k_{NH_3} = 1.35 \cdot 10^{11} \cdot \exp -5829.9/T \qquad k'_{NH_3} = 4.75 \cdot 10^{20} \cdot \exp -8316.1/T \tag{8.13}$$

The implementation of the reaction rates into the column height estimation was necessary to take into account kinetic effects, which have a great influence on the column design.
The binary diffusivity coefficients in the liquid and gaseous phase were expressed by semi-empirical correlations given in [50].

$$D_{12,g} = \frac{0.604 \cdot 10^{-}8 \cdot T^{1.81} \cdot (\frac{M_1+M_2}{M_1 \cdot M_2})^2}{P \cdot (T_{k,1} \cdot T_{k,2})^{0.1405} \cdot (V_{m,k1}^{0.4} + V_{m,k2}^{0.4})^2} \tag{8.14}$$

$$D_{12,l} = 7.4 \cdot 10^{-8} \cdot \frac{T}{\nu_2} \cdot \frac{(C \cdot M_2)^{0.5}}{V_{m,1}^{0.6}} \tag{8.15}$$

C is an emperical association factor.
Finally the needed mass transfer resistence in the liquid and gaseous phase were calculated by empirical correlations for the Sherwood number of random packings given in [50] for *Raschig* rings.

$$Sh_g = 0.407 \cdot R_g^{0.655} \cdot Sc_g^{1/3} \tag{8.16}$$

$$Re_g = \frac{\dot{V}_g \cdot 4 \cdot \epsilon}{A_q \cdot a \cdot \mu_g} \qquad Sc_g = \frac{\mu_g}{D_{12,g}} \tag{8.17}$$

The mass transfer resistence coefficient is given by

$$\beta_g = \frac{Sh_g \cdot D_{12,g} \cdot a}{4 \cdot \epsilon} \tag{8.18}$$

For the mass transfer resistence of the liquid phase the procedure is generally the same. The main difference are the empirical correlations and the different characteristc length.

$$Sh_l = 0.32 \cdot Re_l^{0.59} \cdot Sc_l^{0.5} \cdot Ga_l^{0.17} \tag{8.19}$$

$$Re_l = \frac{\dot{m}_l \cdot d_p}{\rho_l \cdot A_q \cdot \mu_l} \qquad Sc_l = \frac{\mu_l}{D_{12,l}} \qquad Ga_l = \frac{d_p^3 \cdot g}{\mu_l^2} \tag{8.20}$$

$$\beta_l = \frac{Sh_l \cdot D_{12,l}}{d_p} \tag{8.21}$$

At first, the height of the absorption columns were calculated using the HTU-NTU to get a first estimation of the value.
With the gas flow $\dot{G}_T = (\dot{m}_{g,max} \cdot (1 - w_{CO_2}))/\rho_g$, the specific area of the random packing and an assumed degree of wetting of $\varphi \approx 1$ (due to the lack of detailed property data) the height of one transfer unit could be calculated (HTU).

$$HTU = \frac{\dot{G}_T}{K_{o,g} \cdot a \cdot \varphi \cdot A_q \cdot E} \tag{8.22}$$

For the calculation of the number of transfer units (NTU) the assumption was made, that the partial pressure of CO_2 over the liquid phase is approximately zero. As a result, the NTU value was calculated by a simplified expression depending on the loadings of the ingoing and outgoing gas streams of the absorption columns (cf. [27]).

$$NTU = \int_{Y_{in}}^{Y_{out}} \frac{dY}{Y - Y^*} \approx \ln \frac{Y_{in}}{Y_{out}} \tag{8.23}$$

The total height of the column is calculated by the multiplication of the HTU and the NTU value.

$$H_K = HTU \cdot NTU \tag{8.24}$$

Another possiblity for the identification of the column height is given by [66] (caculation following **[66]**). Thereby, the simulation results for each stage i were used to calculate the transferred mole flow from the gaseous into the liquid phase ($\Phi_{CO_2,i}$) and the mass transfer flux J_i from the gaseous phase into the liquid phase.

$$J_i = K_{o,l}^{'} \Delta C_{CO_2,i} \tag{8.25}$$

$\Delta C_{CO_2,i}$ is the change in the logarithmic concentration difference between the gaseous and liquid phase from stage i to stage $i+1$. It represents the driving force of the mass transfer. The values for the concentration at each stage of the column were calculated from the simulation.

$$\Delta C_{CO_2,i} = \frac{C_{CO_2,i+1}^{gas} - C_{CO_2,i+1}^{liquid}}{\ln \frac{C_{CO_2,i+1}^{gas}}{C_{CO_2,i+1}^{liquid}}} - \frac{C_{CO_2,i}^{gas} - C_{CO_2,i}^{liquid}}{\ln \frac{C_{CO_2,i}^{gas}}{C_{CO_2,i}^{liquid}}} \tag{8.26}$$

The required area for the mass transfer (random packing surface) and therefore the total area can be expressed by the mole flow $\Phi_{CO_2,i}$ and the mass transfer flux J_i.

$$A_{P,i} = \frac{\Phi_{CO_2,i}}{J_i} \qquad A_P = \sum_i A_{P,i} \tag{8.27}$$

$\Phi_{CO_2,i}$ is the mole flow from the gaseous into the liquid phase on stage i. It was determined by the simulation results in the RADFrac^{TM} model.
By the required area of the random packing and the specific area of the random packing the column height could be fixed.

$$H_K^{'} = \frac{A_P \cdot 4}{a \cdot D_K^2 \cdot \pi} \tag{8.28}$$

To get a better estimation of the column height a safety factor of 25% was multiplied $H_K = 1.25 \cdot H_K^{'}$ (see [66]).

The input data used in the calculations described above is listed in table 8.7.

Tab. 8.7: Input data for equipment size

Parameter	**MEA** AC/ DC	**CAP** AC/ DC	**Unit**	Source
ρ_g	1.26/ 1.26	1.56/ 1.56	kg/m^3	Simulation
ρ_l	1412.4/ 1412.4	946.38/ 946.38	kg/m^3	Simulation
ν_{MEA/NH_3} at T	5.45/ 2.155	0.0095/ 0.0153	mPa s	[60]
ν_{H_2O} at T	0.43/ 0.244	0.743/ 0.1694	mPa s	[67]
K_3	0.088	0.088	-	[50]
K_4	0.077	0.077	-	[50]
$\nu_g \approx \nu_{air}$ at T	0.025/	0.017	mPa s	[67]
T	340/ 370	310/ 435	°K	Simulation
$M_g \approx M_{N_2}$	28.014	28.014	kg/kmol	[36]
M_{CO_2}	44.01	44.01	kg/kmol	[36]
T_{k,N_2}	126.2	126.2	°K	[36]
T_{k,CO_2}	304.2	304.2	°K	[36]
V_{k,N_2}	0.089	0.089	$m^3/kmol$	[36]
V_{k,CO_2}	0.093	0.093	$m^3/kmol$	[36]
V_{CO_2}	22.22	22.22	cm^3/mol	-
M_{H_2O}	18.015	18.015	kg/kmol	[32]
M_{MEA/NH_3}	61.08	17.03	kg/kmol	[32]
C_{MEA/NH_3}	2926.3/ 1025	3918/ 982	mol/m^3	Simulation
C	15	0.01	-	-
Y_{in}	0.134/ -	0.134/ -	mol CO_2/ mol Gas	Simulation
Y_{out}	0.012/ -	0.012/ -	mol CO_2/ mol Gas	Simulation

Some of the intermediate results for the calculation can be seen in table 8.8.

Tab. 8.8: Intermediate results for the equipment size

Parameter	**MEA** AC | DC	**CAP** AC | DC	**Unit**
$D_{12,g}$	$2.2 \vert 1.3 \cdot 10^{-5}$	$1.8 \mid 0.17 \cdot 10^{-5}$	m^2/s
$D_{12,l}$	$4 \vert 0.11 \cdot 10^{-9}$	$38.5 \mid 2.3 \cdot 10^{-9}$	m^2/s
Ha	109 | 35	$235 \mid 14 \cdot 10^5$	-
β_g	0.0044 | 0.0029	0.0048 | 0.001	m/s
β_l	0.0003 | 0.0017	0.0002 | 0.0016	m/s
$K_{o,g}$	$95 \mid 0.69 \cdot 10^{-5}$	$65 \mid 29 \cdot 10^{-5}$	m/s
$K'_{o,l}$	0.0044 | 0.0029	0.005 | 0.001	m/s

Using the data set in table 8.7 the diameter and height for the absorber columns can be calculated according to the HTU-NTU concept (cf. section 3.5.2).
By using the simulation results on each equilibrium stage the column height can also be calulated for the absorber and additionally for the desorber columns. The results of the calculations are listed in table 8.9.

Tab. 8.9: Equipment size

Parameter	**MEA Process** HTU-NTU | Simulation	**CAP** HTU-NTU | Simulation	**Unit**
Number of absorbers n	2	1	-
Absorber diameter D_K	13.4	13.3	m
Absorber height H_K	27.7 | 30.7	18.9 | 52.5	m
Number of desorbers n	1	1	-
Desorber diameter D_K	- | 9	- | 7	m
Desorber height H_K	- | 15.3	- | 41.2	m

The calculated column diameters and therefore the number of columns for each plant seem reasonable, since the CAP uses around half of the lean solvent mass stream compared to the MEA Process. Due to the lower flue gas and solvent temperature, the gas stream is also reduced compared to the MEA Process. This leads to the fact, that for the CAP just one absorption column is necessary, whereas for the MEA Process two.
The lower column height of the columns in the MEA Process could result from the slower absorption rate in a 12 wt% ammonia solution. This statement was not ensured by other experimental data. Another reason for the enormous deviations could be the imperfect modelling and therefore the ingoing simulation results. This would explain the deviation between the HTU value and the value calculated according to [66]. The height calculated by the HTU concept must also be seen with caution, since the association factor C has an tremendous effect on the HTU value. For example, if it is varied between 0.001 and 2.6 (water) the absorber height varies between 38.6 and 4.7 m of the CAP absorption column, whereas the height calculations based on the simulation are almost constant.

Pressure Drop Further the pressure drop of the columns was roughly estimated. This was done to evaluate the hydraulic performance of the columns.
The column pressure drop is determined by the dry and the wet pressure drop.

$$\Delta p = \Delta p_t + \Delta p_w \tag{8.29}$$

The calculation for the packing pressure drop was done according to [16]. The dry pressure drop is expressed by the next equation.

$$\Delta p_t = \zeta \frac{\rho_g \cdot w_g^2 (1-\epsilon) \cdot H_K}{2 \cdot \epsilon^3 \cdot d_h} \tag{8.30}$$

Where ζ depends on the Reynolds number and the hydraulic packing diameter, which can be calculated as follows.

$$\zeta = f(Re_g) \qquad Re_g = \frac{w_g \cdot d_h}{(1-\epsilon) \cdot \mu_g} \qquad d_h = 6 \cdot \frac{1-\epsilon}{a} \tag{8.31}$$

ζ was determined by diagrams given in [16].
Moreover the wet pressure drop was fixed by diagrams depending on the dry pressure drop and the trickle density B.

$$B = (\frac{\mu_l}{g^2})^{1/3} \cdot \frac{1-\epsilon}{\epsilon \cdot d_h} \cdot w_l \tag{8.32}$$

These so-called flooding point diagrams can be found for example in [27].
The results from the calculation are given in table 8.10.

Tab. 8.10: Column pressure drop

Parameter	**MEA Process** AC | DC	**CAP** AC | DC	**Unit**
Pressure Drop	128 | 85	486 | 764	mbar

The pressure drop analysis shows, that the pressure drop of the CAP columns is around 3 times higher than the pressure drop of the MEA columns, which would lead to higher blower costs. This results from the fact that the CAP columns are close to the flooding limit.
At this point, it has to be said that a column with such a high pressure drop cannot be operated, since this operation point reaches almost the flooding limit of the column, which leads to such a high pressure drop. As a result, changes in the column design would have to be done. These changes in the column design were not made in this work to restrict the effort of the approximate and qualitative estimation of the equipment size.

8.2.2 Investment Costs

The target of this work was not the exact calculation of the investment costs. The methodology of the cost estimation was chosen to make a qualitative economic comparison of the two processes. In this work only the costs for some of the main components of the capture processes were considered. For a more detailed calculation approach costs for all components must be taken into account.

Cost Indexes Due to the change of costs with time a correction for converting the costs at a past date to equivalent costs at the present time. This is realized by the cost index has to be made.
The cost index shows the costs at the time the original cost was obtained relative to a certain base year. The cost at the present time can be calculated by multiplying the original cost times the ratio of the index value at present time to the index value at time original cost was obtained (for more detailed information see [68]).

$$C_{present} = C_{past} \cdot \frac{index_{present}}{index_{past}} \tag{8.33}$$

Columns Due to the smaller column size and less columns for the CAP compared to the MEA Process, the CAP is advantaged from this point of view. Further smaller column height leads to a lower pressure drop and thus to a smaller amount of the random packing. Hence, the column height is a very important parameter for the investment costs.

A more detailed approach for the column costs is based on correlations given in [69]. For an estimation of the column costs the column weight had to be calculated. Thus it was necessary to calculate the thickness of the column shell. It was estimated by the vessel formula for inner pressure in cylindric shells using a stainless steel (1.4401 with $f = R_{p1,0;T}/1.5 = f_{150°C}/1.5 = 136.6$ MPa and z=0.85, taken from EN 10028-7) (for further information see EN 13445-3).

$$e_K = \frac{p_K \cdot D_K}{2 \cdot f \cdot z + p_K} = \frac{p_K \cdot D_K}{232.22 + p_K} \tag{8.34}$$

Including the density of the stainless steel 1.4401 of around 7960 kg/m^3 the shell weight can be calculated. Mulet et al. [69] gave an empirical correlation for the costs of absorption towers depending on the shell weight. The material of construction factor F_M was estimated to 2.1 for stainless steel.

$$C_K = F_M \cdot (\exp 6.488 + 0.21887 \cdot \ln w_K[kg] + 0.02297 \cdot \ln w_K[kg]) \tag{8.35}$$

To estimate the packing costs correlations from [69] were used again ($C_P = V_K \cdot F_P$). Thereby, the cost of tower packing per unit volume factor was assumend as F_P=600 €/m^3 for metal *Raschig* rings - 50 mm.
The costs for platforms and ladders were estimated from the following correlation given by [69].

$$C_L = 1,017 \cdot D_K^{0.73960} \cdot H_K^{0.70684} \tag{8.36}$$

The so calculated column costs were multiplied with the ratio of the cost indexes. As cost index the *Chemical Engineering Chemical Plant Index* (CECPI) of the Chemical Engineering Journal was used. For the equipment it was estimated to 330 for the year 1981 and 740 for 2009.
The results for the main equipment costs are summarized in table 8.11. For the cost calculations only the values determined by this simulation were used.

Tab. 8.11: Column Costs

Parameter	**MEA Process** AC | DC	**CAP** AC | DC	**Unit**
Shell thickness e_K	5.8 | 8.1	5.7 | 59.8	mm
Column costs	0.67 | 0.21	0.49 | 1.45	M€
Ladder costs C_L	0.35 | 0.08	0.25 | 0.13	M€
Sum of column costs C_K	1.75	2.71	M€
Packing costs	11.65 | 1.50	9.81 | 2.13	M€
Sum of Packing costs C_P	13.15	11.95	M€
SUM $C_C = C_K + C_P$	**14.90**	**14.66**	M€

The calculation results in table 8.11 make clear, that the main costs for the column depend on the packing costs and therefore on the column volume.
As in table 8.11 visible, the equipment costs for the columns in the CAP are lower compared to the MEA Process due to the fact that only one absorption column is necessary.

Pump, Blower and Heat exchanger The approach to estimate the costs for pumps, blowers and heat exchangers is based on the work by Peters [68]. In [68] the component costs are given as a linear function of a certain design parameter for each component.

The costs for the solvent pumps were estimated from diagrams given in [68], in which the costs depend on the delivered power. The delivered power was set equal to the power requirement calculated in ASPEN Plus^{TM}. The results are listed in table 8.12.

The relative costs for the blowers were also estimated from graphics in [68]. These diagrams gave the relation between purchased costs and the capacity of the fan.

More problematic was the estimation of the heat exchanger costs. The CAP in this work is

built with 8 heat exchangers (the heat exchanger, which was necessary to make the stream transfer possible was not taken into account), whereas the MEA Process contains 7. In both capture systems 4 of them work under elevated pressure. For the approximate evaluation in this work only the influence of the pressure and the heat exchanger surface on the costs were estimated. By diagrams in [68] the relative costs per square foot of heating surface were estimated. Due to the lack of more detailed data from the simulation, the average heating surface was determined by the following formula.

$$A_H = \frac{\dot{Q}}{k \cdot \Delta T_{ln}} \tag{8.37}$$

The overal transfer coefficient was estimated to 680 W/(m^2K) for the rich-lean solvent heat exchanger and 1278 W/ (m^2K) for the liquid-liquid heaters and coolers. The higher equipment costs for the rich-lean solvent heat exchanger or the reboiler were not considered in detail due to time effort. These were treated as simple liquid-liquid heat exchangers.
A steam temperature of 125°C/ 185°C, cooling water temperature of 15°C and 5°C for the coolers in the CAP was assumed for this rough estimation. For the calculation of the heat exchanger costs no certain heat exchanger type was considered.
Since a very old book (1960s) was taken for the cost estimation, all costs generated from this source were multiplied by factor 10. This factor was estimated from comparing the diagrams of the older version with a new version, which was available recently. The factor can be seen as the ratio of the index value at present time to the index value at time original cost was obtained.

All results from the cost estimation of the auxiliary components are listed in the following table 8.12.

Tab. 8.12: Pumps, fans and heat exchanger costs

Parameter	**MEA Process**	**CAP**	**Unit**
Solvent pump costs	12,000	120,000	€
Blower costs	900,000	900,000	€
Refrigeration system compressor costs	-	600,000	€
Heat exchanger costs	492,000	497,300	€
Sum	**1.40**	**2.12**	M€

The costs calculated above do not represent real costs of the components, they were just used for the sake of comparison.
A short validation of the relative costs can be done by comparing the results to the cost estimation by [66] for the MEA Process. The relative column costs are around 70% of the total equpiment costs (30% pumps, blowers and heat exchangers). In this work, the column costs are around 90% of the total equipment costs. This discrepancy could result from the fact that in this work the equipment costs for only some of the auxiliary components were estimated.

The sum of the equipment costs is 16.30 M€ for the MEA Process and 16.77 M€ for the CAP. Following this first estimation approach for the purchased equipment costs the MEA Process is around 2.8% cheaper than the CAP. The higher equipment costs for the CAP result from the higher costs for the auxiliary equipment.
At this point it should be mentioned, that the costs for the CO_2 compressor, direct contact cooling columns, additional solvent pumps, tanks and filters are not considered in the estimation of the main components costs.

An advantage of the CAP is that the higher pressure in the desorber leads to a lower energy consumption in the carbon dioxide compression section. Since the CO_2 compression section was not considered in this work, this benefit could not be factored in the equipment cost evaluation. Otherwise, the required slurry pumps for the CAP are more expensive than a usual solvent pump. Since the rich solvent is formed as a slurry, higher demands for the heat exchanger and the desorption column must be made. In this cost estimation the effect of the slurry on the pump costs was not concerned. The issue of fouling of the heat exchangers should also be taken into account for a more detailed calculation of the equipment costs.

Adding the equipment costs considered in the paragraphs above, the specific equipment costs wer calculated for each process.
The specific equipment costs for the MEA Process is 44.5€/(kg/h CO_2) and for the CAP it is 45.4€/(kg/h CO_2).

Estimated Investment Costs Following [66] respectively [68] the investment costs can be calculated from the purchased equipment costs by using cost factors (listed in table 8.13).
By multiplying the basis times the factor (given in table 8.13) the costs for the additional equipment and indirect costs can be estimated.
PEDC are the purchased equipment costs including the delivery of the equipment. The fixed capital investment (FCI) is the sum of the PEDC, the total direct plant costs and the indirect plant costs including the contractor's fee and the contigency. The final owner costs are the FCI plus the capital costs.

According to this rough estimation of the investment costs these are around 99.5 M€for the MEA Process and 102.4 M€for the CAP.
These specific investment costs (1.26 [€/tCO_2 avoided] for the MEA Process and 1.29 [€/tCO_2 avoided] for the CAP with a plant life time of 25 years) seem to be very low compared to other cost estimations (e.g.: [70]).
One reason for this fact could be that in this estimation for the purchased equipment costs neither the carbon dioxide compression section, the quench cooling columns for the flue gas (direct contact coolers), the head washing columns, filters for solids, additional solvent pumps or heat exchangers (e.g.: reclaimer for the MEA Process) nor storage or separation tanks are implemented. In addition, a cheap packing with 600 €/m^3 and a low pressure drop of 100 mbar were assumed.
Another reason could be, that the cost estimation functions and graphics in [69] and [68] are just a rough estimation approach and more detailed considerations should be made.
A realistic estimation of the investment costs for such capture plants would be probably around 5 times higher than the calculated values.
But for a first qualtitative comparison of the processes, this estimation should be good enough.

To obtain a more realistic value for the specific costs due to the investment costs, they were estimated to 15 [€/t CO_2 avoided] for the MEA Process following [70] (a capture plant life time of 25 years was assumed). Thus, the costs for the carbon dioxide capturing according to the investment costs are around 15.43 [€/t CO_2 avoided] for the CAP.

It can be summarized that the CAP with this configuration is around 3% more expensive than the MEA Process concerning the investment costs. This fact results from the higher equipment costs for the auxiliary equipment.

Tab. 8.13: Investment costs in M€

	MEA	CAP	Factor	Basis
Purchased equipment costs (PEC)	16.30	16.77	1	-
Delivery	1.63	1.68	0.1	PEC
PEC and delivery costs (PEDC)	17.93	18.45	-	
Installation	8.97	9.23	≈ 0.5 - depending on component type	PEDC
Instrumentation and controls	6.46	6.64	0.36	PEDC
Piping	12.19	12.55	0.68	PEDC
Electrical Systems	1.97	2.03	0.11	PEDC
Buildings	3.23	3.32	0.18	PEDC
Yard improvements	1.79	1.85	0.1	PEDC
Service facilities	12.55	12.92	0.7	PEDC
Total direct plant costs	47.16	48.53	-	
Engineering and supervision	5.92	6.09	0.33	PEDC
Construction expenses	7.35	7.57	0.41	PEDC
Legal expenses	0.72	0.74	0.04	PEDC
Total indirect plant costs	13.99	14.39	-	
Contractor's fee	3.06	3.15	0.05	indirect + direct plant costs
Contigency	6.12	6.29	0.1	indirect + direct plant costs
Fixed capital investment (FCI)	70.32	72.36		
Start-up expenses	4.22	4.34	0.06	FCI
Working capital	7.03	7.24	0.1	FCI
Sum (Owner's cost)	**99.50** M€	**102.39** M€		

8.2.3 Operating Costs

Following [34] the operating costs can be distinguished into production costs and general expenses. Production costs include the operation and maintenace costs, cooling water and make up chemicals. The general expenses consist of the research and development costs, administration and marketing.
In this work only the costs for the make-up solvents and water make-up are considered due to lack of detailed information for other costs concerning the CAP.

Make-up Costs The price for the make-up chemicals is 1.2 €/kg for MEA according to [34] and 0.2 €/kg for ammonia (roughly estimated from [71]). The price of water is around 0.2 €/m^3 (see [34]).
This leads to make-up costs for the MEA Process of around 0.14 €/t CO_2 for MEA solvent and 0.1 €/t CO_2 for the make-up water.
In case of the Chilled Ammonia Process the make-up costs for the ammonia are around 5.4 €/t CO_2 and there are no costs for the make-up water stream, since there is no make-up water necessary.

As a result, the make-up costs for the MEA Process are around 3% of the make-up costs for the CAP, because of the larger ammonia loss during the capture process (see table 8.6).

Thereby it must be mentioned, that in this simulation model the make-up costs resulting from the solvent degradation were not considered. This would lead to higher make-up costs for the MEA Process and the CAP. For example, if a MEA degradation rate of 1.6 kg MEA/ t CO_2 is assumed (see [70]) the MEA make-up costs increase to 2.06 €/t CO_2. Further make-up costs in the MEA Process would be the amount of sodium hydroxide in the reclaimer, which is necessary to destroy the HSS.
According to [31] the solvent degradation of ammonia is lower than for MEA. The amount of degraded NH_3 could be sold as fertilizer (for more details see [31]).

Electric Power Demand Table 8.4 shows that the power demand of the pumps and blowers is around 88% higher for the CAP than the power demand of the MEA Process. Thus, the operating power demand and therefore the operating costs are higher for the CAP.

8.3 Ecological Comparison

In this section a short qualitative abstract of the ecological impact of the used solvent in the capture plants on humans and on the environment is given.
A more detailed ecological comparison of both solvents and the processes, for example concerning the production of the solvents or the cooling water consumption, was not done in this work due to effort time.

8.3.1 Human Toxicity

In this subsection the hazards for humans getting into contact with MEA are declared.

Pure Monoethanolamine The acute health effects in case of contact are irritations of skin, eyes and lung. Further it is slightly corrosive.
A particular interest for the capture process is that mist may lead to damage on mucous membrans of eyes, mouth and respiratory tract. The last example is characterized by shortness of breath. Besides, the odor is ammoniacal and therefore unpleasant.

Another aspect for the toxicity of a component are the potential chronic health effects. MEA may be toxic to kidneys, lungs, liver and central nervous system due to prolonged exposure.

Pure Ammonia The acute health hazards of pure ammonia are possibly severe irritation of mucous membran, skin, eyes and lungs. A short term exposure may lead to the lack of sense of smell, vomiting, pain in the chest, headage, lung damage and difficulties at breathing.
Another aspect is that containers filled with pure ammonia may explode, if they are exposed to heat (cf. [72]).

8.3.2 Enivironmental Impact

In this subsection the eco-toxicity of the washing solvents is briefly taken into concern.

Monoethanolamine In large amounts concentrated MEA is toxic to animals (LD50: 1000mg/kg for a Rabbit). The degradation products of MEA are less toxic than the product itself.

Ammonia The main hazard for the environment is the pH change in aqueous systems, which leads for example to fish mortality (cf. [72]).

All in all, both solvents are toxic and need a special treatment in handling. In a qualitative summary ammonia can be seen as more toxic and problematic to humans and the environment. Besides, in these capture processes much more ammonia is emitted than monoethanolamine.

9 Conclusions and Outlook

9.1 Conclusions

In this section a short resumé of the results in section 8 is given.

9.1.1 Energetic Conclusions from the Comparison

It can be seen that the energy demand in the reboiler (table 8.1) of the CAP is lower, although a higher energy quality (temperature) in the reboiler is necessary.
The primary cooling energy consumption is higher than in the MEA Process, shown in table 8.2. This energy demand does not represent the quality of the needed energy and cannot be directly compared. Thus, the cooling duty of the CAP can be expressed by the secondary cooling energy requirement, which is represented by the specific cooling water consumption (table 8.3). The specific cooling water consumption of this model of the CAP is around 70% larger compared to the MEA Process.

The high auxiliary power demand and cooling water consumption for the CAP compared to the MEA Process due to the chilling system leads to a larger power loss for the power plant. This fact results into an around twice as high specific power plant loss for the CAP (see section 8.1.6).

The amount of make-up solvent is also larger for the CAP than for the MEA Process (table 8.6). It should be mentioned that this value could be decreased further by higher pressure and better down-cooling. Further, the degradation of the solvents was not considered in this model and could therefore lead to larger amounts.

One of the main advantages of the CAP is the lower specific solvent flow, which is necessary for the carbon dioxide absorption (table 8.5). Another fact is that due to the higher desorber pressure lower expenses for the carbon dioxide compression section are necessary.

Nevertheless the reboiler duty is lower, the MEA Process can be seen as more energetic efficient as the CAP.

9.1.2 Economic Conclusions from the Comparison

The economic evaluation of both processes on the investment costs in section 8.2 showed, that the CAP investment is around 2.8% higher than the MEA Process investment.
The slightly higher investment costs for the CAP result primary from the additional auxiliary equipment, which is necessary for the refrigeration system.

If the value of the column height calculated with the HTU-NTU concept is used for the equipment costs (approximately 19m for the absorber and estimated 15m for the desorption column, which is around 64% lower compared to the results based on the simulation), the investment costs would decrease from 45.4€/(kg/h CO_2) respectively 15.43 [€/t CO_2 avoided] to around 20.95€/(kg/h CO_2) respectively 7.12 [€/t CO_2 avoided]. This would correspond to around half (53%) of the investment costs compared to the MEA Process. This change in the column height could perhaps be achieved by higher concentrated ammonia solution.

The operating costs are higher for the CAP due to the higher auxiliary power demand, the

higher cooling water and make-up solvent consumption.

Summarized, the results of this work show that the investment costs for the CAP with a 12wt% ammonia solution are are around 3% higher than for the MEA Process.

9.1.3 Summary

The final conclusion of this work is that this specific model of the CAP with its operating parameters (12wt% NH_3, 20bar desorber pressure, solvent to flue gas ratio of 1.45 and a solvent cooler temperature of 10°C) is disadvantaged in an energetic, economic and ecologic way .
The energetic disadvantage comes from the higher auxiliary power demand and the higher cooling water consumption. The economic disadvantage comes from the higher investment costs due to larger columns and more auxiliary components. The ecologic disadvantage comes from the higher toxicity of ammonia to humans and the environment.

The main disadvantage of the CAP compared to the MEA Process is the refrigeration system, which is obligatory to minimize the volatility of the ammonia.

9.2 Outlook

In this section a short outlook for what could be done to achieve more precise simulation results is given.

9.2.1 Monoethanolamine Process

The model used in this work for the MEA Process could be improved by better evaluation of the property data sets given by [18] (ternary system $H_2O - MEA - CO_2$) and a validation of the simulation results with the results of a pilot plant. Moreover, the *RateFrac* unit operation model in ASPEN Plus^{TM} for the absorption column could be used to get more detailed simulation results.

Changes in the operating parameters could lead to a lower power demand (e.g.: desorber pressure of 2.1 bar).

9.2.2 Chilled Ammonia Process

As far as the CAP is concerned various changes in the model could be done to achieve more precise and better simulation results.

The simulation model could be improved by using the UNIQUAC-NRF model for the VLE, proposed by [24], with data from [24]. This thermodynamic model considers the solid-liquid equilibria and the ternary system ($H_2O - NH_3 - CO_2$) more detailed than the model used in this work.
Besides, the *RateFrac* model could achieve more detailed simulation results in the absorption column.

Otherwise, some improvements in the process parameters could be made to increase the significance of the simulation model.
By using higher concentrated aqueous ammonia solutions the solvent amount could be decreased

further. This fact would lead to thinner columns and smaller pumps for the capture process. Moreover a higher concentrated solution would increase the capture efficiency of the solvent and therefore decrease the absorption column height. On the other hand, a higher concentrated solution leads to a higher ammonia slip. This could make an acid head washing system to reduce the ammonia slip necessary. Another possibility for this issue could be an intermediate cooling system for the column.
Another fact, which could lead to smaller auxiliary power demands, is the improvement of the refrigeration system. Beside this, the cooling demand could be decreased by the use of absorption heat pumps for the gas and solvent cooling.

10 Abbreviations

Tab. 10.1: Abbreviations

Abbreviation	Text
GHG	Greenhouse gases
IPCC	Intergovernmental panel on climate change
CCS	Carbon capture and storage
PCC	Post combustion capture
EU	European Union
IGCC	Integrated gasification combined cycle
MEA	Monoethanolamine
CAP	Chilled Ammonia Process
EOR	Enhanced oil recovery
CO_2	Carbon dioxide
NH_3	Ammonia
PSA	Pressure swing adsorption
TSA	Temperature swing adsorption
HTU	Height of one transfer unit
NTU	Number of transfer units
HSS	Heat stable salts
ASPEN	Advanced system for process engineering
NRTL	Non random, two liquid
ELECNRTL	Electrolyte non random, two Liquid
VLE	Vapour-Liquid Equilibrium
PC	Pulverized coal
NRF	Non random factor
wt%	Percent by weight
v%	Percent by volume
AEP	American Electric Power
AC	Absorption column
DC	Desorption column
PEC	Purchased equipment costs
PEDC	Purchased equipment and delivery costs
FCI	Fixed capital investment

11 Nomenclature

11.1 Chapter 3

Tab. 11.1: Nomenclature Chapter 3 - 1

Symbol	Unit	Discription
T	°C	Temperature
p_i	bar	Partial pressure
P	bar	Total pressure
ν_i	-	Stoichiometric coefficient for component i
$[i]$	mol/m^3	Concentration of component i
K	-	Equilibrium constant
ΔG^0	J	Reference state Gibbs free energy
R	$J//kmol \cdot K)$	Gas constant
c_i	mol/m^3	Liquid concentration of component i
x_i	-	Mole fraction of solute in the liquid
G	J	Gibbs free energy
U	J	Inner energy
H	J	Enthalpy
S	J/K	Entropy
V	m^3	Volume
n_i	mol	Mole of component i
μ_i	J/mol	Chemical potential of component i
d	-	Various molar state variable
d^{IM}	-	Molar state variable of an ideal mixture
d_{mix}	-/mol	Molar mixing variable
d_i	-	Molar state variable of component i
D_{mix}	-	Mixing variable
d^E	-	Molar excess variable
H_i	Pa/(mole fraction)	Henry's constant
y_i	-	Mole fraction of fugatvie componenten in the liquid
m_i	-	Minimal solvent ratio
$\dot{L}_{min}$	kg/h	Minimum solvent flow
$\dot{G}$	kg/h	Minimum gas flow
φ_i	-	Fugacy coefficient of component i
γ_i	-	Activity coefficient of component i
f_i	bar	Fugacity
a_i	mol/m^3	Activity
p_i^0	bar	Saturation vapour pressure
φ	-	Vapour phase fugacity coefficient in mixture
φ°	-	Pure solvent vapour phase fugacity coefficient at saturation pressure
H_i^{p0}	Pa	Henry's law constant for component i in water at saturation pressure
v_i^∞	$m^3/kmol$	Partial molar volume of a solute in water at infinite dilution
v_s	$m^3/kmol$	Partial molar volume of a pure component

Tab. 11.2: Nomenclature Chapter 3 - 2

Symbol	Unit	Discription
$\overline{g_i}$	J/mol	Partial molar Gibbs free energy of component i
A_i, B_i, C_i	-	Adjustment parameters
d^E	-	Excess variable
d^{IM}	-	Ideal mixture variable
D_i	m^2/s	Diffusivity coefficient
β_i	m/s	Mass transfer resistance of component i
$\beta^{g/l}$	m/s	Mass transfer resistance in the gaseous / liquid phase
$\beta_0^{g/l}$	m/s	Mass transfer resistance in the gaseous / liquid phase without chemical reaction
$\dot{N}_i$	mol/s	Mole flow
K_o	m/s	Overall mass transport coefficient
$K_{o,g}$	m/s	Overall mass transport coefficient based on the gaseous phase
$\dot{N}_i^{Overall}$	mol/s	Overall mole flow
$\dot{N}_i^{Diff}$	mol/s	Mole flow by diffusion
Ha	-	Hatta number
E	-	Rate enhancement factor
E_i	-	Enhancement factor at an instanteneous reaction
k_2	-	Rate constant
r_i	mol/s	Rate of reaction
$Y/\ X$	mol/mol carrying Gas/ Liquid	Loading of the gas or liquid stream
$\bar{\varrho}_g$	mol/m^3	Molar density of the gaseous phase
Y^*	mol/mol carrying Gas	Equilibrium loading
A_q	m^2	Column cross section
$\varphi^{'}$	-	Degree of wetting
Y_e	mol/mol carrying Gas	Exit Loading
Y_a	mol/mol carrying Gas	Entry Loading

11.2 Chapter 4

Tab. 11.3: Nomenclature Chapter 4 - 1

Symbol	Unit	Discription
z_i	-	Iteration step
z_{i+1}	-	Iteration result
r_i	-	Calculated value from an initial guess
s	-	Acceleration/ attenuation factor
J_i	-	Jacobi Matrix
t_i	-	Linearization parameter for the Jacobi matrix (slope)
R	$J/(kmol \cdot K)$	Gas constant
v	m^3/mol	Specific volume
$a(T)$	-	Parameter in the Soave equation
a_c	-	Value of $a(T)$ at critical temperature
$\alpha(T) = \frac{a}{a_c}$	-	Correction factor
m	-	Slope of α against reduced temperature
ω	-	Acentric factor
a	-	Attraction paramter for the mixture
a_{ij}	-	Parameter for component i in j
$a_{i/j}$	-	Paramter for component i or j
b	-	Covolume paramter
b_i	-	Parameter for component i
$b_{i/j}$	-	Paramter for component i or j
T_c	K	Critical temperature
P_c	bar	Critical pressure
g^E	J/mol	Molar free excess Gibbs energy
g^E_∞	J/mol	Molar free excess Gibbs energy at inifinite pressure
x_{ij}	mol/mol	Mole fraction of component j in the immediate neighbourhood to molecule i
α_{12}	-	Characteristic of the nonrandomness of a mixture
$\tau_{12/21}$	-	Temperature dependent adjustment parameter
$G_{12/21}$	-	Temperature dependent adjustable parameter
ρ	-	The"Closest approach" parameter
M	g/mol	Molecular weight
D	$(A \cdot s)/(V \cdot m)$	Dielectric Constant
I_x	-	Ionic strength on a mole fraction basis
A_ϕ	-	Debye-Hückel parameter/ constant for osmotic coefficient
z_i	-	Elecrical charge of component i
r_i	-	Born radius of component i
D_s	-	Dielectric constant of the mixed solvent
ϱ	kg/m^3	Density
k_{ij}	-	Adjustment Parameter
A	J/mol	Molar Helmholtz energy

Tab. 11.4: Nomenclature Chapter 4 - 2

Symbol	Unit	Discription
a^E	-	Partial molar Helmholtz energy of mixture
Z	-	Configurational partition function
U_0	-	Potential energy of a lattice containing $\sum_i^n N_i$ molecules
U_{ij}	-	Potential energy characterizing ij interaction
N_i	-	Number of molecules of component i
q	-	Pure component area paramter
r	-	Pure component volume parameter
ω_i	-	Combinatorial factor for component i
Γ_{ii}	-	Area fraction
ϵ_0	$(A \cdot s)/(V \cdot m)$	Dielectric's constant of vacuum
a, b, A_i, B_i, C_i	-	Adjustment parameters
U	J	Inner Energy
H	J	Enthalpy
ΔH_i^{vap}	J/kmol	Standard enthalpy of vaporization
T_{ri}	-	Reduced temperature
T_{ci}	K	Critical temperature of component i
$c_{p,i}^{\infty}$	$J/(kmol \cdot K)$	Heat capacity at infinite dilution
$C_p^{0,s}$	$J/(kmol \cdot K)$	Solid heat capacity
f_i^0	bar	Saturation fugacy
T_{ref}	K	Reference temperature
v_m	mol/m^3	Liquid Molar Volume
v_m^s	mol/m^3	Solid molar volume
k_i^H	$Pa/$(mole fraction)	Henry's constant of component i

11.3 Chapter 5

Tab. 11.5: Nomenclature Chapter 5

Symbol	Unit	Discription
X	mol CO_2/ mol Solvent (MEA/ NH_3)	Liquid loading
n_i	kmol/s	Mole flow of component i
K_3	-	Empirical constant for the packed-bed
K_4	-	Empirical constant for the packed-bed
a	m^2/m^3	Specific packing area
ϵ	m^3/m^3	Porosity of the random packing
d_p	mm	Hydraulic packing diameter

11.4 Chapter 6

Tab. 11.6: Nomenclature Chapter 6

Symbol	Unit	Discription
K_i	-	Equilibrium constant for reaction i
C_i	-	Adjustment parameters
A, B, C, D E, F, G	- -	Adjustment parameters
T	°C	Temperature
m	-	Minimal solvent ratio
E	-	Enhancement factor

11.5 Chapter 7

Tab. 11.7: Nomenclature Chapter 7

Symbol	Unit	Discription
K_i	-	Equilibrium constant
T	°C	Temperature
ϵ_r	$(A \cdot s)/(V \cdot m)$	Dielectric constant
D_{NH_3}	$(A \cdot s)/(V \cdot m)$	Dielectric constant of ammonia
v_m^s	cm^3/mol	Solid molar volume
M_s	g/mol	Solid mole mass
ρ_s	g/cm^3	Solid density
C_i	-	Adjustment parameters

11.6 Chapter 8

Tab. 11.8: Nomenclature Chapter 8-1

Symbol	Unit	Discription
p_{loss}	GJ/kg captured CO_2	Specific power loss
P_{loss}	MW	Power loss
P_{cap}	MW	Power duty for CO_2 capture
P_{comp}	MW	Power duty for CO_2 compression
P_{CW}	MW	Power duty for additonal cooling water supply
P_{reg}	MW	Power loss due to steam extraction for reboiler
q	GJ/t CO_2	Specific reboiler duty
$\epsilon^{'}$	-	CO_2 capture rate
T_{cond}	K	Main condenser temperature in the water steam cycle
T_{ext}^{sat}	K	Saturation temperature of extracted steam
p_{ext}	bar	Pressure of extracted steam
w_l	m/s	Liquid velocity
$\dot{m}_{l,max}$	kg/s	Maximum liquid mass flow
D_K	m	Column diameter
$w_{g,0}$	m/s	Maximum surface gas velocity
K_i	-	Empirical constants
ν_l	mPa s	Liquid viscosity
$\dot{V}_g$	m^3/s	Maximum gas volume flux
K_o / $K_o^{'}$	m/s	Mass transfer coefficient based on the gaseous phase
$\bar{\varrho_{g/l}}$	mol/m^3	Molar density of the gas/ liquid phase
β_g	m/s	Gas phase mass transfer resistence
β_l	m/s	Liquid phase mass transfer resistence
m	-	Dimensionless solubility
P	bar	Total pressure
E	-	Enhancement factor
Ha	-	Hatta number
k_{MEA/NH_3}		Rate of reaction
D_{CO_2}	m^2/s	Binary gaseous diffusivity coefficient of CO_2 in gas phase
C_{MEA/NH_3}	mol/m^3	Concentration of free solvent
T	°K	Temperature
$D_{12,g}$	m^2/s	Binary diffusivity coefficient of component 1 in 2 (gaseous)
$D_{12,l}$	m^2/s	Binary diffusivity coefficient of component 1 in 2 (liquid)
M_i	kg/kmol	Molar mass of component i
$T_{k,i}$	K	Critical temperature of component i
$V_{m,ki}$	mol/m^3	Critical molar volume of component i
ν_i	mPa s	dynamic Viscosity of component i
C	-	Empirical association factor
$Sh_{g/l}$	-	Sherwood number of the gas or liquid phase
$Re_{g/l}$	-	Reynolds number of the gas or liquid phase
$Sc_{g/l}$	-	Schmidt number of the gas or liquid phase
Ga_l	-	Galilei number of the liquid phase

Tab. 11.9: Nomenclature Chapter 8-2

Symbol	Unit	Discription
ϵ	-	Porosity of the random packing
a	m^2/m^3	Specific area of the random packing
A_q	m^2	Cross sectional area of the column
$\mu_{g/l}$	m^2/s	Kinematic viscosity of the gas or liquid phase
ρ_l	kg/m^3	Density of the liquid phase
$\dot{m}_l$	kg/s	Liquid mass flow
d_p	m	Hydraulic random packing diameter
$\dot{G}_T$	m^3/s	Carrying gas flow
HTU	m	Height of one transfer unit
NTU	-	Number of transfer units
H_K	m	Column height
Y	mol/mol solvent	Gas loading
Y^*	mol/mol solvent	Equilibrium gas loading
$Y_{in/out}$	mol/mol solvent	Ingoing/ outgoing gas load
J_i	$mol/m^2 \cdot s$	Mass transfer flux
$\Delta C_{CO_2,i}$	mol/m^3	Concentration difference between gas and liquid phase on stage i
$A_{p,i}$	m^2	Required packing surface for stage i
$\Phi_{CO_2,i}$	mol/s	Carbon dioxide mole flow on stage i
e_K	mm	Column shell thickness
p_K	MPa	Column pressure
f	MPa	Material Resistance
$R_{p1,0;T}$	MPa	1% yield strength at temperture T
z	-	Welding factor
F_M	-	Construction factor
w_K	kg	Column weight
C_K	€	Column costs
C_P	€	Packing costs
$\dot{Q}$	W	Heat flow
k	$W/(m^2K)$	Overal heat transfer coefficient
A_H	m^2	Heat exchanger surface
ΔT_{ln}	K	Logarithmic temperature difference
Δp	mbar	Total pressure drop
Δp_t	mbar	Dry pressure drop
Δp_w	mbar	Wet pressure drop
ζ	-	Drag factor
w_g	m/s	Gas velocity
d_h	m	Hydraulic diameter
μ_l	m^2/s	Liquid kinematic viscosity
g	m/s^2	Gravity

List of Figures

List of Tables

References

[1] Working Group III of the Intergovernmental Panel on Climate Change. *IPCC Special Report on Carbon Dioxide Capture and Storage.* Cambridge University Press, December 2005.

[2] Working Group III: R.E.H. Sims, R.N. Schock, A. Adegbululgbe, J. Fenhann, I. Konstantinaviciute, W. Moomaw, H.B. Nimir, B. Schlamadinger, J. Torres-Martínez, C. Turner, Y. Uchiyama, S.J.V. Vuori, N. Wamukonya, and X. Zhang. *IPCC Report 2007: Energy supply. In Climate Change 2007: Mitigation. Contribution of Working Group III to the Fourth Assessment Report of the Intergovernmental Panel on Climate Change [B. Metz, O.R. Davidson, P.R. Bosch, R. Dave, L.A. Meyer (eds)].* Cambridge University Press, Cambridge, United Kingdom and New York, NY, USA., 2007.

[3] United Nations. Kyoto protocol. 1997.

[4] United Nations. Rio declaration. 1992.

[5] J. Oexmann and A. Kather. *Post-Combustion CO_2-Abtrennung in Kohlekraftwerken*, volume 1/2. 2009.

[6] M. Lucquiaud, H. Chalmers, and J. Gibbins. *Capture-ready supercritical coal-fired power plants and flexible post-combustion CO_2 capture.* 2008.

[7] EIG Inc. Ultra cleaning of combustion gas including the removal of co2, 2006.

[8] Literaturstudie. *Abscheidung und Speicherung von CO_2 aus Kraftwerken.* 2002.

[9] I.M. Smith, C. Nilsson, and D.M.B. Adams. Greenhouse gases - perspectives on coal. technical report. Technical report, IEA Coal Research, 1994.

[10] *VDI-GET Tagung Köln*, 2003.

[11] Thomas Hochleitner. *CO_2-Abscheidung in österreichischen Kraftwerken.* 2004.

[12] Z. Zhang, G. Wang, P. Massarotto, and V. Rudolph. *Optimization of pipline transport for CO_2 sequestration*, volume 47. 2006.

[13] The Zero Emission Fossil Fuel Power Plants Technology Platform. *A Vision for Zero Emission Fossil Fuel Power Plant.* 2006.

[14] Z. E. Heinemann. *Möglichkeiten der Einlagerung von Kohlendioxid in geologischen Strukturen in Östereich.* 2004.

[15] C. F. Alie. co_2 capture with mea: Integrating the absorption process and steam cycle of an existing coal-fired power plant. Master's thesis, University of Waterloo, 2004.

[16] Ao. Univ.-Prof. DI Dr. techn. Anton Friedl. *Skriptum Thermische Verfahrenstechnik I.* self-published, 2003.

[17] D. M. Austgen, G. T. Rochelle, X. Peng, and C. Chen. *Model of Vapor-Liquid Equilibria for Aqueous Acid Gas-Alkanolamine Systems Using the Electrolyte-NRTL Equation*, volume 28. 1986.

[18] M. D. Hilliard. *A Predictive Thermodynamic Model for an Aqueous Blend of Potassium Carbonate, Piperanzine and Monoethanolamine for Carbon Dioxide Capture from Flue Gas.* PhD thesis, University of Texas at Austin, 2008.

[19] Ao. Univ.-Prof. DI Dr. techn. Anton Friedl, Ass. Prof. DI Dr. techn. Michael Harasek, and DI Dr. techn. Walter Wukovits. *Script to the lecture in Process Simulation.* self-published, 2008.

[20] Ralf Dohrn. *Berechnung von Phasengleichgewichten.* Vieweg, 1994.

[21] T. Pröll. Dynamic modeling and simulation of co_2 absorption into carbonate solution. Master's thesis, Vienna University of Technology, 2001.

[22] P. W. Atkins. *Physikalische Chemie.* VCH.

[23] Ao. Univ.-Prof. DI Dr. techn. Andreas Werner. *Script to the lecture in "Umweltschutz bei thermischen Energieanlagen".* self-published, 2010.

[24] K. Thomsen and P. Rasmussen. *Modeling of vapor-liquid-solid equilibrium in gas-aqueous electrolyte systems*, volume 54. 1999.

[25] Puxty Graeme, Rowland Robert, and Attalla Moetaz. *Comparison of the rate of CO_2 absorption into aqueous ammonia and monoethanolamine*, volume 65. 2010.

[26] P. Usubharatana and P. Tontiwachwuthikul. *Enhancement factor and kinetics of CO_2 capture by MEA-menthanol hybrid solvents*, volume 1. 2009.

[27] B. Lohrengel. *Einführung in die thermischen Trennverfahren.* Oldenburg, 2007.

[28] S. Freguia and G.T. Rochelle. *Modelling of CO_2 Capture by Aqueous Monoethanolamine.* 2003.

[29] J. Davis and G. T. Rochelle. *Thermal degradation of monoethanolamine at stripper conditions*, volume 1. 2009.

[30] A. Sexton and G. T. Rochelle. *Oxidation products of amines in CO_2 capture*, volume 8.

[31] G.S. Esber. Carbon dioxide capture technology for the coal-powered electricity industry: A systematic prioritization of research needs. Master's thesis, Ohio University, June 2006.

[32] C. E. Mortimer and U. Müller. *Das Basiswissen der Chemie.* Thieme, 2003.

[33] V. Darde, K. Thomsen, W. J. M. van Well, and E. H. Stenby. *Chilled ammonia process for CO_2 capture*, volume I. Energy Procedia, 2009.

[34] J. Oexmann and A. Kather. *Post-Combustion CO_2 capture in coal fired power plants: comparison of integrated chemical absorption processs with piperazine promoted potassium carbonate and MEA.* 2008.

[35] G. Valenti, D. Bonalumi, and E. Macchi. *Energy and exergy analyses for the carbon capture with the Chilled Ammonia Process (CAP).*

[36] Univ.-Prof. DI Dr. techn. Markus Haider. *Script to the lecture "Thermodynamik in der Energietechnik".* self-published, 2010.

[37] G. Soave. *Equilibrium constants from a modified Redlich-Kwong equation of state*, volume 27. 1972.

[38] E. A. Guggenheim. *Statistical thermodynamic of mixtures with non-zero energies of mixing.* 1944.

[39] G. M. Wilson. *J. Am. Chem. Soc.*, 86:127, 1964.

[40] H. Renon and J. M. Prausnitz. *Local Compositions in Thermodynamic Excess Functions for Liquid Mixtures*, volume 14 (1). 1968.

[41] R.L. Scott. *J. Chem. Phys.*, 25:193, 1956.

[42] C. C. Chen and L. B. Evans. *A Local Composition Model for the Excess Gibbs Energy of Aqueous Electrolyte Systems*, volume 32(3). 1986.

[43] P. Scauflaire, D. Richards, and C. C. Chen. *Ionic Activity Coefficients of Mixed-Solvent Electrolyte Systems*, volume submitted. 1989.

[44] D. S. Abrams and J. M. Prausnitz. *Statistical Thermodynamics of Liquid Mixtures: A New Expression for the Excess Gibbs Energy of Partly of Completely Miscible Systems*, volume 21, No. 1. 1975.

[45] G. R. Pazuki, H. Pahlevanzadeh, and A. Mosheni Ahooei. *Prediction of phase behavior of $CO_2 - NH_3 - H_2O$ system by using the UNIQUAC-Non Random Factor (NRF) model*, volume 242. 2006.

[46] Aspen Tech. *Aspen Plus User Guide - Steady State Simulation, Version 10, Volume 1-2.* Aspen Technology Inc., 1998.

[47] M. Bolhar-Nordenkampf. Modelling simultaneous absorption of co_2 and h_2s in aqueous solutions of methyldiethanolamine using the ratefrac module of aspen plus. Master's thesis, Vienna University of Technology, June 2001.

[48] P. A. Bouillon, S. Hennes, and C. Mahieux. *ECO2: Post-combustion or Oxyfuel - A comparison between coal power plants with integrated CO_2 capture*, volume 1. Engergy Procedia, 2009.

[49] J. Liu, S. Wang, B. Zhao, H. Tong, and C. Chen. *Absorption of carbon dioxide in aqueous ammonia*, volume 1. Energy Procedia I, 2009.

[50] K. Sattler and T. Adrian. *Thermische Trennverfahren.* WILEY-VCH, 2007.

[51] J. Gmehling, U. Onken, W. Arlt, P. Grenzheuser, U. Weidlich, B. Kolbe, and J. Rarey. *DECHEMA Chemistry Data Series - Volume I: Vapor-Liquid Eiquilibrium Data Collection.*

[52] Cambridge (MA), editor. *Aspen Plus 10.1. Computer program.* Aspen Technology Inc., 1999.

[53] M. R. M. Abu-Zahra, L. H. J. Schneiders, J. P. M. Niederer, P. H. M. Feron, and G. F. Versteeg. *CO_2 capture from power plants Part I. A parametric study of the technical performance based on monoethanolamine*, volume I. International Journal of Greenhouse Gas control, 2007.

[54] P. L. Thiez, G. Mosditchian, T. Torp, P. Feron, I. Ritsema, P. Zweigel, and E. Lindberg. *An Innovative European Integrated Project: Castor - CO_2 from Capture to Storage.* 2006.

[55] J. N. Knudsen, J. N. Jensen, P. J. Vilhelmsen, and O. Biede. *Experience with CO_2 capture from coal flue gs in pilot scale: Testing of different amine solvents*, volume I. 2009.

[56] Aspen Technology Inc. *Rate-Based Model of the CO_2 Capture Process by NH_3 using Aspen Plus.* 2008.

[57] F. Kurz, B. Rumpf, and G. Maurer. *Vapor-Liquid-solid equilibria in the system $NH_3 - CO_2 - H_2O$ from around 310 to 470 K: New experimental data and modeling*, volume 104. 1995.

[58] T. J. Edwards, G. Maurer, J. Newman, and J. M. Prausnitz. *Vapor-Liquid Equilibria in Multicomponent Aqueous Solution of Volatile Weak Electrolytes*, volume 24 (6). 1978.

[59] P. M. Mathias, S. Reddy, and J. P. O'Connell. *Quantitative Evaluation of the Aqueous-Ammonia Process for CO_2 Capture Using Fundamental Data and Thermodynamic Analysis*, volume 1. 2009.

[60] David R. Lide, editor. *CRC Handbook of Chemistry and Physics 90th Edition*. Internet Version 2010.

[61] *http://clippercontrols.com/info/dielectric_constants.html*. Clipper Controls Inc.

[62] M. Gray. *Carbon Capture & Storage with Alstom's Chilled Ammonia Process at AEP's Mountaineer Plant*. Presentation, 2009.

[63] R. Rhudy and S. Black. *Chilled Ammonia Process Update - Proceeding*. 2007.

[64] F. Kozak, A. Petig, E. Morris, R. Rhudy, and D. Thimsen. *Chilled Ammonia Process for CO_2 Capture*. GHGT - 9, 2008.

[65] V. Darde, K. Thomsen, W. van Well, and E. H. Stenby. *Using fundamental advanced thermodynamics to model CO_2 capture using aqueous ammonia*. Presentation at the 12^{th} meeting of the international post-combustion capture network, Regina, Canda, 2009.

[66] J. Oexmann, C. Hensel, and A. Kather. *Post-combustion CO_2-capture from coal-fired power plants: Preliminary evaluation of an integrated chemical absorption process with piperazine-promoted potassium carbonate*, volume 2. International Journal of Greenhouse Gas control, 2008.

[67] R. H. Perry and D. W. Green. *Perry's Chemical Engineers' Handbook*. McGraw-Hill, 1997.

[68] M. S. Peters. *Plant Design and Economics for Chemical Engineers*. Mc Graw-Hill Book Comp., Inc., 1958.

[69] A. Mulet, A. B. Corripio, and L. B. Evans. *Estimate Costs of Distillation and Absorption Towers via Correlations*. Chem. Eng., Dec. 28, 1981.

[70] D. Singh, E. Croiset, P. L. Douglas, and M. A. Douglas. *Techno-economic study of CO_2 capture from an existing coal-fired power plant: MEA scrubbing vs. O_2/CO_2 recycle combustion*, volume 44. Energy Conversion and Management, 2003.

[71] *http://www.agrarberatung-hessen.de/markt/analysen/2004/01032004012701.html*. Landesbetrieb Landwirtschaft Hessen.

[72] Robert E. Lenga, editor. *The Sigma-Aldrich library of chemical safety data*. Sigma-Aldrich Corp., 1988.

A Flowsheets

A.1 MEA Process

A.2 CAP

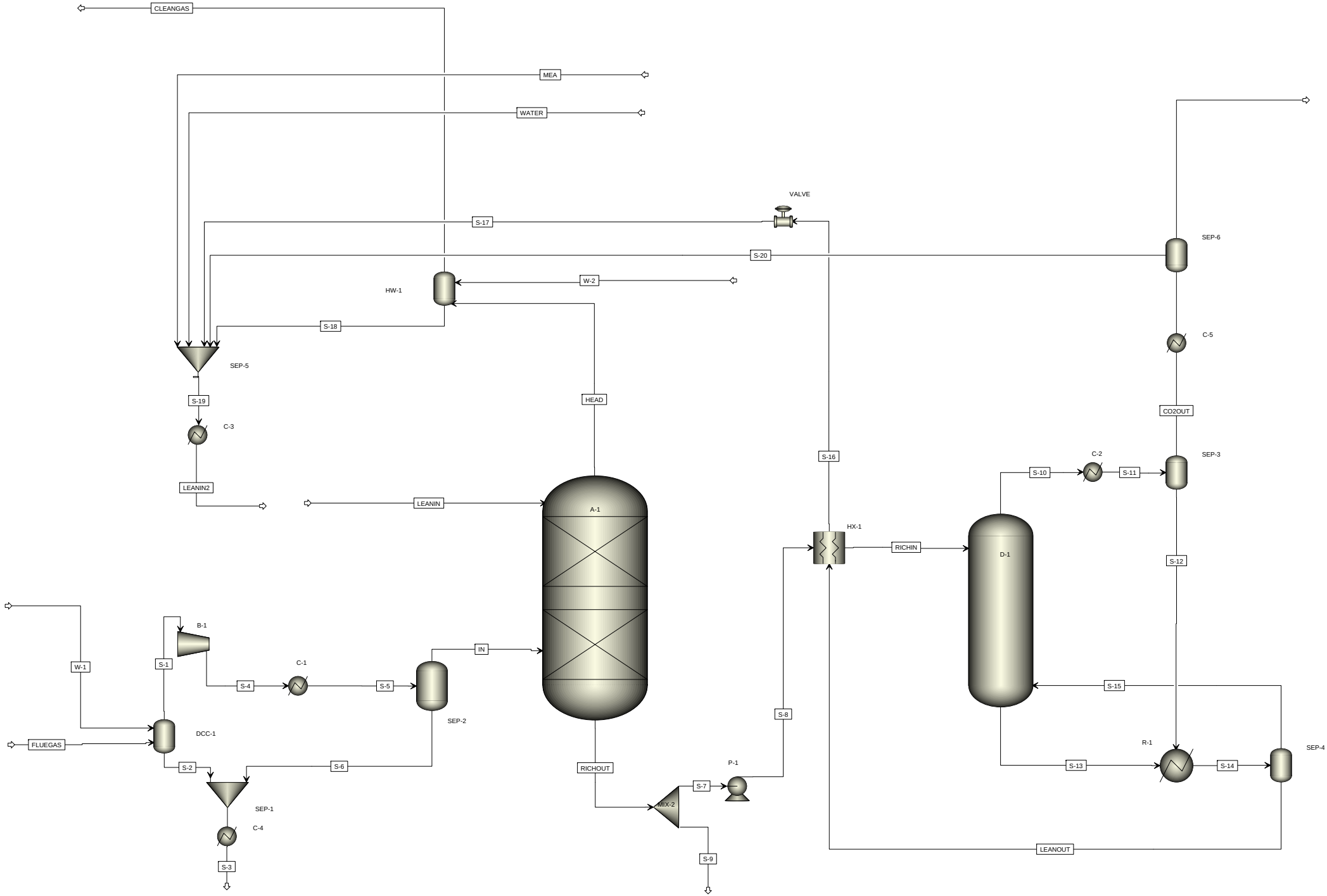
CLEANGAS
MEA
WATER
VALVE
S-17
S-20
SEP-6
HW-1
W-2
S-18
C-5
SEP-5
S-19
HEAD
CO2OUT
C-3
S-16
C-2
SEP-3
S-10
S-11
LEANIN2
LEANIN
A-1
HX-1
RICHIN
D-1
S-12
B-1
W-1
S-1
C-1
IN
S-4
S-5
S-15
SEP-2
S-8
DCC-1
FLUEGAS
R-1
SEP-4
S-2
S-6
S-13
S-14
RICHOUT
P-1
SEP-1
S-7
MIX-2
C-4
S-9
S-3
LEANOUT

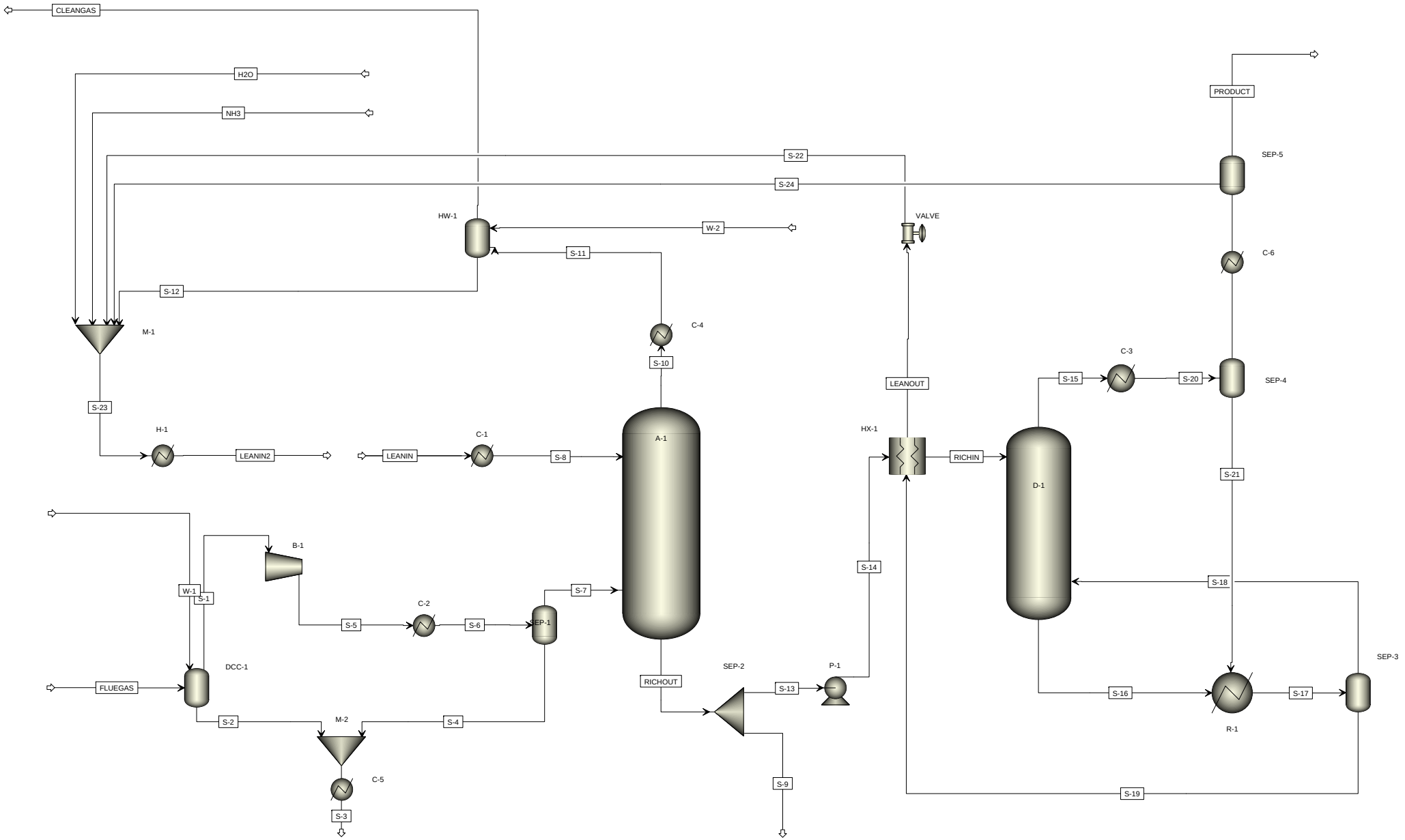
CLEANGAS
H2O
NH3
S-22
S-24
PRODUCT
SEP-5
HW-1
W-2
S-11
VALVE
C-6
S-12
M-1
C-4
S-10
C-3
S-15
S-20
SEP-4
LEANOUT
S-23
H-1
LEANIN2
LEANIN
C-1
S-8
A-1
HX-1
RICHIN
D-1
S-21
B-1
S-14
W-1
S-1
S-7
S-18
C-2
S-5
S-6
SEP-1
DCC-1
SEP-2
P-1
SEP-3
FLUEGAS
RICHOUT
S-13
S-16
S-17
R-1
S-2
M-2
S-4
C-5
S-9
S-19
S-3